Environmental Interfaces and Emerging Contaminants: PFAS Interactions with Microplastics and Dissolved Organic Matter

by

Soleil A. Sklencar

A thesis submitted to the Graduate Faculty of
Auburn University
in partial fulfillment of the
requirements for the Degree of
Crop, Soil, and Environment Science Master of Science

Auburn, Alabama
May 2nd, 2026

Key words: chemistry, adsorption, fluorescence, polyethylene, weathering

Approved by

Yaniv Olshansky, Chair, Assistant Professor of Crop, Soil, and Environmental Science
Thorsten Knappenberger, Associate Professor of Crop, Soil, and Environmental Science
Tham Hoang, Associate Professor of Fisheries, Aquaculture, and Aquatic Sciences

Abstract

Per- and polyfluoroalkyl substances (PFAS) are a diverse class of over 4,000 synthetic chemicals widely used in industrial and consumer products, including non-stick cookware, food packaging, textiles, and aqueous film-forming foams (AFFFs). Their unique amphiphilic structure, consisting of a hydrophobic fluorinated carbon chain and a hydrophilic functional head group, imparts exceptional chemical stability and environmental persistence. As a result, PFAS are frequently detected in environmental systems where they interact with co-occurring materials such as microplastics (MPs) and dissolved organic matter (DOM).

Microplastics are ubiquitous in terrestrial and aquatic environments and exist as either pristine particles or weathered forms resulting from abiotic and biotic processes. In this study, polyethylene microbeads were incubated in an aquatic mesocosm for 15 months to simulate environmental weathering. Compared to pristine MPs, weathered MPs exhibited significant physicochemical alterations, including increased surface oxidation and heterogeneity. Fourier-transform infrared (FTIR) and X-ray photoelectron spectroscopy (XPS) analyses revealed the formation of oxygen-containing functional groups (e.g., carbonyl and carboxyl), while scanning electron microscopy (SEM) showed surface cracks, divots, and mineral attachments. Adsorption–desorption experiments demonstrated that weathered MPs enhanced the adsorption of long-chain PFAS relative to pristine MPs and MP-free sediments, whereas short-chain PFAS exhibited negligible adsorption, likely due to their greater affinity for the aqueous phase.

In agricultural systems, PFAS inputs are often associated with the land application of organic amendments such as biosolids and manure, which introduce both PFAS and DOM. While DOM is known to influence PFAS partitioning, the mechanisms governing this process remain poorly constrained. DOM can facilitate PFAS adsorption through bridging interactions with soil colloids or through direct complexation, but may also compete for sorption sites. Using fluorescence excitation–emission matrix (EEM) spectroscopy, changes in DOM fluorophore intensity were evaluated in response to PFAS exposure. Results indicate that PFAS–DOM interactions are highly dependent on DOM composition and environmental conditions. Protein-like fluorophores exhibited an inverse relationship between humification index (HIX) and relative fluorophore intensity (F/F_0), suggesting fluorophore enhancement through restricted molecular motion and reduced solvent-mediated quenching.

Collectively, these findings demonstrate that PFAS behavior is strongly influenced by interactions with environmental interfaces, including weathered microplastics and heterogeneous DOM. These interactions can significantly alter PFAS adsorption, mobility, and environmental fate, underscoring the need to consider complex multiphase systems when predicting PFAS transport in natural environments.

Artificial Intelligence (AI) Use Disclosure Statement

In the preparation of this thesis, the following Artificial Intelligence (AI) tools were used: ChatGPT. These tools were used primarily for document organization and troubleshooting code. The author acknowledges full responsibility for the intellectual content of this work and has ensured that all AI-assisted sections have been reviewed and revised for accuracy and appropriate academic style. All AI-generated content was reviewed and validated for relevance, appropriateness, and accuracy before incorporation into the final document to maintain scholarly integrity of this research.

Digital Accessibility Disclosure Statement

In the preparation of this thesis, the following digital accessibility tools were used to ensure this document complies with federal requirements: Microsoft Word for document preparation and accessibility review, EndNote for citation management, and R for statistical analysis and figure generation. The author acknowledges full responsibility for the intellectual content of this work and has made a good faith effort to comply with digital accessibility requirements in publishing, wherein the nature of the content does not significantly change in order to do so. Furthermore, all content has been reviewed and revised to meet these requirements prior to final publication.

Acknowledgments

I would like to express my sincere gratitude to Dr. Olshansky for the opportunity to pursue my studies here and for your continued support, both professionally and personally. I am deeply grateful for your guidance and encouragement throughout this journey. Additionally, Dr. Knappenberger and Dr. Hoang for all their assistance on my committee and throughout this project. I am also thankful to the U.S. Department of Agriculture National Institute of Food and Agriculture for funding this research. I am beyond grateful to the friends I made in Auburn, and to those waiting for me at home, for their friendship and support. Finally, I would like to thank my family for their unwavering encouragement, and to honor the memory of my late father, whose work ethic was passed on to me and continues to guide me.

Table of Contents

List of Tables

List of Figures

List of Abbreviations

MPs	Microplastics
PE	Polyethylene
DOM	Dissolved organic matter
PFAS	Per- and polyfluoroalkyl substances
PFAAs	Perfluoroalkyl acids
PFSAs	Perfluoroalkyl sulfonic acids
PFCAs	Perfluoroalkyl carboxylic acids
PFOS	Perfluorooctane sulfonate
PFOA	Perfluorooctanoate
PFHpA	Perfluoroheptanoate
PFHxS	Perfluorohexane sulfonate
PFBS	Perfluorobutane sulfonate
SEM	Scanning electron microscopy
FTIR	Fourier-transform infrared spectroscopy
XPS	X-ray photoelectron spectroscopy
EEM	Excitation–emission matrix
UV-Vis	Ultraviolet–visible spectroscopy
ANOVA	Analysis of variance

1 Introduction

1.1 PFAS Composition and Contamination

Per- and polyfluoroalkyl substances (PFAS) are a diverse class of over 4,000 synthetic organic fluorinated compounds characterized by a fully or partially fluorinated alkyl backbone (Buck, 2011; Glüge, 2020). Structurally, PFAS consist of a hydrophilic functional head group (e.g., carboxylate, sulfonate, sulfonamide) attached to a hydrophobic and oleophobic perfluoroalkyl or polyfluoroalkyl carbon chain, commonly represented as C_nF_{2n+1}-R, where R denotes the functional moiety. The degree of fluorination distinguishes perfluoroalkyl substances, in which all hydrogen atoms are replaced by fluorine, from polyfluoroalkyl substances, which contain at least one non-fluorinated carbon.

PFAS were identified as persistent organic pollutants (POPs) at the Stockholm Convention in 2009 (Decision SC-4/17). The exceptional physicochemical properties of PFAS arise primarily from the carbon–fluorine (C–F) bond, which is the strongest single covalent bond in organic chemistry (≈485 kJ mol^{-1}). This bond strength is attributed to fluorine's high electronegativity and small atomic radius, resulting in a highly polarized and tightly bound C-F linkage. Consequently, PFAS exhibit remarkable resistance to thermal degradation, hydrolysis, photolysis, and biological transformation, leading to their persistence in environmental systems (Zhang, 2022). The surfactant behavior enables PFAS to accumulate at air-water, solid-water, and organic-aqueous interfaces. These amphiphilic properties strongly influence PFAS transport and fate in environmental matrices (Higgins, 2006; Buck, 2011). The fluorinated tail promotes partitioning to

hydrophobic phases such as organic matter, sediments, and microplastics, while the charged or polar head group facilitates aqueous mobility and electrostatic interactions with mineral and organic surfaces (Le, 2021). Variations in chain length, functional group identity, and degree of fluorination further control PFAS behavior, with long-chain PFAS generally exhibiting greater sorption affinity and bioaccumulation potential compared to their short-chain counterparts.

Owing to their unique combination of chemical stability, surface activity, and resistance to heat and oils, PFAS have been extensively used since the mid-20th century in industrial, commercial, and consumer applications. Major uses include aqueous film-forming foams (AFFFs) for firefighting, fluoropolymer manufacturing, metal plating, textile and paper coatings, and surface treatments for stain, grease, and water repellency. PFAS are also widely present in consumer products such as non-stick cookware, waterproof and breathable fabrics, food packaging, cosmetics, pesticides, industrial lubricants, and certain medical devices (Wang, 2017b; Sunderland, 2019). While these applications highlight the functional advantages of PFAS, their widespread use has led to pervasive environmental contamination and raised significant concerns, as the strong carbon–fluorine (C–F) bonds that define these compounds confer exceptional resistance to chemical, thermal, and biological degradation, resulting in high environmental persistence, mobility, and potential impacts on ecosystems and human health. In response to regulatory restrictions and voluntary phase-outs of legacy long-chain PFAS such as PFOA and PFOS, manufacturers introduced “replacement PFAS,” typically shorter-chain or structurally modified fluorinated compounds designed to reduce bioaccumulation while maintaining performance characteristics. However, emerging

evidence suggests that many replacement PFAS remain environmentally persistent and highly mobile (Kwiatkowski, 2020).

Many of the most environmentally persistent PFAS contain acidic functional groups, such as carboxylates and sulfonates, with pK_a values well below environmentally relevant pH, resulting in predominant deprotonation and anionic speciation in natural waters, soils, and sediments. This anionic form contributes to their chemical stability, high aqueous mobility, and strong electrostatic interactions with charged environmental constituents, including mineral surfaces and dissolved organic matter (DOM). As a result, anionic PFAS are more prevalent in industrial applications and have been more extensively studied than their cationic or zwitterionic counterparts (Buck, 2011; Xiao, 2019). In contrast, cationic PFAS, typically containing protonated amine or quaternary ammonium groups, exhibit enhanced adsorption to negatively charged surfaces, while nonionic PFAS (e.g., fluorotelomer alcohols) preferentially partition into organic phases. Zwitterionic PFAS, which contain both positively and negatively charged functional groups, display pH-dependent speciation and complex interfacial behavior. These differences in PFAS charge state and functional group chemistry strongly influence interactions with environmental matrices, such as soils and sediments, where electrostatic attraction, hydrophobic partitioning, and interfacial accumulation collectively govern PFAS transport, retention, and bioavailability in environmental systems (Buck, 2011; Xiao, 2019).

1.2 Environmental Occurrence

The widespread use of PFAS has led to their widespread release into the environment through multiple pathways, ranging from primary manufacturing to the use

and disposal of PFAS-containing products. Environmental contamination arising from industrial activities and routine product use creates numerous exposure routes for organisms in terrestrial, aquatic, and agricultural ecosystems, ultimately leading to human exposure.

Studies have examined the effects of PFAS in terrestrial systems, where exposure occurs through contaminated water and soil, as well as through trophic transfer via the consumption of other organisms (Xu, 2021; Miranda, 2022). Earthworms occupy a critical position at the base of the terrestrial food web and serve as a primary food source for birds, rodents, amphibians, and small mammals. Due to their reliance on soil ingestion and constant contact with contaminated substrates, earthworms are among the most affected organisms in PFAS-contaminated soils. A statistical analysis of 25 peer-reviewed studies found that increased chain length was positively correlated with bioaccumulation in earthworms (Burkhard, 2023). Another study identified that a biosolid-amended soil increased PFAS concentrations in earthworms by 1.5-fold (Navarro, 2016), indicating that biosolids serve not only as a direct source of PFAS but may also enhance PFAS bioavailability, uptake, and subsequent bioaccumulation in soil-dwelling organisms by increasing dissolved organic matter (DOM) content, which can complex with PFAS and promote their mobility and accessibility to biota.

In addition to soil fauna, terrestrial vegetation represents an important exposure pathway for PFAS entry into food webs. Plant uptake is strongly influenced by PFAS chain length and functional group chemistry with numerous studies demonstrating that short-chain perfluoroalkyl carboxylates (PFCAs) exhibit greater mobility in soil and sediment porewater and are more readily taken up and translocated within plants, whereas long-

chain perfluoroalkyl sulfonates (PFSAs), such as PFOS, tend to sorb more strongly to soils and accumulate primarily in roots (Qi, 2022a; Costello, 2024). Across multiple species, shorter-chain PFAS are preferentially transported to aboveground tissues, including leaves and shoots, while longer-chain compounds remain concentrated in root systems (Shende, 2023).

Agricultural systems are particularly vulnerable to PFAS contamination from biosolid amendments and reclaimed wastewater irrigation, while additional inputs may also arise from broader environmental sources such as aqueous film-forming foams (AFFFs) and atmospheric deposition. Increased biosolid application has been directly associated with elevated PFAS concentrations in agricultural soils and enhanced plant uptake (Ghisi, 2019; Sunderland, 2019). Wastewater treatment plants (WWTPs) serve as convergence points for PFAS originating from industrial discharges, consumer products, and domestic waste streams. Because PFAS are resistant to conventional treatment processes, they accumulate in sewage sludge, which is frequently land-applied as biosolids for agricultural fertilization (Lindstrom, 2011). This practice redistributes PFAS to croplands, where they may persist in soils, be taken up by plants, or leach to groundwater, thereby creating a potential pathway for human exposure through food ingestion (Sunderland, 2019; Johnson, 2022).

Across crop species, PFAS accumulation is strongly governed by carbon chain length and functional group chemistry. Shorter-chain PFAS exhibit greater mobility in soil porewater and are more readily translocated to aboveground tissues, whereas longer-chain compounds preferentially accumulate in roots due to stronger sorption to soil and plant matrices. In maize and potato, plant uptake generally decreases with increasing

chain length, with shorter-chain compounds more frequently detected in shoots and edible tissues (Costello, 2024; Shen, 2024). Although edible portions often contain lower concentrations than roots, the detection of compounds such as PFOA and PFOS in crop tissues underscores the potential for dietary exposure. These chain-length-dependent partitioning patterns highlight the importance of physicochemical properties in governing PFAS mobility and food-chain transfer within agricultural systems.

The atmosphere serves as an important transport pathway for PFAS originating from manufacturing emissions, landfills, wastewater treatment, vehicle exhaust, firefighting, and consumer products (Faust, 2023). Certain neutral PFAS precursors, particularly fluorotelomer alcohols (FTOHs), are sufficiently volatile to undergo long-range atmospheric transport. In the presence of hydroxyl radicals, FTOHs undergo oxidative transformation to form terminal perfluoroalkyl carboxylic acids (PFCAs), such as PFOA and PFNA, which subsequently deposit in terrestrial and aquatic environments (Ellis, 2004). This coupled transport–transformation mechanism contributes to the detection of PFAS in remote and otherwise isolated regions.

In addition to precursor volatilization, recent work identifies aerosolization as an underrecognized pathway for PFAS transfer from contaminated water bodies to the atmosphere. Aerosolization efficiency is strongly influenced by PFAS molecular structure, with longer-chain compounds and fluorotelomer sulfonates (e.g., 8:2 FTS) exhibiting enhanced enrichment in aerosols relative to shorter-chain homologs. Functional head group chemistry further modulates this behavior, with perfluoroalkyl sulfonates (PFSAs) generally demonstrating greater aerosolization potential than perfluoroalkyl carboxylates (PFCAs). Following regulatory phase-outs of legacy long-chain PFAS such as PFOA and

PFOS, alternative fluorotelomer-based “replacement” PFAS were introduced. Notably, Kizhakkethil et al. (Kizhakkethil, 2024) demonstrated that 4:2 FTS and 8:2 FTS could aerosolize from contaminated water at levels up to 3.6% and 33%, respectively. These findings suggest that aeration-based processes, including wastewater treatment, artificial lake destratification, and river oxygenation, may inadvertently enhance atmospheric redistribution of both legacy and replacement PFAS.

Through long-range atmospheric transport and aerosol deposition, PFAS are redistributed across regional and global scales, ultimately entering marine systems that serve as terminal reservoirs for anthropogenic contaminants. The global ocean represents a major terminal reservoir for anthropogenic contaminants delivered via wastewater effluent, surface runoff, and riverine transport, thereby increasing the potential for exposure and bioaccumulation within marine food webs. A review on marine PFAS exposure in seawater showed that the Indian Ocean is most contaminated with PFAS, with the sum of all PFAS in the dataset being 46.1 ng L^{-1}, based on 31 independent studies (Khan, 2023). Following the Indian Ocean are the North Pacific (12.8 ng L^{-1}), North Atlantic (4.0 ng L^{-1}), South Atlantic (2.6 ng L^{-1}), Arctic (1.1 ng L^{-1}), and South Pacific (0.5 ng L^{-1}). In marine sediments, long-chain PFAS were detected more frequently than in seawater, reflecting the greater solubility and volatility of short-chain species (Khan, 2023). All taxonomic groups studied, excluding plankton, showed dominance of long-chain carboxyl-containing PFAS, indicating the importance of chain length and functional group on PFAS interactions (Khan, 2023). PFAS concentrations in seawater have been shown to align with the global thermohaline circulation pattern described by Broecker’s “global conveyor belt,” suggesting that open-ocean currents facilitate long-range transport

and redistribution of PFAS on a global scale (Yamashita, 2008). Consistent with this large-scale transport mechanism, PFAS have been detected in marine sediments in regions lacking identifiable local sources, leading researchers to characterize their distribution as “unnatural” and indicative of widespread anthropogenic dispersal (Boitsov, 2024). Replacement PFAS such as perfluorobutane sulfonamide (FBSA) and hexafluoropropylene oxide-dimer acid (HFPO-DA, Gen-X) were also recently found in sediment, showing the shift from legacy to emerging PFAS (Zhong, 2021). Sediments and soils are well suited for investigating PFAS interactions with dissolved organic matter and other soil constituents because they function as environmental sinks; additionally, their relatively low mineral surface area enhances the role of organic phases and added constituents in governing PFAS partitioning.

Collectively, these findings demonstrate that PFAS are not confined to a single environmental compartment but are continuously redistributed among soils, sediments, biota, the atmosphere, and marine systems. Their persistence, mobility, and chain-length-dependent partitioning govern their transport across terrestrial and aquatic interfaces, while bioaccumulation in invertebrates, plants, and marine organisms facilitates entry into food webs. This interconnected cycling across environmental media ultimately increases the likelihood of human exposure through contaminated water, agricultural products, and seafood consumption.

1.3 Human and Animal Health Impacts and Toxicology

Human exposure to PFAS occurs through multiple environmental and occupational pathways, including ingestion of contaminated food and drinking water, inhalation of air and dust, dermal contact, and direct exposure during manufacturing or

use of PFAS-containing products. For the general population, dietary intake and drinking water are the dominant exposure routes, whereas inhalation and dermal contact are more relevant in occupational settings (Panieri, 2022). PFAS-treated materials, including non-stick cookware, may contribute to dietary exposure (Sunderland, 2019). Food ingestion was identified as the primary exposure pathway for PFOS and PFOA among Norwegian women, with additional contributions from drinking water, dust, and air (Haug, 2011). Contamination of cereals, fruits, vegetables, milk, and other food sources further contributes to indirect exposure through bioaccumulation in the food chain (Panieri, 2022). Monitoring studies reinforce the importance of drinking water, particularly in contaminated regions; for example, ultra-short-chain PFAS accounted for 49–99% of total PFAS detected in groundwater and treated drinking water in the Netherlands (Sadia, 2023). Epidemiological and biomonitoring data consistently demonstrate positive associations between PFAS concentrations in community water supplies and corresponding increases in human serum levels (Domingo, 2019).

Dietary exposure remains a major pathway, with seafood consumption of particular concern due to the bioaccumulative properties of PFAS in aquatic organisms. PFAS partition into protein-rich tissues, and biomagnification within marine food webs leads to elevated concentrations in higher trophic level species consumed by humans. Longer-chain PFAS, particularly perfluoroalkyl sulfonates such as PFOS, exhibit greater bioaccumulation potential than shorter-chain homologs and carboxylates, reflecting stronger protein binding and slower elimination (Sunderland, 2019). Fish, crustaceans, and mollusks frequently contain measurable PFAS concentrations, with accumulation influenced by species, trophic position, and habitat (Torres, 2023). Together, these

findings identify seafood as an important vector of PFAS transfer from aquatic systems to humans.

Once internalized, PFAS exhibit chain-length-dependent toxicokinetics that influence persistence and health risk. Biological half-lives vary substantially by carbon chain length. For example, the short-chain compound PFBA has a half-life of approximately 6–9 hours in male rats and approximately 3 days in humans, whereas the longer-chain PFNA persists for 31–55 days in rats and 2.5–4.3 years in humans (Fenton, 2021). Similar prolonged elimination has been documented for PFOS and PFOA following exposure through contaminated drinking water (Panieri, 2022). These differences underscore the enhanced bioaccumulation potential of longer-chain PFAS and their relevance for chronic toxicity.

Regulatory agencies have incorporated epidemiological data into health-based guidance values. The European Food Safety Authority (EFSA) CONTAM Panel established tolerable weekly intake (TWI) values of 13 ng kg^{-1} body weight for PFOS and 6 ng kg^{-1} body weight for PFOA, based on associations with increased serum cholesterol, reduced antibody response to immunization in children, decreased birth weight, and elevated liver enzyme levels. Exposure estimates indicate that a subset of the population exceeds these thresholds (EFSA, 2018). Epidemiological evidence further links PFAS exposure to endocrine- and metabolism-related outcomes, including childhood and adult obesity, impaired glucose tolerance and gestational diabetes, reduced birthweight, reduced semen quality, polycystic ovarian syndrome (PCOS), endometriosis, and breast cancer (Khan, 2023). The evidence base is strongest for associations with fetal growth restriction and metabolic dysfunction, consistent with the concept that prenatal and early-

life exposures can disrupt hormonal and metabolic programming with effects that manifest later in life. Importantly, dose–response relationships for endocrine disruptors may be non-monotonic, and susceptibility is heightened during sensitive developmental windows, emphasizing the need to evaluate PFAS exposures across the lifespan.

Mechanistic studies support these epidemiological observations. In vitro experiments demonstrate that PFOS and PFOA inhibit iodide uptake and reduce thyroid peroxidase activity in thyroid follicular cells, indicating direct interference with thyroid hormone synthesis. Consistent with this, human studies report associations between PFAS exposure and altered circulating thyroid hormone levels, including disruptions in free thyroxine (T4) and thyroid-stimulating hormone (TSH), particularly in prenatal and early-life exposures (Panieri, 2022) Because thyroid hormones play a critical role in growth, metabolism, and neurodevelopment, such disruption provides a biologically plausible pathway linking PFAS exposure to reduced birth weight and developmental effects.

With respect to carcinogenicity, PFOA has been classified as Group 2B (possibly carcinogenic to humans) by the International Agency for Research on Cancer. Epidemiological studies in highly exposed communities and occupational cohorts suggest the strongest associations for kidney and testicular cancer (Sunderland, 2019). Across study designs, kidney cancer has consistently been linked to higher PFOA exposure, particularly in highly exposed populations and in large cohort-based analyses. Testicular cancer shows a similar exposure–response pattern, although findings are based on smaller case numbers. Evidence for other malignancies remains limited and inconsistent,

and mechanistic pathways relevant to human carcinogenesis continue to be investigated (Steenland, 2021).

The magnitude and nature of PFAS-associated health effects depend on exposure dose, duration, route of exposure, and host-specific characteristics such as age, sex, health status, and genetic susceptibility, additionally PFAS structure. Given the expanding diversity of PFAS chemistries and their persistence in human tissues, substantial uncertainty remains regarding the long-term health implications of chronic, low-level exposure to both legacy and emerging PFAS.

1.4 PFAS in Soils and Sediments

PFAS contaminate multiple environmental media, including soil, sediment, water, and air. In terrestrial systems, contamination commonly arises from land application of biosolids and other agricultural amendments (Lindstrom, 2011), as well as the use of aqueous film-forming foams (AFFFs) at military installations and airports. More than 300 U.S. military bases have reported PFAS-contaminated drinking water attributed to AFFF releases, with compounds migrating through the vadose zone into underlying groundwater (Ruyle, 2023). Industrial discharges and manufacturing emissions represent additional major sources of environmental PFAS (De Silva, 2021).

Soils and sediments function as important sinks for PFAS, particularly long-chain compounds that exhibit greater molecular weight, hydrophobicity, and persistence compared to short-chain analogs (Higgins, 2006; Guelfo, 2020). Sorption to soil colloids is the primary mechanism governing PFAS retention, mediated by electrostatic interactions, hydrophobic partitioning, and associations with mineral surfaces and soil organic matter (Li, 2018). Organic fractions and electrolyte composition of the soil solution

further influence PFAS adsorption behavior by altering surface charge and competitive binding dynamics.

1.5 PFAS Adsorption

The retention and mobility of PFAS in soils and sediments are governed by interactions between PFAS molecular structure, solid-phase constituents, and solution chemistry. PFAS occur as anionic species under environmentally relevant pH conditions, resulting in sorption mechanisms that involve a combination of electrostatic interactions, hydrophobic partitioning, hydrogen bonding, and surface complexation (Ehsan, 2026). Soil organic matter (SOM) plays a central role in PFAS sorption and retention (Li, 2019). The fluorinated chain can preferentially associate with nonpolar domains of organic matter, increasing PFOS/PFOA partitioning as organic carbon content increases (Jeon, 2011), while functional groups may interact with polar sites through hydrogen bonding or dipole interactions (Qi, 2022b). Sorption generally increases with PFAS chain length, reflecting stronger hydrophobic interactions and greater molecular surface area. Consequently, long-chain perfluoroalkyl sulfonates (PFSAs) and carboxylates (PFCAs) typically exhibit higher sorption affinity than short-chain analogues (Buck, 2011).

Mineral surfaces also contribute to PFAS retention, particularly metal oxides and clay minerals. Variable-charge minerals such as iron and aluminum oxides can promote electrostatic attraction between negatively charged PFAS headgroups and positively charged surface sites under acidic to neutral pH conditions (Campos-Pereira, 2020). Clay minerals, through their high specific surface area and surface charge characteristics, provide additional adsorption domains. Surface area itself is an important controlling factor, as soils with greater specific surface area offer more reactive sites for adsorption

(Xiang, 2018). The presence of co-contaminants and particulate phases, including microplastics and mineral-associated organic matter, may further modify PFAS adsorption by introducing additional hydrophobic or charged interfaces, altering surface heterogeneity and adsorption capacity (Yu, 2024).

Solution chemistry strongly modulates PFAS adsorption behavior. pH influences both PFAS speciation and surface charge of soil constituents (Nguyen, 2020). Although many PFAS are strong acids and remain deprotonated across typical environmental pH ranges, decreasing pH can increase positive surface charge on metal oxides, enhancing electrostatic attraction and sorption (Campos-Pereira, 2020). Ionic strength influences PFAS retention primarily through electrostatic screening effects. Increasing ionic strength compresses the electric double layer and suppresses repulsive forces between negatively charged PFAS headgroups and negatively charged mineral surfaces, thereby facilitating sorption. Polyvalent cations (e.g., Ca^{2+}, Mg^{2+}, Al^{3+}) are particularly effective in enhancing sorption due to their greater ability to shield surface charge and reduce intermolecular repulsion compared to monovalent ions (Cai, 2022). In most environmental systems, polyvalent cations may also promote cation bridging between PFAS headgroups and negatively charged surfaces, further enhancing adsorption relative to monovalent ions (Higgins, 2006; Campos-Pereira, 2018). Conversely, competing anions may reduce PFAS sorption by occupying available surface sites.

These factors demonstrate that PFAS adsorption in soils and sediments is a dynamic process controlled by both solid-phase composition and aqueous geochemistry. Understanding these interacting mechanisms is essential for predicting PFAS fate, transport, and long-term persistence in contaminated environments.

Laboratory investigations of PFAS adsorption commonly employ batch equilibrium experiments and column transport studies. Batch systems assess equilibrium sorption behavior under controlled conditions, while column experiments simulate advective flow and more closely approximate natural transport processes. Both approaches are widely used and considered statistically robust, and they are often applied in tandem to improve mechanistic interpretation (Van Glubt, 2021). Kinetic studies show that PFAS adsorption often follows a biphasic pattern, with measurable uptake occurring almost immediately and substantial adsorption developing within the first several hours, followed by a slower phase that approaches equilibrium within about 48 h (Li, 2019). This behavior is frequently described using a biexponential model with fast (k_1) and slow (k_2) rate constants (Li, 2019). Equilibrium may require more than 48 hours, with longer-chain PFAS exhibiting stronger affinity for the solid phase and shorter-chain compounds remaining preferentially in the aqueous phase (Li, 2019; Zhou, 2021). These observations underscore the importance of both equilibrium and kinetic controls in determining PFAS persistence and transport in soil-sediment systems.

1.6 Dissolved Organic Matter and PFAS

1.6.1 DOM Characterization

Dissolved organic matter (DOM) is a complex and heterogeneous mixture of organic compounds dissolved in water, typically operationally defined as the fraction of organic matter that passes through a 0.45 μm filter membrane (Bolan, 2011). DOM originates from plant litter, microbial byproducts, soil organic matter decomposition, and anthropogenic inputs, and plays a central role in environmental systems by influencing nutrient cycling, metal speciation, pollutant transport, microbial metabolism, and soil

mineral interactions. Chemically, DOM contains a wide range of compounds, including carbohydrates, amino acids, proteins, lipids, low-molecular-weight organic acids, and humic substances. Among these, humic substances are often divided into humic acids and fulvic acids. Humic acids are generally larger, more aromatic, and less soluble under acidic conditions, whereas fulvic acids are smaller, more oxygenated, and remain soluble across a broader pH range. In general, humic-like fractions tend to be more chemically recalcitrant and enriched in conjugated structures, whereas protein- and other microbially derived fractions are typically considered more labile.

Ultraviolet-visible spectrometry (UV-VIS), along with fluorescence spectrometry, identifies the nature of DOM in solutions. A fraction of DOM that has the capacity to release a photon, referred to as fluorescent dissolved organic matter (FDOM), is used to track DOM mechanisms and composition. Fluorescence is the phenomenon where a molecule is excited to a higher electron state by absorption of UV-visible light and emits photons to return to the ground state. Delocalized π electrons found in alkenes and aromatic molecules become excited more easily at lower wavelengths. Greater π bonds in humic substances relate to humic acids, which are more recalcitrant, whereas fulvic acids are labile with fewer π bonds (Piccolo, 2001). Organic substances that are more recalcitrant and humic-like have higher molecular weight compared to protein- or fatty acid-like labile substances (Chin, 1994). Therefore, the molecular structure of DOM includes different fluorophores, molecules that fluoresce by releasing a photon.

DOM fluorescence spectra are thought to represent the average of individual compounds in the mixture. Whereas UV absorbance shows mainly the aromatic carbons at a wavelength of 254 nm. Fluorescence data are commonly collected using a

spectrofluorometer and expressed as excitation–emission matrices (EEMs), which resolve spectral features and quantify the relative contributions of excitation and emission regions. The majority of naturally derived DOM are aromatic compounds with polar functional groups. Additionally, amino acids that fluoresce include phenylalanine, tyrosine, and tryptophan. pH directly affects DOM fluorescence from the protonation and deprotonation of acidic and basic compounds bound to fluorophores. Parallel factor analysis (PARAFAC) is frequently applied to EEM datasets to deconvolute individual fluorescent components. Using EEM-PARAFAC, Ifon et al. (2022), reported increased intensities of humic-like and protein-like fluorophores in the presence of PFAS. In contrast, a separate sediment-based study observed reduced DOM aromaticity following PFAS exposure, attributing this effect to preferential PFAS association with protein-like DOM fractions and competitive adsorption driven by carboxyl and hydroxyl functional groups across sulfonic and carboxylic PFAS (Shi, 2025). PFAS-DOM interactions can either enhance or quench DOM fluorescence, depending on DOM composition, PFAS molecular structure, and interaction proximity.

1.6.2 DOM and PFAS

The fate of PFAS in soils is strongly influenced by interactions with clay minerals, soil organic matter (SOM), metal oxides, and dissolved organic matter (DOM). In agricultural systems, contaminated organic amendments such as biosolids, manures, and wastewater effluent introduce both PFAS and substantial amounts of DOM, creating conditions where these components interact dynamically. Because DOM is chemically reactive and compositionally heterogeneous, its presence can substantially modify PFAS retention and mobility.

DOM influences PFAS behavior through multiple mechanisms. Positively charged functional groups within DOM can electrostatically attract anionic PFAS headgroups (Bolan, 2011), while hydrophobic domains facilitate partitioning of the fluorinated carbon tail, particularly for longer-chain compounds. These interactions may enhance PFAS adsorption by creating additional binding domains within soil matrices or alternatively decrease adsorption through competitive sorption for mineral surface sites. Smaller DOM molecules may compete more effectively for adsorption sites than larger macromolecular organic matter (Du, 2014). Accordingly, sediment–water distribution coefficients (Kd) often increase with total organic carbon content (Du, 2014), yet the presence of mobile DOM can simultaneously increase PFAS solubility and reduce overall removal from soil systems (Qi, 2022b). Importantly, DOM effects are highly source dependent. For example, adding 100 mg C L^{-1} DOM from biosolids and animal wastes increased PFOS adsorption (up to ~90%), whereas DOM from plant/terrestrial sources decreased adsorption (up to ~40%), showing that DOM can either enhance or suppress retention depending on its chemistry (Olshansky, 2025).

Recent high-resolution molecular analyses further demonstrate that PFAS contamination can alter DOM composition and stability. Fourier Transform Ion Cyclotron Resonance Mass Spectrometry (FT-ICR-MS) revealed increased thermodynamic stability of DOM in PFAS-contaminated soils compared to uncontaminated systems (Chen, 2025). Contaminated soils exhibited reduced O/C ratios in tannin-like compounds and enrichment in protein- and lipid-like fractions, along with decreased aromaticity, suggesting a shift toward more microbially derived DOM pools (Olshansky, 2025). These

compositional changes may limit carbon cycling and nutrient availability while promoting persistent PFAS–DOM associations (Xia, 2015; Longstaffe, 2016; Chen, 2025)

1.7 Microplastics

Commercial plastic production began in the 1950s and has grown exponentially since its introduction. Plastics are synthetic organic polymers derived primarily from petroleum or natural gas. Their versatility, durability, and relatively low production cost have made them integral to food and beverage packaging, construction, textiles, consumer goods, transportation, and countless other sectors. As a result, daily life in modern society is deeply intertwined with plastic-based materials. Approximately 450 million tons of plastic are produced annually, with nearly 50% designed for single-use applications (Ritchie, 2018; Ritchie, 2026). Its extensive production and consumption have led to significant waste generation and widespread environmental pollution.

Plastics are primarily composed of low-density polymers such as polyethylene (PE) and polypropylene (PP). However, higher-density polymers, including high–density polyethylene (HDPE), polyethylene terephthalate (PET), polycarbonate (PC), and certain forms of polypropylene, are also widely produced (Hale et al., 2020). PE is the most widely produced plastic globally, accounting for approximately 31% of total plastic production and 33% of plastic waste generation (Xu, 2020; Wang, 2021). In addition to the base polymer, various chemical additives (e.g., plasticizers, stabilizers, pigments, and flame retardants) are incorporated to modify the physical properties, durability, and appearance of plastic materials (Marturano, 2017).

Environmental weathering and degradation of plastics generate microplastics (MPs). MPs may be intentionally manufactured as primary particles (e.g., in personal care

products) (Guerranti, 2019) or form as secondary particles through the physical, chemical, and biological breakdown of larger plastic debris. They are defined by the National Oceanic and Atmospheric Administration as being less than 5 mm in diameter (NOAA, 2024). MPs enter environmental systems through improper disposal, inadequate waste management, industrial releases, and fragmentation of discarded materials.

Abiotic degradation typically initiates this breakdown; photodegradation (photooxidation), driven by solar UV, produces free radicals, promotes oxidation, and introduces oxygen-containing (polar) functional groups that reduce surface hydrophobicity and weaken the polymer. Thermal oxidation can contribute through heat-driven radical formation and peroxide/hydroperoxide pathways, while mechanical abrasion (e.g., waves, sand, freeze–thaw) accelerates fragmentation (Zhang, 2021). Biotic processes may then further break down plastics by physical digestion/fragmentation and, more slowly, microbial degradation and mineralization (e.g., bacteria/fungi), often facilitated after abiotic weathering increases surface defects and bioavailability (Arp, 2021).

The widespread presence of MPs raises concerns regarding ecological and human health impacts. In humans, ingestion is considered the primary exposure pathway, with estimates suggesting that individuals may consume approximately 39,000–52,000 microplastic particles annually (Cox, 2019). Microplastic exposure has been associated with inflammatory responses, oxidative stress, cytotoxicity, and potential metabolic and reproductive effects in experimental and epidemiological studies, although standardized human health risk frameworks remain under development (Kim, 2021; Hoang, 2025).

Improper handling of plastics has resulted in plastic accumulation in the ocean and plastics being found ubiquitously in the soil and freshwater environments. Elevated MPs concentrations have been reported in freshwater systems, with Bei Lake in China reaching 8,925 particles m^{-3} (Wang, 2017a). In soils, concentrations in industrial areas have been reported between 300 and 67,500 mg kg^{-1} (Fuller, 2016). In terrestrial systems, MPs can disrupt soil structure, alter physicochemical properties, influence nutrient availability, modify microbial activity, and affect crop growth and seed germination (Sajjad, 2022).

Beyond their physical presence, MPs also function as reactive environmental interfaces. Organic pollutants are known to adsorb onto MP surfaces and may be transported across environmental compartments (Sajjad, 2022). MPs can act as vectors for co-contaminants, including persistent organic pollutants, heavy metals, pharmaceuticals, and other hydrophobic organic compounds, thereby influencing contaminant transport and bioavailability (Hoang, 2025). The potential for bioaccumulation and contaminant transfer raises important questions regarding interactions between MPs and emerging contaminants such as per- and polyfluoroalkyl substances (PFAS). Notably, a review of 91 MP–PFAS interaction studies found that the majority relied on pristine plastics (Costigan, 2022). Pristine plastics possess relatively homogeneous surfaces and uniform chemical structure, which do not accurately represent environmentally weathered MPs. Environmental aging alters MP surface morphology, generating cracks, fractures, divots, and pores (Shi, 2024), and increases surface oxygen content through the formation of oxidized functional groups (Shi, 2023a; Shi, 2024). These physicochemical changes may substantially modify adsorption

behavior and contaminant interactions, underscoring the importance of studying environmentally relevant, aged microplastics.

1.8 Microplastics and PFAS

PFAS are frequently co-occurring with microplastics (MPs) in consumer products such as food packaging, waterproof textiles, and nonstick cookware (Schellenberger, 2019; Fu, 2021; Luo, 2022; Yashwanth, 2025). Shi et al. (2023b) examined PFAS adsorption to weathered microplastics under controlled laboratory conditions in the absence of environmental media and reported reduced adsorption of four PFAS, perfluorobutanoic acid (PFBS), perfluorooctanoic acid (PFOA), and perfluorooctane sulfonate (PFOS), onto weathered low-density polyethylene compared with pristine microplastics. This reduction was attributed to weakened hydrophobic interactions following weathering. Notably, however, the study did not incorporate organic matter, which is a major contributor to PFAS–microplastic interactions under environmentally relevant conditions (Campos-Pereira, 2023).

Field-based studies further highlight the importance of MPs' composition in PFAS transport. (Cheng, 2021) analyzed MPs collected from an estuarine environment for the occurrence and abundance of 21 PFAS and found that polypropylene and polyethylene were the most prevalent polymer types. The authors suggested that PP, PE, and textile-fiber microplastics may enhance PFAS transport and accumulation within aquatic systems. Similarly, Salawau et al. (2024) investigated PET particles shredded from water bottles under controlled conditions without environmental physicochemical alteration and observed a higher adsorption capacity for PFSAs than for PFCAs. This trend was attributed to the greater hydrophobicity of sulfonate functional groups. The authors also

reported decreased adsorption of long-chain PFAS with decreasing pH, which they attributed to reduced electrostatic repulsion between negatively charged PET surfaces and anionic PFAS headgroups. Additionally, PFAS adsorption was shown to displace water molecules bound to the PET surface, indicating that adsorption is dominated by hydrophobic interactions between fluorinated PFAS chains and the polymer surface.

The role of polymer type and environmental context was further explored in a study investigating the adsorption of several PFAS (PFHxS, PFOA, fluorotelomer sulfonic acid, and GenX) to polyamide microplastics (commonly used in nylon) incorporated into a soil matrix (Sun, 2024). Polyamide–soil mixtures were incubated in the dark at room temperature for 0, 7, and 14 days. Batch adsorption isotherms demonstrated that the presence of polyamide microplastics increased PFAS adsorption capacity, with adsorption to microplastics alone being substantially greater than adsorption to soil. However, PFAS adsorption decreased with increasing incubation time, suggesting that aging processes or competitive interactions within the soil matrix may limit long-term PFAS retention on microplastic surfaces. Laboratory experiments using pristine or minimally altered polymers have provided insight into hydrophobic and electrostatic controls (Fu, 2021; Parashar, 2023). They often exclude environmentally relevant factors such as natural organic matter, mineral surfaces, and aging processes. Field observations further suggest that polymer composition and environmental weathering may significantly influence PFAS transport and accumulation in aquatic systems (Parashar, 2023). However, results remain inconsistent regarding whether weathering enhances or diminishes PFAS adsorption, and few studies have evaluated environmentally aged microplastics within realistic sediments or soil matrices. Given the

ubiquity of polyethylene in global plastic production and waste streams, and the known co-occurrence of PFAS and microplastics in contaminated environments, there remains a critical need to evaluate PFAS interactions with environmentally weathered polyethylene under environmentally relevant conditions. Understanding how long-term weathering alters microplastic surface chemistry and subsequent PFAS adsorption and desorption behavior is essential for predicting contaminant fate, transport, and persistence in sediment systems. It is hypothesized that environmental weathering will significantly alter the surface of polyethylene microbeads through the formation of oxygenated functional groups (e.g., hydroxyl and carbonyl moieties). These surface modifications are expected to increase PFAS adsorption and influence desorption behavior in sediments by enhancing surface polarity and creating additional sorption sites.

1.9 Research Questions and Hypotheses

1.9.1 Weathered Microplastic Classification, Quantification, and Interactions with Per and Polyfluoroalkyl Substances (PFAS)

Research questions are to identify the distinct chemical and physical transformations in pristine microplastics and those exposed to abiotic and biotic factors over time, and to determine how these modifications affect the adsorptive properties of contaminated sediment. The specific objectives are (1) to determine the chemical modifications of microplastics during weathering under environmentally relevant conditions in aquatic mesocosms, and (2) to determine the impact of pristine and weathered MPs in sediments on the adsorption and desorption of PFAS with varied chain length and head group. Microplastics are expected to gain oxygenated functional groups,

increasing polar interactions after weathering, and increasing adsorption capacity with PFAS.

1.9.2 Effects of Per and Polyfluoroalkyl Substances (PFAS) on Dissolved Organic Matter Mechanisms and Composition

The goal of this study is to evaluate the impact of PFAS on DOM fluorophores to elucidate underlying interaction mechanisms. Specific objectives are to determine how the DOM source, pH, and background electrolyte affect PFAS–DOM interactions and to identify the DOM fractions most responsive to PFAS exposure. It is hypothesized that PFAS–DOM interactions will be stronger at lower pH, and that the extent of interaction will vary among DOM sources according to their chemical composition. In particular, PFAS are expected to influence DOM at the fluorophore level, with protein-like components exhibiting measurable changes in fluorescence intensity and relationships with humification index (HIX), reflecting composition-dependent interactions.

References

Arp HPH, Kuhnel D, Rummel C, MacLeod M, Potthoff A, Reichelt S, Rojo-Nieto E, Schmitt-Jansen M, Sonnenberg J, Toorman E, Jahnke A. 2021. Weathering Plastics as a Planetary Boundary Threat: Exposure, Fate, and Hazards. Environ Sci Technol 55:7246-7255 https://doi.org/10.1021/acs.est.1c01512.

Boitsov S, Bruvold A, Hanssen L, Jensen HK, Ali A. 2024. Per-and polyfluoroalkyl substances (PFAS) in surface sediments of the North-east Atlantic Ocean: a non-natural PFAS background. Environmental Advances 16:100545 https://doi.org/10.1016/j.envadv.2024.100545.

Bolan NS, Adriano DC, Kunhikrishnan A, James T, McDowell R, Senesi N. 2011. Dissolved organic matter: biogeochemistry, dynamics, and environmental significance in soils. Advances in agronomy 110:1-75 https://doi.org/10.1016/B978-0-12-385531-2.00001-3.

Buck RC, Franklin J, Berger U, Conder JM, Cousins IT, De Voogt P, Jensen AA, Kannan K, Mabury SA, van Leeuwen SP. 2011. Perfluoroalkyl and polyfluoroalkyl substances in the environment: terminology, classification, and origins. Integrated Environmental Assessment and Management 7:513-541 https://doi.org/10.1002/ieam.258.

Burkhard LP, Votava LK. 2023. Review of per-and polyfluoroalkyl substances (PFAS) bioaccumulation in earthworms. Environmental advances 11:100335 https://doi.org/10.1016/j.envadv.2022.100335.

Cai W, Navarro DA, Du J, Ying G, Yang B, McLaughlin MJ, Kookana RS. 2022. Increasing ionic strength and valency of cations enhance sorption through hydrophobic interactions of PFAS with soil surfaces. Science of the Total Environment 817:152975 https://doi.org/10.1016/j.scitotenv.2022.152975.

Campos-Pereira H, Kleja DB, Ahrens L, Enell A, Kikuchi J, Pettersson M, Gustafsson JP. 2023. Effect of pH, surface charge and soil properties on the solid-solution partitioning of perfluoroalkyl substances (PFASs) in a wide range of temperate soils. Chemosphere 321:138133 https://doi.org/10.1016/j.chemosphere.2023.138133.

Campos-Pereira H, Kleja DB, Sjostedt C, Ahrens L, Klysubun W, Gustafsson JP. 2020. The Adsorption of Per- and Polyfluoroalkyl Substances (PFASs) onto Ferrihydrite Is Governed by Surface Charge. Environ Sci Technol 54:15722-15730 https://doi.org/10.1021/acs.est.0c01646.

Campos-Pereira H, Ullberg M, Kleja DB, Gustafsson JP, Ahrens L. 2018. Sorption of perfluoroalkyl substances (PFASs) to an organic soil horizon–Effect of cation composition and pH. Chemosphere 207:183-191 https://doi.org/10.1016/j.chemosphere.2018.05.012.

Chen Y, Cao D, Li X, Jia X, Shi Y, Cai Y. 2025. Interactive Effects of Soil Dissolved Organic Matter (DOM) and Per-and Polyfluoroalkyl Substances on Contaminated Soil Site: DOM Molecular-Level Perspective. Journal of Hazardous Materials 137372 https://doi.org/10.1016/j.jhazmat.2025.137372.

Cheng Y, Mai L, Lu X, Li Z, Guo Y, Chen D, Wang F. 2021. Occurrence and abundance of poly-and perfluoroalkyl substances (PFASs) on microplastics (MPs) in

Pearl River Estuary (PRE) region: Spatial and temporal variations. Environmental Pollution 281:117025 https://doi.org/10.1016/j.envpol.2021.117025.

Chin Y-P, Aiken G, O'Loughlin E. 1994. Molecular weight, polydispersity, and spectroscopic properties of aquatic humic substances. Environmental science & technology 28:1853-1858 https://doi.org/10.1021/es00060a015.

Costello MCS, Lee LS. 2024. Sources, fate, and plant uptake in agricultural systems of per-and polyfluoroalkyl substances. Current Pollution Reports 10:799-819 https://doi.org/10.1007/s40726-020-00168-y.

Costigan E, Collins A, Hatinoglu MD, Bhagat K, MacRae J, Perreault F, Apul O. 2022. Adsorption of organic pollutants by microplastics: Overview of a dissonant literature. Journal of Hazardous Materials Advances 6:100091 https://doi.org/10.1016/j.hazadv.2022.100091.

Cox KD, Covernton GA, Davies HL, Dower JF, Juanes F, Dudas SE. 2019. Human consumption of microplastics. Environmental science & technology 53:7068-7074 https://doi.org/10.1021/acs.est.9b01517.

De Silva AO, Armitage JM, Bruton TA, Dassuncao C, Heiger-Bernays W, Hu XC, Kärrman A, Kelly B, Ng C, Robuck A. 2021. PFAS exposure pathways for humans and wildlife: a synthesis of current knowledge and key gaps in understanding. Environmental toxicology and chemistry 40:631-657 https://doi.org/10.1002/etc.4935.

Domingo JL, Nadal M. 2019. Human exposure to per-and polyfluoroalkyl substances (PFAS) through drinking water: A review of the recent scientific literature. Environmental research 177:108648 https://doi.org/10.1016/j.envres.2019.108648.

Du Z, Deng S, Bei Y, Huang Q, Wang B, Huang J, Yu G. 2014. Adsorption behavior and mechanism of perfluorinated compounds on various adsorbents--a review. J Hazard Mater 274:443-454 https://doi.org/10.1016/j.jhazmat.2014.04.038.

Ehsan MN. 2026. Per-and polyfluoroalkyl substances in aquatic sediments: Global distribution, partitioning behavior, and ecological consequences. Journal of Environmental Quality 55:e70148 https://doi.org/10.1002/jeq2.70148.

Ellis DA, Martin JW, De Silva AO, Mabury SA, Hurley MD, Sulbaek Andersen MP, Wallington TJ. 2004. Degradation of fluorotelomer alcohols: a likely atmospheric source of perfluorinated carboxylic acids. Environmental science & technology 38:3316-3321 https://doi.org/10.1021/es049860w.

Faust JA. 2023. PFAS on atmospheric aerosol particles: a review. Environmental Science: Processes & Impacts 25:133-150 https://doi.org/10.1039/D2EM00002D.

Fenton SE, Ducatman A, Boobis A, DeWitt JC, Lau C, Ng C, Smith JS, Roberts SM. 2021. Per-and polyfluoroalkyl substance toxicity and human health review: Current state of knowledge and strategies for informing future research. Environmental toxicology and chemistry 40:606-630 https://doi.org/10.1002/etc.4890.

Fu L, Li J, Wang G, Luan Y, Dai W. 2021. Adsorption behavior of organic pollutants on microplastics. Ecotoxicology and Environmental Safety 217:112207 https://doi.org/10.1016/j.ecoenv.2021.112207.

Fuller S, Gautam A. 2016. A procedure for measuring microplastics using pressurized fluid extraction. Environmental science & technology 50:5774-5780 https://doi.org/10.1021/acs.est.6b00816.

Ghisi R, Vamerali T, Manzetti S. 2019. Accumulation of perfluorinated alkyl substances (PFAS) in agricultural plants: A review. Environmental research 169:326-341 https://doi.org/10.1016/j.envres.2018.10.023.

Glüge J, Scheringer M, Cousins IT, DeWitt JC, Goldenman G, Herzke D, Lohmann R, Ng CA, Trier X, Wang Z. 2020. An overview of the uses of per-and polyfluoroalkyl substances (PFAS). Environmental Science: Processes & Impacts 22:2345-2373 https://doi.org/10.1039/D0EM00291G.

Guelfo JL, Wunsch A, McCray J, Stults JF, Higgins CP. 2020. Subsurface transport potential of perfluoroalkyl acids (PFAAs): Column experiments and modeling. J Contam Hydrol 233:103661 https://doi.org/10.1016/j.jconhyd.2020.103661.

Guerranti C, Martellini T, Perra G, Scopetani C, Cincinelli A. 2019. Microplastics in cosmetics: environmental issues and needs for global bans. Environmental Toxicology and Pharmacology 68:75-79 https://doi.org/10.1016/j.etap.2019.03.007.

Haug LS, Huber S, Becher G, Thomsen C. 2011. Characterisation of human exposure pathways to perfluorinated compounds--comparing exposure estimates with biomarkers of exposure. Environ Int 37:687-693 https://doi.org/10.1016/j.envint.2011.01.011.

Higgins CP, Luthy RG. 2006. Sorption of perfluorinated surfactants on sediments. Environmental Science & Technology 40:7251-7256 https://doi.org/10.1021/es061000n.

Hoang HG, Nguyen NSH, Zhang T, Tran H-T, Mukherjee S, Naidu R. 2025. A review of microplastic pollution and human health risk assessment: current knowledge and future outlook. Frontiers in Environmental Science 13:1606332 https://doi.org/10.3389/fenvs.2025.1606332.

Ifon BE, Kiki C, Lasisi KH, Suanon F, Adyari B, Wotto V, Yu C-P, Hu A. 2022. Effects of bisphenols and perfluoroalkylated substances on fluorescence properties of humic and amino acids substances of dissolved organic matter: EEM-PARAFAC and ATR-FTIR analysis. Journal of Environmental Chemical Engineering 10:108186 https://doi.org/10.1016/j.jece.2022.108186.

Jeon J, Kannan K, Lim BJ, An KG, Kim SD. 2011. Effects of salinity and organic matter on the partitioning of perfluoroalkyl acid (PFAs) to clay particles. Journal of Environmental Monitoring 13:1803-1810 https://doi.org/10.1039/C0EM00791A.

Johnson GR. 2022. PFAS in soil and groundwater following historical land application of biosolids. Water Research 211:118035 https://doi.org/10.1016/j.watres.2021.118035.

Khan B, Burgess RM, Cantwell MG. 2023. Occurrence and bioaccumulation patterns of per-and polyfluoroalkyl substances (PFAS) in the marine environment. ACS ES&T Water 3:1243-1259 https://doi.org/10.1021/acsestwater.2c00296.

Kim J-H, Yu Y-B, Choi J-H. 2021. Toxic effects on bioaccumulation, hematological parameters, oxidative stress, immune responses and neurotoxicity in fish exposed to microplastics: A review. Journal of Hazardous Materials 413:125423 https://doi.org/10.1016/j.jhazmat.2021.125423.

Kizhakkethil JP, Shi Z, Bogush A, Kourtchev I. 2024. Aerosolisation of per-and polyfluoroalkyl substances (PFAS) during aeration of contaminated aqueous solutions. Atmospheric Environment 334:120716 https://doi.org/10.1016/j.atmosenv.2024.120716.

Kwiatkowski CF, Andrews DQ, Birnbaum LS, Bruton TA, DeWitt JC, Knappe DR, Maffini MV, Miller MF, Pelch KE, Reade A. 2020. Scientific basis for managing PFAS as a chemical class. Environmental science & technology letters 7:532-543

Le S-T, Kibbey TC, Weber KP, Glamore WC, O'Carroll DM. 2021. A group-contribution model for predicting the physicochemical behavior of PFAS components for understanding environmental fate. Science of The Total Environment 764:142882 https://doi.org/10.1016/j.scitotenv.2020.142882.

Li F, Fang X, Zhou Z, Liao X, Zou J, Yuan B, Sun W. 2019. Adsorption of perfluorinated acids onto soils: kinetics, isotherms, and influences of soil properties. Science of The Total Environment 649:504-514 https://doi.org/10.1016/j.scitotenv.2018.08.209.

Li Y, Oliver DP, Kookana RS. 2018. A critical analysis of published data to discern the role of soil and sediment properties in determining sorption of per and polyfluoroalkyl substances (PFASs). Science of the Total Environment 628:110-120 https://doi.org/10.1016/j.scitotenv.2018.01.167.

Lindstrom AB, Strynar MJ, Delinsky AD, Nakayama SF, McMillan L, Libelo EL, Neill M, Thomas L. 2011. Application of WWTP biosolids and resulting perfluorinated compound contamination of surface and well water in Decatur, Alabama, USA. Environ Sci Technol 45:8015-8021 https://doi.org/10.1021/es1039425.

Longstaffe JG, Courtier-Murias D, Simpson AJ. 2016. A nuclear magnetic resonance study of the dynamics of organofluorine interactions with a dissolved humic acid. Chemosphere 145:307-313 https://doi.org/10.1016/j.chemosphere.2015.11.080.

Luo Y, Gibson CT, Chuah C, Tang Y, Naidu R, Fang C. 2022. Raman imaging for the identification of Teflon microplastics and nanoplastics released from non-stick cookware. Science of The Total Environment 851:158293 https://doi.org/10.1016/j.scitotenv.2022.158293.

Marturano V, Cerruti P, Ambrogi V. 2017. Polymer additives. Physical Sciences Reviews 2:20160130 https://doi.org/10.1515/psr-2016-0130.

Miranda DdA, Peaslee GF, Zachritz AM, Lamberti GA. 2022. A worldwide evaluation of trophic magnification of per-and polyfluoroalkyl substances in aquatic ecosystems. Integrated environmental assessment and management 18:1500-1512 https://doi.org/10.1002/ieam.4579.

Navarro I, De la Torre A, Sanz P, Pro J, Carbonell G, de los Ángeles Martínez M. 2016. Bioaccumulation of emerging organic compounds (perfluoroalkyl substances and halogenated flame retardants) by earthworm in biosolid amended soils. Environmental Research 149:32-39 https://doi.org/10.1016/j.envres.2016.05.004.

Nguyen TMH, Bräunig J, Thompson K, Thompson J, Kabiri S, Navarro DA, Kookana RS, Grimison C, Barnes CM, Higgins CP. 2020. Influences of chemical properties, soil properties, and solution pH on soil–water partitioning coefficients of per-and polyfluoroalkyl substances (PFASs). Environmental Science & Technology 54:15883-15892 https://doi.org/10.1021/acs.est.0c05705.

Olshansky Y, Lawhon J, Ojeda A, Melina N, Knappenberger T. 2025. Impact of dissolved organic matter chemical properties on perfluorooctane sulfonate solution binding affinities and adsorption on soils. 0047-2425. Wiley Online Library.

Panieri E, Baralic K, Djukic-Cosic D, Buha Djordjevic A, Saso L. 2022. PFAS molecules: a major concern for the human health and the environment. Toxics 10:44 https://doi.org/10.3390/toxics10020044.

Parashar N, Mahanty B, Hait S. 2023. Microplastics as carriers of per-and polyfluoroalkyl substances (PFAS) in aquatic environment: Interactions and ecotoxicological effects. Water Emerging Contaminants & Nanoplastics 2:N/A-N/A https://doi.org/10.20517/wecn.2023.25.

Piccolo A. 2001. The supramolecular structure of humic substances. Soil science 166:810-832

Qi L, Li R, Wu Y, Lin X, Chen G. 2022a. Effect of solution chemistry on the transport of short-chain and long-chain perfluoroalkyl carboxylic acids (PFCAs) in saturated porous media. Chemosphere 303:135160 https://doi.org/10.1016/j.chemosphere.2022.135160.

Qi Y, Cao H, Pan W, Wang C, Liang Y. 2022b. The role of dissolved organic matter during Per- and Polyfluorinated Substance (PFAS) adsorption, degradation, and plant uptake: A review. J Hazard Mater 436:129139 https://doi.org/10.1016/j.jhazmat.2022.129139.

Ritchie H. 2018. FAQs on plastics. Our World in Data

Ritchie H, Samborska V, Roser M. 2026. Plastic pollution. [cited 2026]. Available from: https://ourworldindata.org/plastic-pollution

Ruyle BJ, Thackray CP, Butt CM, LeBlanc DR, Tokranov AK, Vecitis CD, Sunderland EM. 2023. Centurial Persistence of Forever Chemicals at Military Fire Training Sites. Environ Sci Technol 57:8096-8106 https://doi.org/10.1021/acs.est.3c00675.

Sadia M, Nollen I, Helmus R, Ter Laak TL, Been F, Praetorius A, van Wezel AP. 2023. Occurrence, Fate, and Related Health Risks of PFAS in Raw and Produced Drinking Water. Environ Sci Technol 57:3062-3074 https://doi.org/10.1021/acs.est.2c06015.

Sajjad M, Huang Q, Khan S, Khan MA, Liu Y, Wang J, Lian F, Wang Q, Guo G. 2022. Microplastics in the soil environment: A critical review. Environmental Technology & Innovation 27:102408 https://doi.org/10.1016/j.eti.2022.102408.

Salawu OA, Olivares CI, Adeleye AS. 2024. Adsorption of PFAS onto secondary microplastics: a mechanistic study. Journal of Hazardous Materials 470:134185 https://doi.org/10.1016/j.jhazmat.2024.134185.

Schellenberger S, Jonsson C, Mellin P, Levenstam OA, Liagkouridis I, Ribbenstedt A, Hanning A-C, Schultes L, Plassmann MM, Persson C. 2019. Release of side-chain fluorinated polymer-containing microplastic fibers from functional textiles during washing and first estimates of perfluoroalkyl acid emissions. Environmental Science & Technology 53:14329-14338 https://doi.org/10.1021/acs.est.9b04165.

Shen L, Zhou J, Ma Y, Su Q, Mao H, Su E, Tang KHD, Wang T, Zhu L. 2024. Characterization of the bioavailability of per-and polyfluoroalkyl substances in farmland soils and the factors impacting their translocation to edible plant tissues. Environmental Science & Technology 58:15790-15798 https://doi.org/10.1021/acs.est.4c04009.

Shende T, Andaluri G, Suri R. 2023. Chain-length dependent ultrasonic degradation of perfluoroalkyl substances. Chemical Engineering Journal Advances 15: https://doi.org/10.1016/j.ceja.2023.100509.

Shi Y, Almuhtaram H, Andrews RC. 2023a. Adsorption of per-and polyfluoroalkyl substances (PFAS) and microcystins by virgin and weathered microplastics in freshwater matrices. Polymers 15:3676 https://doi.org/10.3390/polym15183676.

Shi Y, Shi L, Huang H, Ye K, Yang L, Wang Z, Sun Y, Li D, Shi Y, Xiao L, Gao S. 2024. Analysis of aged microplastics: a review. Environmental Chemistry Letters 22:1861-1888 https://doi.org/10.1007/s10311-024-01731-5.

Shi Y, Zheng L, Huang H, Tian Y-C, Gong Z, Liu P, Wu X, Li W-T, Gao S. 2023b. Formation of nano- and microplastics and dissolved chemicals during photodegradation of polyester base fabrics with polyurethane coating. Environmental Science & Technology 57:1894-1906 https://doi.org/10.1021/acs.est.2c05063.

Shi Y-b, Hua Z-l, Chen Z-w. 2025. Impact of long-term submerge-emerge alternation on the fate of per-and polyfluoroalkyl substances (PFASs) in sediment-water systems: Insight from dissolved organic matter. Environmental Pollution 126822 https://doi.org/10.1016/j.envpol.2025.126822.

Steenland K, Winquist A. 2021. PFAS and cancer, a scoping review of the epidemiologic evidence. Environmental research 194:110690 https://doi.org/10.1016/j.envres.2020.110690.

Sun J, Xiang H, Jiang X, Wang X, Luo X, Fu J, Fan J. 2024. Effects of polyamide microplastics on the adsorption of perfluoroalkyl substances in soil. Journal of Hazardous Materials Advances 13:100391 https://doi.org/10.1016/j.hazadv.2023.100391.

Sunderland EM, Hu XC, Dassuncao C, Tokranov AK, Wagner CC, Allen JG. 2019. A review of the pathways of human exposure to poly- and perfluoroalkyl substances (PFASs) and present understanding of health effects. Exposure Science & Environmental Epidemiology 29:131-147 https://doi.org/10.1038/s41370-018-0094-1.

Torres FG, De-la-Torre GE. 2023. Per-and polyfluoroalkyl substances (PFASs) in consumable species and food products. Journal of Food Science and Technology 60:2319-2336 https://doi.org/10.1007/s13197-022-05545-7.

Van Glubt S, Brusseau ML, Yan N, Huang D, Khan N, Carroll KC. 2021. Column versus batch methods for measuring PFOS and PFOA sorption to geomedia. Environ Pollut 268:115917 https://doi.org/10.1016/j.envpol.2020.115917.

Wang C, Liu Y, Chen WQ, Zhu B, Qu S, Xu M. 2021. Critical review of global plastics stock and flow data. Journal of Industrial Ecology 25:1300-1317 https://doi.org/10.1111/jiec.13125.

Wang W, Ndungu AW, Li Z, Wang J. 2017a. Microplastics pollution in inland freshwaters of China: A case study in urban surface waters of Wuhan, China. Science of the Total Environment 575:1369-1374 https://doi.org/10.1016/j.scitotenv.2016.09.213.

Wang Z, DeWitt JC, Higgins CP, Cousins IT. 2017b. A Never-Ending Story of Per- and Polyfluoroalkyl Substances (PFASs)? Environ Sci Technol 51:2508-2518 https://doi.org/10.1021/acs.est.6b04806.

Xia X, Dai Z, Rabearisoa AH, Zhao P, Jiang X. 2015. Comparing humic substance and protein compound effects on the bioaccumulation of perfluoroalkyl substances by Daphnia magna in water. Chemosphere 119:978-986 https://doi.org/10.1016/j.chemosphere.2014.09.034.

Xiang L, Xiao T, Yu PF, Zhao HM, Mo CH, Li YW, Li H, Cai QY, Zhou DM, Wong MH. 2018. Mechanism and Implication of the Sorption of Perfluorooctanoic Acid by

Varying Soil Size Fractions. J Agric Food Chem 66:11569-11579 https://doi.org/10.1021/acs.jafc.8b03492.

Xiao F, Jin B, Golovko SA, Golovko MY, Xing B. 2019. Sorption and Desorption Mechanisms of Cationic and Zwitterionic Per- and Polyfluoroalkyl Substances in Natural Soils: Thermodynamics and Hysteresis. Environ Sci Technol 53:11818-11827 https://doi.org/10.1021/acs.est.9b05379.

Xu B, Liu S, Zhou JL, Zheng C, Weifeng J, Chen B, Zhang T, Qiu W. 2021. PFAS and their substitutes in groundwater: Occurrence, transformation and remediation. Journal of Hazardous Materials 412:125159 https://doi.org/10.1016/j.jhazmat.2021.125159.

Xu W, Chen W-Q, Jiang D, Zhang C, Ma Z, Ren Y, Shi L. 2020. Evolution of the global polyethylene waste trade system. Ecosystem Health and Sustainability 6:1756925 https://doi.org/10.1080/20964129.2020.1756925.

Yamashita N, Taniyasu S, Petrick G, Wei S, Gamo T, Lam PK, Kannan K. 2008. Perfluorinated acids as novel chemical tracers of global circulation of ocean waters. Chemosphere 70:1247-1255 https://doi.org/10.1016/j.chemosphere.2007.07.079.

Yashwanth A, Huang R, Iepure M, Mu M, Zhou W, Kunadu A, Carignan C, Yegin Y, Cho D, Oh JK. 2025. Food packaging solutions in the post-per-and polyfluoroalkyl substances (PFAS) and microplastics era: a review of functions, materials, and bio-based alternatives. Comprehensive Reviews in Food Science and Food Safety 24:e70079 https://doi.org/10.1111/1541-4337.70079.

Yu F, Wu J, Wang H, Bao Y, Xing H, Ye W, Li X, Huang M. 2024. Interaction of microplastics with perfluoroalkyl and polyfluoroalkyl substances in water: A review of the fate, mechanisms and toxicity. Science of The Total Environment 948:175000 https://doi.org/10.1016/j.scitotenv.2024.175000.

Zhang K, Hamidian AH, Tubić A, Zhang Y, Fang JK, Wu C, Lam PK. 2021. Understanding plastic degradation and microplastic formation in the environment: A review. Environmental pollution 274:116554 https://doi.org/10.1016/j.envpol.2021.116554.

Zhang Z, Sarkar D, Biswas JK, Datta R. 2022. Biodegradation of per-and polyfluoroalkyl substances (PFAS): A review. Bioresource technology 344:126223 https://doi.org/10.1016/j.biortech.2021.126223.

Zhong H, Zheng M, Liang Y, Wang Y, Gao W, Wang Y, Jiang G. 2021. Legacy and emerging per-and polyfluoroalkyl substances (PFAS) in sediments from the East China Sea and the Yellow Sea: Occurrence, source apportionment and environmental risk assessment. Chemosphere 282:131042 https://doi.org/10.1016/j.chemosphere.2021.131042.

Zhou D, Brusseau ML, Zhang Y, Li S, Wei W, Sun H, Zheng C. 2021. Simulating PFAS adsorption kinetics, adsorption isotherms, and nonideal transport in saturated soil with tempered one-sided stable density (TOSD) based models. Journal of hazardous materials 411:125169 https://doi.org/10.1016/j.jhazmat.2021.125169.

2 Environmental Weathering of Polyethylene Microbeads Controls PFAS Adsorption on Sediments

2.1 Abstract

Microplastics (MPs) are pervasive environmental contaminants that undergo physicochemical alterations during environmental weathering. Perfluoroalkyl substances (PFAS) are persistent synthetic compounds found in similar environments. This study investigates the surface characteristics of polyethylene (PE) MP following weathering in aquatic sediments and their effects on PFAS adsorption. Weathering of MP occurred during 15 months of incubation in an aquatic mesocosm. MP surfaces were analyzed using X-ray photoelectron spectroscopy (XPS), Fourier-transform infrared spectroscopy (FTIR), and scanning electron microscopy (SEM). Batch adsorption and desorption experiments were conducted with six common PFAS on aquatic sediment containing no MP, or 2.5 mg MPs g^{-1} of pristine or weathered MP. Our results show that weathering of MP increased surface roughness and the formation of hydroxyl and carbonyl groups, thereby enhancing surface polarity and providing potential adsorption sites. The presence of pristine MP decreased PFOS adsorption by 40% but did not affect PFNA adsorption. However, the presence of weathered MP did not affect PFOS adsorption but increased PFNA adsorption by 40%. Adsorption of short-chain PFAS was below the limit of quantification. A pronounced apparent adsorption-desorption hysteresis was measured for both PFNA and PFOS on sediments containing pristine MPs, but only for PFNA on sediments containing weathered MPs. These results demonstrate that MP affects PFAS fate in aquatic systems even at low concentrations. Moreover, the study shows that

weathered MP exhibits distinct properties and thus affects the fate of PFAS and potentially other contaminants in the environment.

2.2 Introduction

Plastic production has increased rapidly over the past century, becoming integral to modern society due to its durability, versatility, and low cost. As a result, plastic materials are now used across nearly all industrial sectors. However, this widespread use has led to growing environmental concern, as plastic waste is continuously introduced into natural systems through improper disposal, tire wear, textile fibers, and general litter. Among the various plastic types, polyethylene (PE) is the most widely produced, accounting for approximately 31% of the global plastic production rate and 33% of plastic waste (Xu, 2020; Wang, 2021).

A significant fraction of environmental plastic contamination exists as microplastics (MPs), defined as plastic particles smaller than 5 mm in diameter (NOAA, 2024). These particles may be introduced directly as primary microplastics, such as manufactured microbeads used in personal care products, or formed indirectly as secondary microplastics through the breakdown of larger plastic debris (Guerranti, 2019). Environmental weathering processes, including ultraviolet (UV) radiation, thermal exposure, mechanical abrasion, and biodegradation, play a critical role in this transformation (Fu, 2021).

As plastics undergo weathering, their physicochemical properties are altered substantially. In contrast to pristine materials, which are typically designed to be relatively inert, weathered microplastics exhibit increased surface roughness and chemical heterogeneity (Shi, 2024). Oxidative degradation of polyolefins such as PE and polypropylene (PP) proceeds through radical-mediated reactions that break down hydrocarbon chains and introduce oxygen-containing functional groups, including

carbonyl (R–C=O) and carboxyl (R–COOH) moieties (Shi, 2023b). Hence, these transformations increase surface polarity, hydrophilicity, and hydrogen-bonding capacity (Fu et al., 2021). Collectively, these changes enhance the capacity of microplastics to interact with co-occurring contaminants. As a result, weathered MPs may serve as vectors for organic pollutants, facilitating their transport and persistence in both aquatic and terrestrial environments (Bellasi, 2020; Rafa, 2024).

Per- and polyfluoroalkyl substances (PFAS) are a class of synthetic surfactants that contain a hydrophobic perfluoroalkyl backbone and a polar head group (Buck, 2011). The most abundant PFAS are perfluoroalkyls with carboxylate or sulfonate headgroups and varying length of C_nF^{2n+1} backbone (Buck, 2011; Sunderland, 2019). Particularly, perfluorooctane sulfonate (PFOS) perfluorooctanoate (PFOA), heptadecafluorononanoate (PFNA), perfluoroheptanoate (PFHpA), perfluorohexane sulfonate (PFHxS), and perfluorobutanesulfonate (PFBS) are frequently found in the environment due to their prolonged commercial use or the transformation of PFAS precursors to one of these stable compounds (Lenka, 2021; Lyu, 2022). Due to their low pKa (<3), these acids are anions under most environmental conditions (Higgins, 2006; Nguyen, 2020). In soils and sediments, PFAS mobility varies with chain length. Short-chain (<6 perfluorinated carbons) are constantly more mobile than long-chain (≥7) (Sunderland, 2019; Brusseau, 2023). The prevalence of commercial use, high stability under environmental conditions, and toxicity for humans and other organisms make PFAS organic pollutants of emerging concern.

PFAS partitioning in sediments is primarily governed by mineral surfaces and natural organic matter. Field and laboratory studies show that adsorption of PFOS and

PFOA in sediments is strongly influenced by organic matter content, oxide composition, and prior PFAS loading, with concentration gradients between sediment and overlying water driving either retention or remobilization (Reif, 2022). These findings demonstrate that sediments can function as both sinks and secondary sources of PFAS depending on environmental conditions. In such mineral- and organic matter-dominated systems, microplastics must compete with abundant natural sorbents, raising important questions regarding their relative contribution to PFAS retention and mobility.

PFAS are often found in conjunction with microplastics (MPs) in consumer products such as food packaging, waterproof clothing, and nonstick pans (Schellenberger, 2019; Fu, 2021; Luo, 2022; Yashwanth, 2025). MPs can act as mobile sorbents for PFAS in aquatic environments, influencing their transport, persistence, and bioavailability. Because PFAS are amphiphilic molecules with hydrophobic fluorinated chains and charged headgroups, their interactions with polymer surfaces are governed by a combination of hydrophobic, electrostatic, and interfacial water-mediated processes. Understanding these interactions is therefore critical for predicting how polymer type and environmental conditions influence PFAS fate.

Adsorption of PFAS on pristine polyethylene terephthalate (PET) microplastics derived from water bottles was controlled by PFAS head group, chain length and aqueous conditions (Salawu, 2024). Higher adsorption was measured for perfluoroalkyl sulfonic acids (PFSAs) compared to perfluoroalkyl carboxylic acids (PFCAs), attributed to the greater hydrophobicity of sulfonate functional groups. Adsorption of long-chain PFAS increased with decreasing pH, consistent with reduced electrostatic repulsion between the negatively charged PET surface and anionic PFAS headgroups. The authors further

demonstrated that PFAS adsorption displaced water molecules bound to the PET surface, indicating that sorption was dominated by hydrophobic interactions facilitated by the disruption of structured interfacial water. Molecular-scale simulations support these observations, showing that PFAS structure and polymer chemistry alone can drive strong sorption selectivity, with long-chain and sulfonated PFAS (e.g., PFOS and PFHxS) exhibiting the strongest affinity for polyethylene surfaces due primarily to van der Waals interactions (Enyoh, 2024). Using a similar simplified approach, Shi et al. (2023a) examined PFAS adsorption to weathered low-density polyethylene microplastics in the absence of environmental media and reported decreased adsorption of PFBS, PFOA, and PFOS relative to pristine MPs, which they attributed to weakened hydrophobic interactions following weathering. While these findings provide insight into surface-property changes, such experiments do not capture the influence of environmentally relevant matrices or geochemical interactions. In contrast, field-based evidence demonstrates the importance of microplastics as vectors for transporting PFAS in natural systems. Enhanced transport of PFAS by microplastics was documented in an estuarine environment by Cheng et al. (2021), where polypropylene (PP) and polyethylene were the dominant polymer types recovered, and PFAS concentrations associated with MPs were substantially higher than those measured in surrounding waters. Similarly, Sun et al. (2024) investigated the adsorption of PFHxS, PFOA, fluorotelomer sulfonic acid, and GenX to polyamide microplastics incorporated into a soil matrix and found that the presence of microplastics increased PFAS adsorption capacity, with adsorption to microplastics alone exceeding that in soil.

Polyamide remains the only polymer, to date, for which weathered microplastic–PFAS interactions have been evaluated within a soil or sediment matrix. Considering the environmental prevalence of polyethylene and its documented role in PFAS sorption in aquatic systems, the lack of studies addressing environmentally weathered polyethylene in mineral- and organic matter-dominated matrices limits our ability to predict PFAS behavior in terrestrial and sedimentary environments. This study examined how environmental weathering of PE MPs in freshwater mesocosms influences PFAS adsorption and desorption on MPs-containing sediments. We first confirm the chemical and physical transformations of MP following 15 months of incubation in an aquatic mesocosm. We then compared the adsorption and desorption of three PFSAs and three PFCAs on sediments containing pristine, weathered, or no-MP conditions. The results shed new light on the importance of MPs' weathering on the fate of PFAS in aquatic systems.

2.3 *Materials and Methods*

Red colored PE microbeads with 150 µm diameter (hereafter MPs) were purchased from Cospheric (Cospheric LLC, Somis, California). Perfluoroalkyl substances (Table 1) were purchased from Matrix Scientific (Matrix Scientific, Columbia, SC). Isotopically labeled PFAS (Table 1) were purchased from Wellington Laboratories (Guelph, ON). Ultrapure water (18.2 MΩ) was obtained from a Smart2Pure system (Thermo Scientific, Waltham, WI). LC-MS grade methanol and calcium chloride dihydrate (VWR International, Radnor, PA).

2.3.1 Aquatic Mesocosm Incubation

The weathered microplastic used in this study was from a mesocosm study by Jenna Molaro. Briefly, the aquatic mesocosm was prepared by adding 40 L of sediment into a 340 L glass aquarium, followed by adding 50 L of pond water and approximately 200 L of city water treated with an activated carbon filter to remove chlorine and heavy metals. Sediment and pond water were collected from the Chicago Botanical Garden in Illinois, USA (42° 8’ 29’’ N, 87° 47’14’’ W), and added to the mesocosm as an algal seed source to initiate the system. This design was to mimic a natural lentic ecosystem (Hoang, 2021). The sediments consist of a loamy sand texture, specific surface area of 2.95 ± 0.01 m^2 g^{-1}, pH 7.1 ± 0.3, and organic content of 3.22% ± 0.47% (Text Appx. 1). Preliminary analysis showed that MPs content in the sediment was negligible before contracting the mesocosms. The mesocosm was allowed to grow for three months before the introduction of microplastics. After the growing phase, MPs were added to the system at a concentration of 100 mg L^{-1} and incubated for an additional 15 months. More details can be seen in Molaro (2023). Following incubation, sediment cores were collected from each mesocosm and air-dried before further analysis and use in batch adsorption experiments.

2.3.2 Microplastic Collection, Separation, and Characterization

MPs were extracted from sediment using a density separation and vacuum filtration procedure (Quinn, 2017). To disperse the MPs, 5 g of sediments were suspended in 40 mL of ultra-pure water in a PP centrifuge tube, vortexed for 10 min, and placed on a reciprocal shaker for 8 hours. Then, 13 g of NaCl (~5.6 M) were added to

each tube to achieve a final density of 1.21 g cm^{-3}. Samples were allowed to settle overnight, then centrifuged at 330 relative centrifugal force (g) for 10 min at 25° C. The MPs were collected from the supernatant on 105° C dry and pre-weighted on Whatman 5 filter paper (Cytiva, Marlborough, MA). The filters were thoroughly washed with ultrapure water, dried at 105° C, and reweighed. The red MPs were clearly visible on the filter, and MP-free sediments were used as a negative control. Before further characterization, MPs were washed with ultrapure water and ethanol, then air-dried on a watch glass. A subset of unwashed MPs was also analyzed (Table Appx. 3,Figure Appx. 1). Pristine MPs were treated the same way and used as a control of unweathered MPs. For scanning electron microscopy (SEM) analysis, samples were mounted on aluminum support stubs with double-stick carbon tape and coated with gold using an Electron Microscopy Sciences Q150R sputter coater (Electron Microscopy Sciences, Hatfield, PA). Sputter-coated samples were imaged with an EVO50 Scanning Electron Microscope (SEM) at 20kV (Zeiss, White Plains, NY).

The chemical image of MPs was measured with an IRT 7200 (Jasco, Tokyo, Japan) Fourier Transform Infrared microscope (μFTIR) equipped with a view-through Ge ATR microscope objective (ClearView™), IQ Mapping, and a linear-array 16-element MCT detector. Washed pristine and weathered MPs were placed on a PTFE filter membrane and mounted on the auto-stage. The scanned size is 180 μm X 180 μm and the wavenumber ranged between 3500-950 cm^{-1}, at a spectral resolution of 4 cm^{-1}, with 16 scans accumulated per measurement.

Carbon and oxygen speciation at the MP surface were determined using a Thermo K-Alpha X-ray photoelectron spectroscopy (XPS) system (Thermo Scientific, Waltham,

USA) equipped with a monochromatic Al Kα X-ray source (1486.6 eV) and a 60 μm spot size. MPs were affixed onto double-sided adhesive tape. The XPS energy scale was calibrated with internal gold, silver, and copper standards, Au 4f (84 eV), Ag 3d (368.4 eV), and Cu 2p (932.6 eV) reference peaks. Charge compensation was achieved using a low-energy ionized argon flood gun. All spectra were charge-corrected by referencing the aliphatic C–C/C–H peak to 284.8 eV. High-resolution spectra were deconvoluted into individual components using a mixed Voigt function in Advantage software (v. 5.99, Thermo Scientific, Waltham, USA).

2.3.3 *Batch Adsorption and Desorption*

PFAS adsorption was measured using the batch method. Three adsorbents were used: sediments incubated without MPs (MPFS), sediments incubated with MPs (WMPS), and sediments that were incubated without MPs and fortified with pristine MPs (PMPS). The concentration of pristine MPs added was comparable to that of weathered MPs accumulated in the sediments collected at the end of the incubation experiment. Surface area. Ten g of adsorbent were added to 50 mL Falcon PP centrifuge tubes and pre-equilibrated with 5mM $CaCl_2$ solution for 12 hours on a reciprocal shaker (150 RPM) at 25 °C in the dark. Subsequently, a cocktail of six PFAS (Table 1) was added at concentrations ranging from 0.5 to 50 $\mu g\ L^{-1}$ for each PFAS. Each concentration was prepared in duplicate. The suspensions were placed on a reciprocal shaker (150 RPM) at 25 °C in the dark and equilibrated for 48 h. The Sediments were separated by centrifugation at 572 g for 5 minutes. Fifteen milliliters of supernatant were withdrawn from just below the liquid surface to avoid collecting microplastics, which were retained with the sediment infranatant. The supernatant was filtered through a 0.22 μm PP syringe

filter (Foxx Life Sciences, Salem, OR) before PFAS analysis. The desorption step was followed by the addition of 15 mL of PFAS-free 5 mM $CaCl_2$ to the respective tube. The samples were equilibrated for an additional 48 hours and prepared for PFAS quantification as described for the adsorption step. The adsorbed concentration of each PFAS was calculated from the difference between the initial and equilibrium concentrations. The adsorption and desorption isotherms were fitted to the Freundlich equation (Eq. 1) using nonlinear least squares estimates (Wickham, 2016; Posit team, 2026; R Core Team, 2026).

$$q_e = K_f C_e^n \quad (1)$$

Where, q_e is the concentration of the adsorbate (μg kg^{-1}), C_e is the concentration of adsorptive at equilibrium (μg L^{-1}), K_f is the Freundlich coefficient [(μg kg^{-1}) (μg $L^{-1})^{-n}$], and n describes isotherm linearity (dimensionless). Freundlich parameters were estimated using linearized regression. Combined adsorption and desorption data were analyzed using a linearized Freundlich model. Tukey-adjusted pairwise comparisons were used to evaluate differences in K_f, with statistically homogeneous groups indicated by superscript letters ($p < 0.05$).

2.3.4 PFAS Quantification

An aliquot of 0.6 mL of filtered supernatant was mixed with 0.6 mL of methanol. Subsequently, 10 µL of an isotopically labeled internal standard mixture (Table 1) was added to achieve a final concentration of 4 µg L^{-1} for each labeled compound. PFAS were quantified using a Vanquish Flex Binary ultra-performance liquid chromatography system coupled to a quadrupole Orbitrap mass spectrometer (Orbitrap Exploris 120, Thermo Scientific) operated with heated electrospray ionization in negative mode. PFAS-free LC

hardware was used throughout the analysis. Detailed chromatographic and mass spectrometric parameters are provided in the Appendix, Text Appx. 3.

2.4 Results

2.4.1 Microplastic Characterization

The final concentration of aged plastic-contaminated sediment was 0.41 ± 0.15 mg g^{-1}. The surface area of the sediment was 2.95 ± 0.01, 3.03 ± 0.01, and 2.40 ± 0.01 m^2 g^{-1} for MFPS, WMPS, and PMPS, respectively (Text Appx. 1). Given the low concentration of MPs in the sediment, little variability in surface area was anticipated.

Weathering processes in the aquatic mesocosm substantially changed the surface morphology of the MPs. SEM imaging of pristine MPs (Figure 1) demonstrates a smooth surface, while the weathered microplastics exhibited pronounced surface heterogeneity characterized by cracks with a length of 6.5 - 12.9 µm, divots 2.9 - 6.5 µm in diameter, and mineral attachments (6.5–11.2 µm). The µFTIR chemical imaging of the pristine MP (Figure 2) exhibited absorption bands around 2975, 2918, and 1462 cm^{-1}, corresponding to the asymmetric and symmetric C–H stretching vibrations of methylene ($-CH_2-$) groups, and methylene bending (scissoring), respectively (Coates, 2000; Charles, 2009). The chemical image of weathered MPs shows a distinct region of interest (ROI). Most ROI exhibited spectra similar to that of pristine MPs. However, for some ROI additional bands appeared between 3400–3500 and 1700–1750 cm^{-1}, assigned to O–H and C=O stretching vibrations, respectively (Coates, 2000). An additional band at 1100 cm^{-1} can be assigned to C–O or Si–O–Si stretching (Smith, 2018). Similar chemical speciation was obtained by XPS analysis (Figure 3). The abundance of C decreased from 95% in pristine MPs to 67% in weathered MPs, while the O and Si abundances increased from 5% to

24%, and 0% to 6%, respectively (Table Appx. 2).The high-resolution C1s spectrum of pristine MPs (Figure 3) shows a predominant (90%) peak at binding energy 284.5 eV, the C–C bond, and a minor peak at 285.9 eV, the C–OH bond (Kuwabara, 2007). For weathered MPs, the 284.5 eV peak decreased by 77%, whereas the 285.9 eV peak increased by 15%. An additional peak was observed at 288.5 eV, which is C=O in carboxyl (Rotger et al., 1995), and accounts for 8% of the C1s spectrum. The O1s spectra of pristine MPs show only one peak at 531.3 eV assigned for the C–O bond (Kolodziejczyk et al., 2023), while the spectra of weathered MPs show an additional peak at 532.7 eV, assigned to the Si–O bond (Rotger, 1995). The spectrum of Si2p (Table Appx. 2) of weathered MPs shows only one peak at 102.2 eV, assigned for the Si–O bond (Rotger, 1995). When weathered MPs were not washed extensively with water and ethanol before XPS analysis, additional peaks appeared for N, Fe, Al, Na, and Cl, indicating that MPs were weakly associated with other organic and mineral constituents of the aquatic sediments (Table Appx. 3, Figure Appx. 1).

2.4.2 *Adsorption and Desorption Experiments*

Adsorption of short and medium-chain PFAS on the aquatic sediments with and without MP was negligible (Figure Appx. 3). The adsorption and desorption of PFOS and PFNA exhibited pronounced L-type isotherms (Figure 4). These isotherms fitted well to the Freundlich equation with K_f values ranging from 1.86 to 16.53 [(mg kg^{-1})(mg L^{-1})$^{-n}$] and *n* values ranging from 0.72 to 1.13 (Figure 4, Table 2). Adsorption isotherms of PFOS exhibited larger K_f values and lower *n* values compared with PFNA (Table 2,). Similar PFOS adsorption was measured on WMPS and MPFS. In contrast, adsorption on PMPS was significantly lower. Pairwise comparisons of K_f values further resolved these

differences (Table 2), showing that PFOS adsorption on PMPS was significantly lower than on WMPS. In contrast, MPFS exhibited intermediate behavior and was not significantly different from either treatment. In contrast, PFNA adsorption was significantly enhanced in the presence of microplastics, with both PMPS and WMPS exhibiting greater K_f values than MPFS. Both MPFS and WMPS exhibited reversible adsorption, but apparent hysteresis between adsorption and desorption was observed for PMPS (Figure 4). Similar to PFOS, the adsorption of PFNA was highest on WMPS. However, adsorption of PFNA on PMPS and MPFS was similar (Table 2). Moreover, apparent hysteresis between PFNA adsorption and desorption was observed for both WMPS and PMPS, but not for MPFS (Figure 4).

2.5 *Discussion*

Our results demonstrate substantial physical and chemical weathering of polyethylene microplastics following 15 months of environmentally relevant incubation. The observed surface roughening, cracking, and oxidation are consistent with characteristics commonly reported for PE MPs recovered from aquatic and sedimentary environments, as well as MPs subjected to prolonged, but not overly aggressive, laboratory weathering (Gulmine, 2003; Shi, 2023b). These similarities suggest that the mesocosm-based weathering approach captures key environmental weathering processes that are often absent from short-term or highly oxidative laboratory treatments. The progressive loss of PE-characteristic C–C bonds and the formation of oxygen-containing functional groups reflect oxidative weathering that increases surface polarity and chemical heterogeneity, trends widely documented in environmental MP surveys. In parallel, the detection of silicon and other sediment-associated elements indicates

interactions between MPs and surrounding mineral phases. Hence, demonstrating environmental exposure that is rarely reproduced in simplified laboratory systems. Notably, unwashed weathered MPs exhibited enrichment in sediment-derived elements that were removed by solvent washing, indicating weakly bound surface associations rather than permanent chemical incorporation. This behavior is consistent with the formation of an environmentally derived surface coating, often described as an “eco-corona,” composed of mineral and organic constituents accumulated during environmental residence (Yao, 2023). Such coatings represent a key distinction between environmentally weathered MPs and artificially weathered particles and underscore the importance of incorporating realistic aging processes when assessing MP reactivity and contaminant interactions.

Prior studies report increasing PFAS adsorption with chain length and greater affinity of PFSAs relative to PFCAs (Higgins, 2006; Buck, 2011; Brusseau, 2023). The low surface area and limited adsorption sites of the sediments used in this work explain the negligible adsorption of short-chain PFAS (Figure Appx. 2, Figure 4), consistent with their high aqueous mobility (Luft, 2022; Dong, 2024). Competitive interactions among the six PFAS further limited short-chain sorption (Li, 2019). While both sediments and weathered MPs carry a net negative surface charge, the introduction of oxidized functional groups and mineral-associated features on weathered MPs likely enables additional interaction pathways not available on pristine polyethylene surfaces (Li, 2018; Salawu, 2024). These include electrostatic interactions, Ca^{2+} bridging, and associations with organic and mineral constituents attached to the MPs surface, which together may explain the enhanced adsorption of both PFOS and PFNA on weathered MPs. Overall,

compound-specific behavior was observed, with PFOS exhibiting stronger adsorption consistent with its sulfonate head group and higher hydrophobicity, whereas PFNA adsorption varied more strongly with changes in microplastic surface chemistry, particularly the introduction of oxygen-containing functional groups.

Greater hysteresis in PMPS suggests that, even as aqueous PFAS concentrations decline, hydrophobic partitioning into the polymer matrix remains more favorable than desorption to the aqueous phase. This, combined with diffusion limitations within the polyethylene structure, restricts PFAS release and promotes apparent irreversibility. Although equilibrium partitioning of PFAS into polyethylene may be limited, restricted access to near-surface amorphous polymer regions can result in slow back-diffusion during desorption (Ahmad, 2024; Salawu, 2024). In contrast, weathering introduces oxidized functional groups and mineral coatings that favor surface-associated, reversible sorption pathways. Overall, PFAS adsorption appears to arise from multiple interacting mechanisms, including hydrophobic interactions, electrostatic effects, cation bridging, and associations with mineral and organic constituents, with the relative importance of these processes varying between pristine and weathered MPs surfaces.

2.6 *Conclusions*

This study demonstrates that environmentally relevant weathering of polyethylene microplastics fundamentally alters PFAS sorption behavior by increasing surface heterogeneity, enhancing adsorption capacity, and reducing sorption hysteresis relative to pristine MPs. These findings raise important questions regarding the role of microplastic aging in controlling PFAS mobility rather than long-term sequestration in sediments. In particular, the greater reversible sorption observed for weathered MPs

suggests that weathered MPs may facilitate PFAS transport under dynamic environmental conditions, whereas pristine MPs may promote kinetically constrained retention and delayed release, and the hydrophobic forces are greater than diffusive forces. Notably, even at low concentrations relative to sediment mass, MPs substantially altered PFAS adsorption and desorption dynamics, indicating that microplastics can act as active modifiers of PFAS fate rather than passive co-contaminants. Future research should therefore focus on quantifying PFAS transport and release from microplastics under environmentally relevant flow, ionic strength, and aging conditions, and on evaluating how ongoing eco-corona development influences PFAS bioavailability in groundwater–sediment systems.

References

Ahmad A, Tian K, Tanyu B, Foster GD. 2024. Sorption and diffusion of per-polyfluoroalkyl substances (PFAS) in high-density polyethylene geomembranes. Waste Management 174:15-23 https://doi.org/10.1016/j.wasman.2023.11.015.

Bellasi A, Binda G, Pozzi A, Galafassi S, Volta P, Bettinetti R. 2020. Microplastic contamination in freshwater environments: a review, focusing on interactions with sediments and benthic organisms. Environments 7:30 https://doi.org/10.3390/environments7040030.

Brusseau ML. 2023. Influence of chain length on field-measured distributions of PFAS in soil and soil porewater. Journal of Hazardous Materials Letters 4 100080: https://doi.org/10.1016/j.hazl.2023.100080.

Buck RC, Franklin J, Berger U, Conder JM, Cousins IT, De Voogt P, Jensen AA, Kannan K, Mabury SA, van Leeuwen SP. 2011. Perfluoroalkyl and polyfluoroalkyl substances in the environment: terminology, classification, and origins. Integrated Environmental Assessment and Management 7:513-541 https://doi.org/10.1002/ieam.258.

Charles J. 2009. Qualitative analysis of high density polyethylene using FTIR spectroscopy. Asian Journal of Chemistry 21:4477

Cheng Y, Mai L, Lu X, Li Z, Guo Y, Chen D, Wang F. 2021. Occurrence and abundance of poly-and perfluoroalkyl substances (PFASs) on microplastics (MPs) in Pearl River Estuary (PRE) region: Spatial and temporal variations. Environmental Pollution 281:117025 https://doi.org/10.1016/j.envpol.2021.117025.

Coates J. 2000. Interpretation of infrared spectra, a practical approach. Encyclopedia of Analytical Chemistry 12:10815-10837 https://doi.org/10.1002/9780470027318.a5606.

Dong Q, Min X, Zhao Y, Wang Y. 2024. Adsorption of per-and polyfluoroalkyl substances (PFAS) by ionic liquid-modified clays: effect of clay composition and PFAS structure. Journal of Colloid and Interface Science 654:925-934 https://doi.org/10.1016/j.jcis.2023.10.112.

Enyoh CE, Wang Q, Wang W, Chowdhury T, Rabin MH, Islam R, Yue G, Yichun L, Xiao K. 2024. Sorption of per-and polyfluoroalkyl substances (PFAS) using polyethylene (PE) microplastics as adsorbent: grand canonical Monte Carlo and molecular dynamics (GCMC-MD) studies. International Journal of Environmental Analytical Chemistry 104:2719-2735 https://doi.org/10.1080/03067319.2022.2070016.

Fu L, Li J, Wang G, Luan Y, Dai W. 2021. Adsorption behavior of organic pollutants on microplastics. Ecotoxicology and Environmental Safety 217:112207 https://doi.org/10.1016/j.ecoenv.2021.112207.

Guerranti C, Martellini T, Perra G, Scopetani C, Cincinelli A. 2019. Microplastics in cosmetics: environmental issues and needs for global bans. Environmental Toxicology and Pharmacology 68:75-79 https://doi.org/10.1016/j.etap.2019.03.007.

Gulmine J, Janissek P, Heise H, Akcelrud L. 2003. Degradation profile of polyethylene after artificial accelerated weathering. Polymer Degradation and Stability 79:385-397 https://doi.org/10.1016/S0141-3910(02)00338-5.

Higgins CP, Luthy RG. 2006. Sorption of perfluorinated surfactants on sediments. Environmental Science & Technology 40:7251-7256 https://doi.org/10.1021/es061000n.
Hoang TC, Brausch JM, Cichra MF, Phlips EJ, Van Genderen E, Rand GM. 2021. Effects of zinc in an outdoor freshwater microcosm system. Environmental Toxicology and Chemistry 40:2051-2070 https://doi.org/10.1002/etc.5050.
Kuwabara A, Kuroda S-i, Kubota H. 2007. Polymer surface treatment by atmospheric pressure low temperature surface discharge plasma: its characteristics and comparison with low pressure oxygen plasma treatment. Plasma Science and Technology 9:181 https://doi.org/10.1088/1009-0630/9/2/14.
Lenka SP, Kah M, Padhye LP. 2021. A review of the occurrence, transformation, and removal of poly-and perfluoroalkyl substances (PFAS) in wastewater treatment plants. Water Research 199:117187 https://doi.org/10.1016/j.watres.2021.117187.
Li F, Fang X, Zhou Z, Liao X, Zou J, Yuan B, Sun W. 2019. Adsorption of perfluorinated acids onto soils: kinetics, isotherms, and influences of soil properties. Science of The Total Environment 649:504-514 https://doi.org/10.1016/j.scitotenv.2018.08.209.
Li Y, Oliver DP, Kookana RS. 2018. A critical analysis of published data to discern the role of soil and sediment properties in determining sorption of per and polyfluoroalkyl substances (PFASs). Science of the Total Environment 628:110-120 https://doi.org/10.1016/j.scitotenv.2018.01.167.
Luft CM, Schutt TC, Shukla MK. 2022. Properties and mechanisms for PFAS adsorption to aqueous clay and humic soil components. Environmental Science & Technology 56:10053-10061 https://doi.org/10.1021/acs.est.2c00499.
Luo Y, Gibson CT, Chuah C, Tang Y, Naidu R, Fang C. 2022. Raman imaging for the identification of Teflon microplastics and nanoplastics released from non-stick cookware. Science of The Total Environment 851:158293 https://doi.org/10.1016/j.scitotenv.2022.158293.
Lyu X, Xiao F, Shen C, Chen J, Park CM, Sun Y, Flury M, Wang D. 2022. Per-and polyfluoroalkyl substances (PFAS) in subsurface environments: occurrence, fate, transport, and research prospect. Reviews of Geophysics 60:e2021RG000765 https://doi.org/10.1029/2021RG000765.
Molaro J, Peterson C, Hoang T. 2023. Microplastics can alter phytoplankton community structure in aquatic systems. Preprint available at SSRN 4548560 https://doi.org/10.2139/ssrn.4548560.
National Oceanic and Atmospheric Administration. 2024. What are microplastics? Available from: https://oceanservice.noaa.gov/facts/microplastics.html
Nguyen TMH, Bräunig J, Thompson K, Thompson J, Kabiri S, Navarro DA, Kookana RS, Grimison C, Barnes CM, Higgins CP. 2020. Influences of chemical properties, soil properties, and solution pH on soil–water partitioning coefficients of per-and polyfluoroalkyl substances (PFASs). Environmental Science & Technology 54:15883-15892 https://doi.org/10.1021/acs.est.0c05705.
Posit team. 2025. RStudio: integrated development environment for R. 2025.5.1.513 ed. Posit Software, PBC, Boston, MA.

Quinn B, Murphy F, Ewins C. 2017. Validation of density separation for the rapid recovery of microplastics from sediment. Analytical Methods 9:1491-1498 https://doi.org/10.1039/C6AY02542K.
R Core Team. 2025. R: a language and environment for statistical computing. R Foundation for Statistical Computing.
Rafa N, Ahmed B, Zohora F, Bakya J, Ahmed S, Ahmed SF, Mofijur M, Chowdhury AA, Almomani F. 2024. Microplastics as carriers of toxic pollutants: source, transport, and toxicological effects. Environmental Pollution 343:123190 https://doi.org/10.1016/j.envpol.2023.123190.
Reif D, Zoboli O, Wolfram G, Amann A, Saracevic E, Riedler P, Hainz R, Hintermaier S, Krampe J, Zessner M. 2022. Pollutant source or sink? Adsorption and mobilization of PFOS and PFOA from sediments in a large shallow lake with extended reed belt. Journal of Environmental Management 320:115871 https://doi.org/10.1016/j.jenvman.2022.115871.
Rotger J, Pireaux J-J, Caudano R, Thorne N, Dunlop H, Benmalek M. 1995. Deposition of silicon oxide onto polyethylene and polyethyleneterephthalate: an x-ray photoelectron spectroscopy interfacial study. Journal of Vacuum Science & Technology A: Vacuum, Surfaces, and Films 13:260-267 https://doi.org/10.1116/1.579408.
Salawu OA, Olivares CI, Adeleye AS. 2024. Adsorption of PFAS onto secondary microplastics: a mechanistic study. Journal of Hazardous Materials 470:134185 https://doi.org/10.1016/j.jhazmat.2024.134185.
Schellenberger S, Jonsson C, Mellin P, Levenstam OA, Liagkouridis I, Ribbenstedt A, Hanning A-C, Schultes L, Plassmann MM, Persson C. 2019. Release of side-chain fluorinated polymer-containing microplastic fibers from functional textiles during washing and first estimates of perfluoroalkyl acid emissions. Environmental Science & Technology 53:14329-14338 https://doi.org/10.1021/acs.est.9b04165.
Shi Y, Almuhtaram H, Andrews RC. 2023a. Adsorption of per-and polyfluoroalkyl substances (PFAS) and microcystins by virgin and weathered microplastics in freshwater matrices. Polymers 15:3676 https://doi.org/10.3390/polym15183676.
Shi Y, Shi L, Huang H, Ye K, Yang L, Wang Z, Sun Y, Li D, Shi Y, Xiao L, Gao S. 2024. Analysis of aged microplastics: a review. Environmental Chemistry Letters 22:1861-1888 https://doi.org/10.1007/s10311-024-01731-5.
Shi Y, Zheng L, Huang H, Tian Y-C, Gong Z, Liu P, Wu X, Li W-T, Gao S. 2023b. Formation of nano- and microplastics and dissolved chemicals during photodegradation of polyester base fabrics with polyurethane coating. Environmental Science & Technology 57:1894-1906 https://doi.org/10.1021/acs.est.2c05063.
Smith BC. 2018. *Infrared Spectral Interpretation: A Systematic Approach*, 1st ed. CRC Press.
Sun J, Xiang H, Jiang X, Wang X, Luo X, Fu J, Fan J. 2024. Effects of polyamide microplastics on the adsorption of perfluoroalkyl substances in soil. Journal of Hazardous Materials Advances 13:100391 https://doi.org/10.1016/j.hazadv.2023.100391.
Sunderland EM, Hu XC, Dassuncao C, Tokranov AK, Wagner CC, Allen JG. 2019. A review of the pathways of human exposure to poly- and perfluoroalkyl substances (PFASs) and present understanding of health effects. Exposure Science &

Environmental Epidemiology 29:131-147 https://doi.org/10.1038/s41370-018-0094-1.
Wang C, Liu Y, Chen WQ, Zhu B, Qu S, Xu M. 2021. Critical review of global plastics stock and flow data. Journal of Industrial Ecology 25:1300-1317 https://doi.org/10.1111/jiec.13125.
Wickham H. 2016. *ggplot2: Elegant Graphics for Data Analysis*. Springer-Verlag New York.
Xu W, Chen W-Q, Jiang D, Zhang C, Ma Z, Ren Y, Shi L. 2020. Evolution of the global polyethylene waste trade system. Ecosystem Health and Sustainability 6:1756925 https://doi.org/10.1080/20964129.2020.1756925.
Yao S, Li X, Wang T, Jiang X, Song Y, Arp HPH. 2023. Soil metabolome impacts the formation of the eco-corona and adsorption processes on microplastic surfaces. Environmental Science & Technology 57:8139-8148 https://doi.org/10.1021/acs.est.3c01877.
Yashwanth A, Huang R, Iepure M, Mu M, Zhou W, Kunadu A, Carignan C, Yegin Y, Cho D, Oh JK. 2025. Food packaging solutions in the post-per-and polyfluoroalkyl substances (PFAS) and microplastics era: a review of functions, materials, and bio-based alternatives. Comprehensive Reviews in Food Science and Food Safety 24:e70079 https://doi.org/10.1111/1541-4337.70079.

Figures and Tables

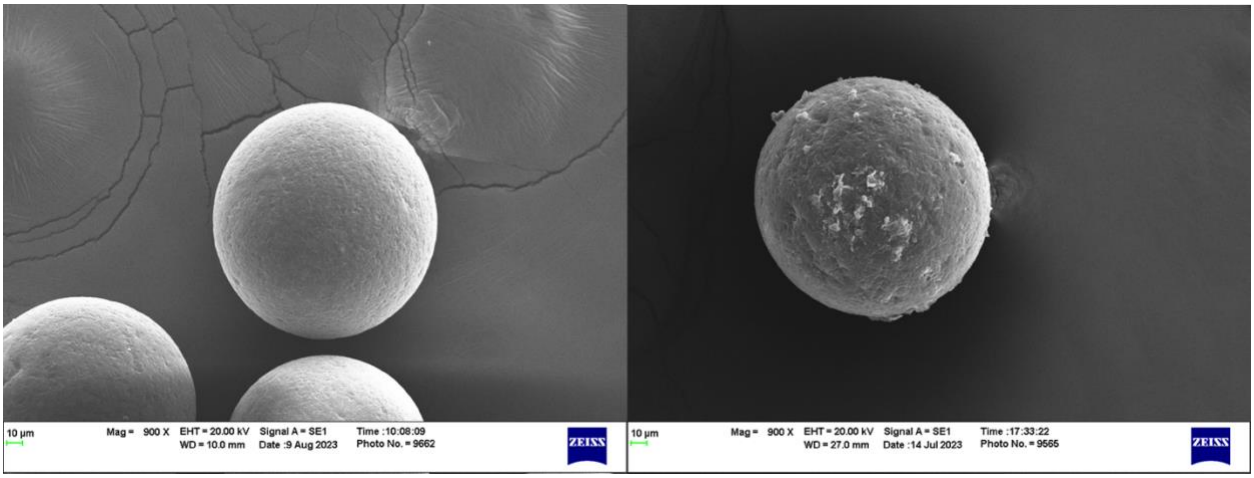

Figure 1 SEM images of pristine and environmentally weathered polyethylene microbeads. Scanning electron microscopy (SEM) images of a pristine polyethylene (PE) microbead (left) and a PE microbead isolated from sediment following 15 months of incubation.

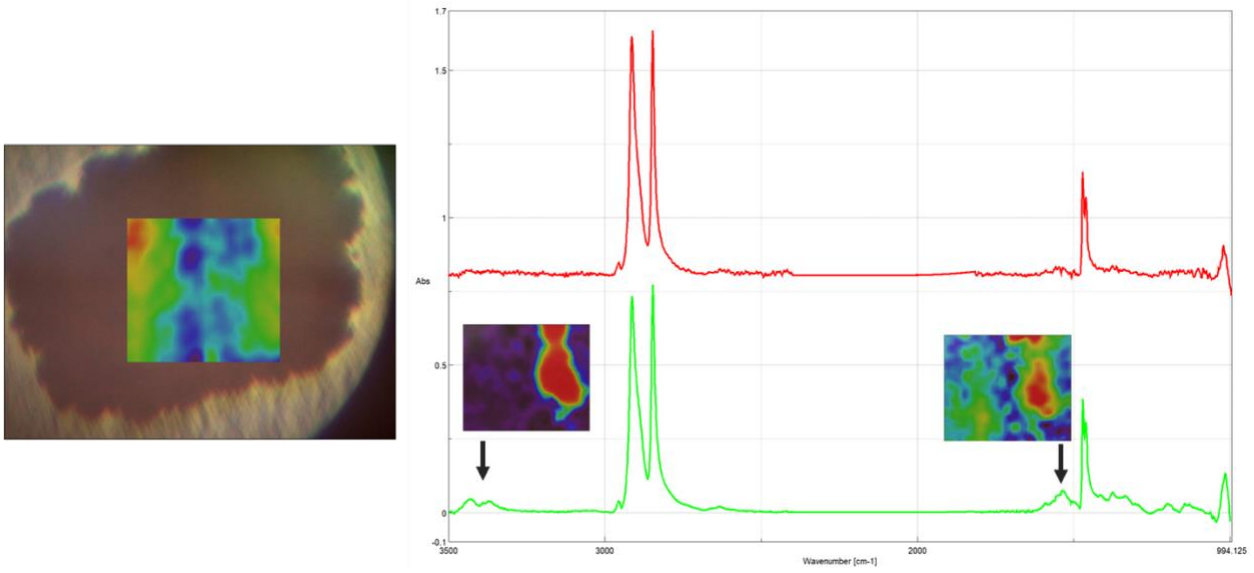

Figure 2 µFTIR chemical imaging of polyethylene (PE) microbeads overlaid on optical images (left). Spectra extracted from regions of interest (ROI) with IR signatures consistent with pristine PE are shown in red (top), while spectra from ROIs exhibiting oxygen-containing functional groups are shown in green (bottom).

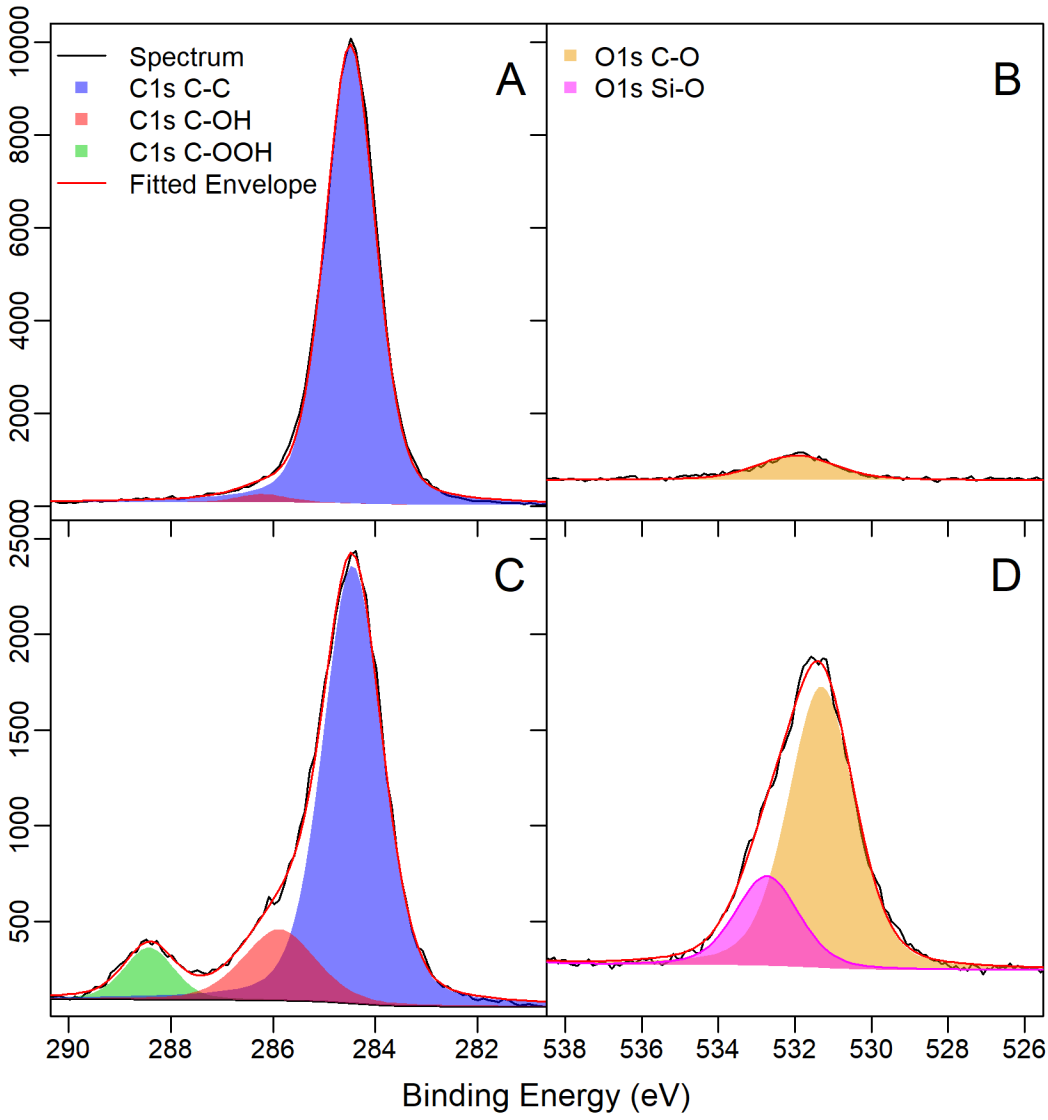

Figure 3 XPS core-level spectra (C1s and O1s) of pristine and weathered microplastics. X-ray photoelectron spectroscopy (XPS), C1s (A, C) and O1s (B, D) core-level spectra and peak deconvolution for pristine MPs (A, B) and weathered MPs (C, D).

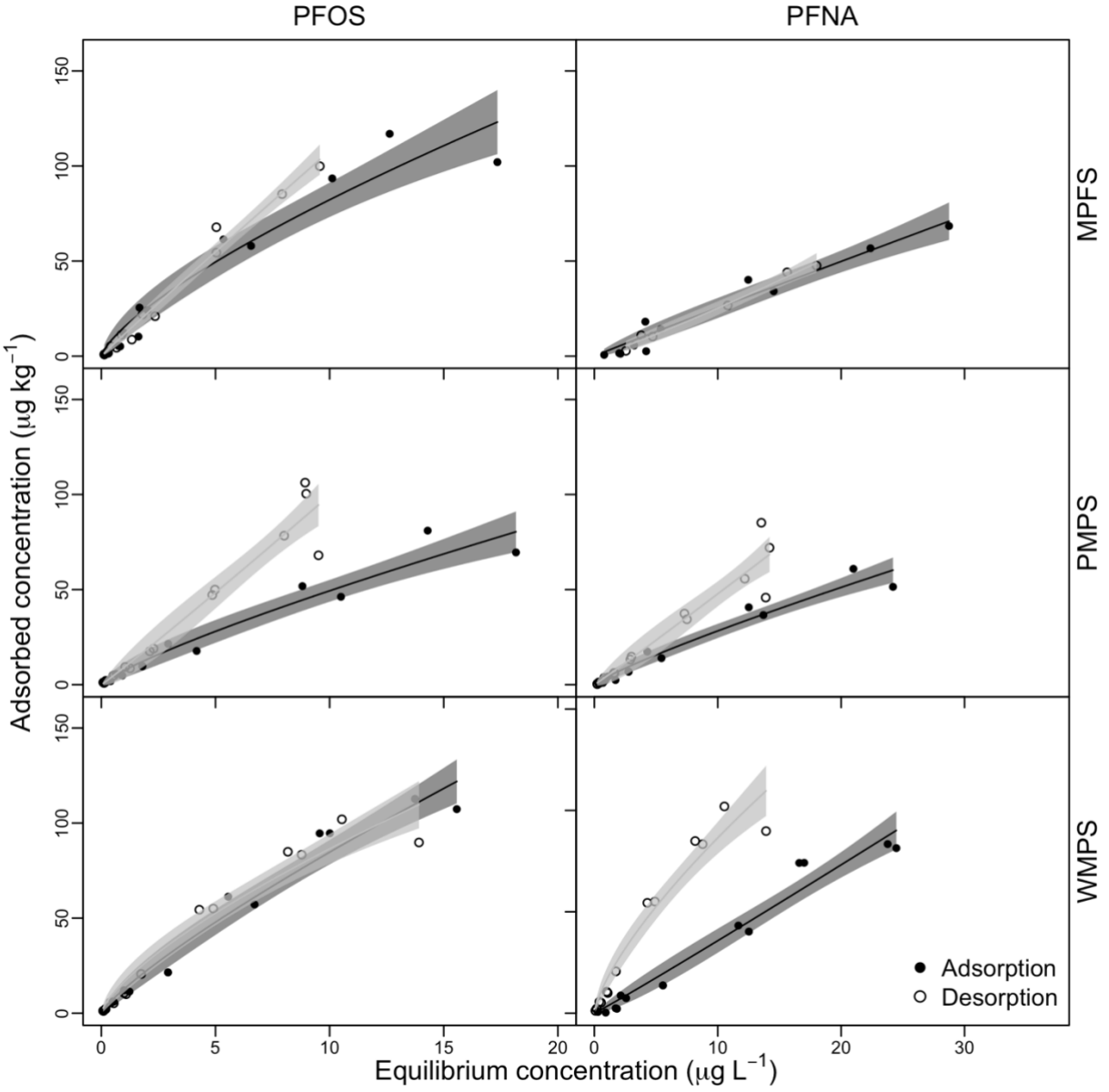

Figure 4 Adsorption–desorption isotherms of pfos and pfna on microplastic-influenced sediments. Adsorption (closed circles) and desorption (open circles) isotherms of PFOS and PFNA on MPs free sediments (MPFS), sediment containing pristine MPs (PMPS), and sediment.

Table 1 List of PFAS compounds used in this study and their corresponding isotopically labeled standards.

PFAS Compound (CF chain length)	Formula	Molar Mass g mol-1	Structure	Internal Standard
PFNA (8)	C9F17O2	462.963	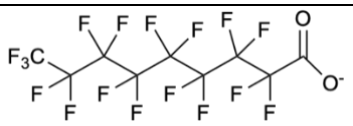	13C8-PFNA
PFOS (8)	C8F17SO3	498.930	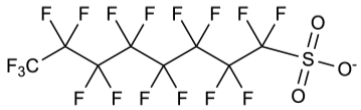	13C8-PFOS
PFOA (7)	C8F15O2	412.966	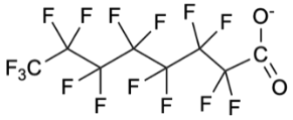	13C7-PFOA
PFHpA (6)	C7F13O2	362.970	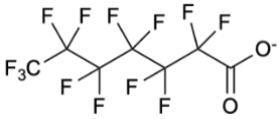	13C6- PFHpA
PFHxS (6)	C6F13SO3	398.937	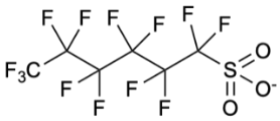	13C6- PFHxS
PFBS (4)	C4F9SO3	298.943	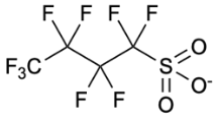	13C4-PFBS

Table 2 Freundlich fitting parameters for PFOS and PFNA adsorption and desorption isotherms on MPs free sediments (MPFS), sediments containing pristine MPs (PMPS), and sediments containing weathered MPs (WMPS). Values represent the parameter estimates ± standard. Superscript letters denote statistically homogeneous groups based on pairwise comparisons ($p < 0.05$), such that treatments sharing at least one letter are not significantly different, whereas treatments with no letters in common are significantly different.

Adsorbent	Process	Parameter	PFOS	PFNA
MPFS	Adsorption	K_f *	15.22 ± 2.98ab	2.68 ± 0.87a
MPFS	Adsorption	n	0.73 ± 0.08	0.98 ± 0.11
MPFS	Adsorption	r^2	0.95	0.96
MPFS	Desorption	K_f *	11.38 ± 1.46b	1.86 ± 0.50a
MPFS	Desorption	n	0.98 ± 0.06	1.13 ± 0.10
MPFS	Desorption	r^2	0.98	0.99
PMPS	Adsorption	K_f *	7.52 ± 1.81a	3.94 ± 0.92b
PMPS	Adsorption	n	0.82 ± 0.09	0.86 ± 0.08
PMPS	Adsorption	r^2	0.95	0.96
PMPS	Desorption	K_f *	9.07 ± 2.68a	4.46 ± 1.85a
PMPS	Desorption	n	1.04 ± 0.14	1.03 ± 0.17
PMPS	Desorption	r^2	0.94	0.92
WMPS	Adsorption	K_f *	12.74 ± 2.22b	3.31 ± 1.02b
WMPS	Adsorption	n	0.82 ± 0.07	1.03 ± 0.10
WMPS	Adsorption	r^2	0.97	0.96
WMPS	Desorption	K_f *	16.53 ± 2.58a	7.44 ± 1.37a
WMPS	Desorption	n	0.72 ± 0.07	0.85 ± 0.07
WMPS	Desorption	r^2	0.96	0.97

*$(\mu g\ kg^{-1})(\ \mu g\ L^{-1})^{-n}$

3 Organic Amendment Dissolved Organic Matter Molecular Interactions with Perfluoroalkyl Substances

3.1 Abstract

Dissolved organic matter (DOM) plays a critical role in controlling the environmental behavior of per- and polyfluoroalkyl substances (PFAS), yet the mechanisms governing PFAS–DOM interactions under environmentally relevant conditions remain poorly constrained. In this study, fluorescence spectroscopy was used to evaluate how DOM fluorescence responds to interactions with three PFAS (PFOS, PFNA, and PFBS) across varying pH and concentration conditions in DOM derived from biosolids, cow manure, and Pahokee muck. Parallel factor analysis (PARAFAC), fluorescence indices, ultraviolet–visible absorbance, and Fourier-transform infrared (FTIR) spectroscopy were applied to characterize compositional and molecular-level changes.

PARAFAC resolved four components, including two humic-like and two protein-like fluorophores, highlighting distinct compositional differences among DOM sources. Bulk fluorescence indices exhibited limited sensitivity to PFAS; however, subtle decreases in humification index (HIX) were observed alongside increases in protein-like fluorophore intensity, indicating a shift in the relative contribution of DOM components. This inverse relationship suggests preferential interactions between PFAS and labile, protein-like DOM fractions. Mechanistically, these responses are consistent with non-covalent PFAS–DOM complexation, driven by hydrophobic interactions between the fluorinated PFAS tail and organic moieties, as well as electrostatic associations with non-

or positive charged functional groups such as amines. These interactions likely modify the local fluorophore microenvironment by restricting molecular motion and reducing solvent-mediated quenching, enhancing fluorescence emission without substantially altering bulk DOM structure.

Type III ANOVA demonstrated that DOM composition, PFAS identity, and pH were the dominant drivers of fluorescence variability ($p < 0.001$), with strong interaction effects indicating that PFAS–DOM behavior is highly dependent on environmental conditions. PFAS concentration was also significant ($p < 0.001$), although its effect was comparatively small. Among PFAS, PFOS exhibited the strongest influence on fluorescence behavior, supported by FTIR evidence showing enhanced sulfonate- and C–F-related bands (~1300–1000 cm^{-1}), indicating association with DOM rather than remaining freely dissolved.

Overall, these findings demonstrate that PFAS alter DOM fluorescence primarily through component-specific interactions rather than compositional changes. The inverse relationship between HIX and protein-like fluorescence highlights the importance of fluorophore-level analysis for resolving PFAS–DOM interactions and suggests that DOM composition and solution chemistry exert a stronger control on PFAS behavior than concentration alone, with important implications for PFAS mobility and transport in natural systems. These findings indicate that PFAS can alter DOM fluorescence even at low, environmentally relevant concentrations, reflecting measurable molecular-scale interactions.

3.2 Introduction

Per- and polyfluoroalkyl substances (PFAS) are a class of over 4,000 synthetic chemicals (Panieri et al., 2022) widely used for their surfactant properties. Their applications include non-stick cookware, waterproof textiles, food packaging, and aqueous film-forming foams (Evich et al., 2022). These properties arise from their unique molecular structure, consisting of a hydrophobic fluorinated carbon chain and a hydrophilic functional head group (Buck et al., 2011). PFAS are commonly categorized by chain length, with short-chain compounds containing fewer than six fluorinated carbons and long-chain compounds containing seven or more (Sunderland et al., 2019). PFAS behavior in the environment is governed by both chain length and functional group. Perfluoroalkyl sulfonic acids (PFSAs) generally exhibit greater adsorption capacity than perfluoroalkyl carboxylic acids (PFCAs), while short-chain PFAS preferentially partition to the aqueous phase, and long-chain PFAS exhibit stronger association with solid phases.

Organic amendments are generally applied to soils to increase nutrient availability and replenish organic carbon. Unlike industrial fertilizers, these materials supply both macro- and micronutrients, including nitrogen, phosphorus, and potassium, while contributing substantial amounts of dissolved organic matter (DOM). Although cow manure and biosolids both originate from organic waste streams, their DOM represents fundamentally different stages of organic matter processing. Fresh cow manure contains predominantly microbially derived, labile DOM, whereas biosolids undergo extensive biological and chemical treatment during wastewater processing, producing more humified and chemically resistant organic matter. These compositional differences are expected to influence the reactivity of DOM with contaminants.

While organic amendments improve soil fertility, they can also act as vectors for emerging contaminants, including PFAS (Johnson, 2022; Masoner et al., 2025; Thompson et al., 2023). Biosolid-based soil amendments have been shown to contain substantially higher concentrations of perfluoroalkyl acids (PFAAs) than non-biosolid composts, with reported concentrations ranging from 9-199 μg kg^{-1} compared with <20 μg kg^{-1} in plant-derived materials (Lazcano et al., 2020). DOM can influence PFAS behavior through several mechanisms. Positively charged functional groups within DOM may electrostatically attract anionic PFAS headgroups (Bolan et al., 2011), while hydrophobic domains facilitate partitioning of the fluorinated carbon tail, particularly for longer-chain PFAS. These interactions may enhance PFAS adsorption by creating additional binding domains within soil matrices or reduce adsorption through competitive sorption for mineral surface sites.

The distribution coefficient (Kd) has been widely used to characterize PFAS interactions with dissolved organic matter (DOM), with variability in the order of magnitude underscoring the importance of DOM chemistry in controlling PFAS behavior (Carmosini & Lee, 2008; Higgins & Luthy, 2006; Xia et al., 2015). Recent work demonstrates that dissolved-phase DOM enhances the mobility of PFCAs through complexation and hydrogen bonding, while exerting a comparatively limited influence in sediment phases due to reduced reactivity and mobility (Xie et al., 2025). Although perfluoroalkyl sulfonic acids (PFSAs) generally exhibit stronger adsorption to solid phases than PFCAs, PFCAs have been shown to associate more readily with DOM in the aqueous phase, promoting their solubility and transport. Importantly, DOM effects are highly source dependent. For example, the addition of 100 mg C L^{-1} DOM derived from biosolids or animal wastes

increased PFOS adsorption to soils by up to ~90%, whereas DOM from plant-derived sources decreased adsorption by up to ~40% (Olshansky et al., 2025). These contrasting responses indicate that DOM composition and reactivity play a critical role in governing PFAS–DOM interactions. Molecular characteristics further influence these processes, as smaller DOM molecules may compete more effectively for adsorption sites than larger macromolecular fractions. Consequently, sediment–water Kd often increases with total organic carbon content, yet the presence of mobile DOM can simultaneously enhance PFAS solubility and reduce overall retention in soil systems (Qi et al., 2022).

Because DOM molecular composition governs polarity, aromaticity, and hydrophobicity, changes in DOM fluorescence provide a sensitive indicator of PFAS–DOM interactions. Specifically, PFAS–DOM interactions were directly assessed through changes in fluorophore intensity (i.e., fluorescence enhancing/quenching behavior) and supported by shifts in functional group signatures observed using Fourier-transform infrared (FTIR) spectroscopy. Variations in fluorescence intensity across humic- and protein-like regions were used to evaluate relative changes in DOM fluorophore environments upon PFAS addition, while FTIR peak shifts were used to identify potential interactions involving carboxyl, aromatic, and oxygen-containing functional groups. Together, these complementary approaches provide insight into the non-covalent interactions governing PFAS–DOM association, including hydrophobic partitioning and electrostatic interactions.

Despite growing recognition that DOM source controls PFAS behavior, the mechanisms linking DOM composition to PFAS interactions remain poorly understood, particularly for DOM derived from common agricultural amendments. Differences in

fluorescence characteristics and FTIR responses among amendment-derived DOM may therefore provide critical insight into the molecular features governing PFAS–DOM interactions. This study aims to address these knowledge gaps by directly evaluating PFAS–DOM fluorescence interactions in agricultural systems amended with organic amendments. It is hypothesized that PFAS–DOM interactions will be enhanced under lower pH conditions and will vary among DOM sources as a function of chemical composition. Specifically, PFAS are expected to influence DOM at the fluorophore level, with protein-like components exhibiting measurable changes in fluorescence intensity and corresponding shifts in humification index (HIX), reflecting composition-dependent interactions.

3.3 Materials and Methods

3.3.1 Materials

Organic amendment sources are listed in Table 3. Fresh cow manure was air-dried for 72 h following collection to preserve labile organic components. Biosolids were oven-dried at 65 °C for 48 h to remove excess moisture associated with wastewater treatment residuals. All samples were subsequently stored in amber bottles prior to extraction. The drying temperatures used were sufficiently low to minimize thermal alteration of DOM composition.

Perfluoroalkyl substances (Table 4), were purchased from Matrix Scientific (Matrix Scientific, Columbia, SC). Ultrapure water (18.2 MΩ) was obtained from a Smart2Pure system (Thermo Scientific, Waltham, WI). Sodium chloride used as a background electrolyte was purchased from VWR (VWR International, Radnor, PA).

3.3.2 Dissolved Organic Matter Extraction

DOM was extracted from solid organic matter sources using an aqueous extraction method. Four grams of organic material were mixed with 20 mL of ultrapure water (18 MΩ cm) in 40 mL high-density polyethylene tube. Tubes were vortexed, then shaken for 16 h at 200 rpm on a reciprocal shaker in the dark to minimize photochemical alteration. Then tubes were centrifuged at 14,000 RPM (13,000 *g*) for 10 min at 25°C using a refrigerated centrifuge (International Equipment Corporation, Needham Heights, MA). The supernatant was vacuum filtered through 0.45 µm Supor® PES membrane filters (Pall Corporation, Port Washington, NY, USA). Prior to filtration, glass filtration assemblies were sequentially rinsed with deionized water, 30% ethanol, 100% ethanol, and deionized water to remove organic residues of varying polarity. Filters were pre-rinsed with 250-500 mL of deionized water before use. Filtrates were collected in pre-combusted amber glass bottles. Solution pH was measured using a calibrated pH electrode and adjusted as necessary using 0.1 M HCl or 0.1 M NaOH. Amber bottles were combusted at 600°C for 4 h prior to use.

Homoionic DOM solutions were produced using dialysis to reduce variability associated with mixed electrolyte backgrounds. Dialysis tubing was rinsed repeatedly with deionized water prior to use. DOM solutions were transferred into dialysis tubing and sealed with polyethylene clips. Dialysis was conducted against NaCl electrolytes. Samples were dialyzed against a 5 mM NaCl electrolyte solution under gentle stirring, with the solution exchanged four times at 2 h intervals. Following dialysis, DOM solutions were recovered and stored in amber glass bottles until analysis.

3.3.3 PFAS-DOM sample preparation

PFAS-DOM interaction solutions were prepared using dialyzed DOM, background electrolyte, and individual PFAS standards. To minimize fluorescence inner-filter effect, DOM solutions were diluted to obtain UV absorbance at 250 nm below 0.10 ± 0.01 (au). The required volume of DOM stock added to each sample was calculated from this absorbance constraint. This determines the DOM volume added to the sample. 15 mL polypropylene centrifuge tubes were labeled according to PFAS concentration and replicate number. Sixteen tubes contained PFAS-DOM samples, while four control treatments were included: (i) PFAS with background electrolyte only, (ii) DOM with background electrolyte only, (iii) background electrolyte only, and (iv) PFAS only. PFAS standards, electrolyte solutions, and DOM aliquots were added gravimetrically, maintaining a mass error ≤ ±0.005 g. Prepared samples were stored in the dark until UV-Vis and fluorescence analyses.

PFAS was added at concentrations ranging from 1 – 5000 μg L^{-1}. For each sample, the calculated volume of DOM (based on UV–Vis absorbance at 250 nm) was added first, followed by PFAS standards, and the remaining volume was adjusted with 5 mM NaCl to a final volume of 15 mL. Prepared samples were stored in the dark until UV–Vis and fluorescence analyses.

3.3.4 DOM analysis

Ultraviolet-visible (UV-Vis) spectroscopy was used to determine appropriate DOM dilution factors before fluorescence analysis and to minimize inner-filter effects by ensuring absorbance values were minimized. Absorbance spectra were collected using a JASCO V-750 UV-Vis spectrophotometer (JASCO Inc., Easton, MD) following a 30 min

warm-up period. Quartz cuvettes were cleaned with ultrapure water and ethanol before analysis. Ultrapure water was used as both the reference and blank. DOM samples were introduced into the cuvette following a double rinse with the sample solution to minimize carryover. Absorbance spectra were visually inspected for baseline irregularities or excessive noise.

Fluorescence excitation-emission matrix (EEM) spectroscopy was conducted to characterize DOM fluorescence and assess quenching effects following PFAS addition. Measurements were performed using a JASCO FP-8500 spectrofluorometer (JASCO Inc., Easton, MD) after a 30 min warm-up period. Quartz cuvettes were cleaned with ethanol and ultrapure water before use. Ultrapure water blanks were collected before sample analysis and evaluated to ensure negligible background fluorescence. EEMs were acquired using the instrument's three-dimensional spectral acquisition mode. Blank spectra were visually inspected in color-scale view to confirm the absence of background signal before sample analysis.

Fourier transform infrared (FTIR) spectroscopy was used to characterize biosolid DOM composition and changes in bands associated with DOM or PFAS functional groups, due to PFAS-DOM interactions. After completion of the PFAS-DOM UV-Vis and EEM experiments, approximately 8 mL of solution remained in each reaction tube. These solutions were freeze-dried, homogenized, and mixed thoroughly with 200 mg of pre-dried potassium bromide (KBr). The DOM-PFAS-KBr mixtures were pressed into transparent pellets using a hydraulic press (International Crystal Laboratories, Erie, NJ).

BS-PFOS analysis was performed to observe the impact PFOS has on DOM functional groups. Controls of 5 mg L^{-1} PFOS were used in a final volume of 10 mL and 5

mL to observe the impact of volume on sublimation during freeze drying in replicates of 5. Five samples of DOM at a concentration of 2.0 mg L^{-1} were prepared to ensure replicability of the method. Finally, samples were prepared with a constant PFOS concentration of 5.0 mg L^{-1} in a final volume of 7.5 mL with BS-DOM concentrations ranging from 0.35 to 1.2 mg L^{-1} to determine the impact of PFOS on increasing concentrations of BS-DOM.

FTIR spectra were collected using an FTIR-6800 spectrometer equipped with a deuterated triglycine sulfate detector (JASCO Inc., Easton, MD) over a spectral range of 600-4000 cm^{-1} with a spectral resolution of 4 cm^{-1} and 64 co-added scans per sample. Background spectra were collected using a pure KBr pellet and subtracted automatically before sample analysis. All spectra were visually inspected for baseline stability and spectral artifacts before interpretation.

3.3.5 *Data Processing and Analysis*

All data processing, visualization, and statistical analyses were performed in RStudio using R (Posit team, 2026; R Core Team, 2026). Data handling and restructuring were conducted using the *dplyr* and *tidyr* packages to standardize sample identifiers, treatments, and replicates across datasets (Wickham, 2026a; Wickham, 2026b).

Fluorescence excitation-emission matrix (EEM) data were processed using the *staRdom* package (Pucher, 2019). Pre-processing steps included Raman scatter removal, inner-filter effect correction, interpolation to a common excitation-emission grid, and subtraction of ultrapure water blanks Rayleigh and Raman scatter regions were removed prior to PARAFAC modeling and excluded from analysis to avoid interference from non-fluorescent scattering signals. Processed EEMs were decomposed to the

underlying fluorophore using both PARAFAC modeling Model robustness was evaluated using split-half analysis, and component similarity was assessed using Tucker congruence coefficients (TCC) to confirm model stability.

Using fluorescence EEMs and absorbance spectra, fluorescence indices were calculated to characterize DOM composition. The fluorescence index (FI; Em470/Em520 at Ex370) distinguishes microbial (≈1.7–2.0) from terrestrial (≈1.2–1.5) DOM sources. The E2/E3 ratio (A250/A365) was used as a proxy for DOM molecular weight and aromaticity, with lower values indicating higher molecular weight and greater aromatic character. The humification index (HIX), calculated as the ratio of integrated emission intensity from 435–480 nm to 300–345 nm at Ex254, reflects the degree of DOM humification and aromaticity. Additionally, fluorescence intensity responses were interpreted in terms of general quenching or enhancement behavior for each PARAFAC component. While fluorescence quenching can arise from dynamic (collisional) or static (complex formation) processes, the heterogeneous nature of DOM precludes strict differentiation; therefore, trends are interpreted qualitatively.

Bulk fluorescence indices (FI, HIX, and E2/E3) were analyzed using linear models with DOM source, PFAS species, and pH as fixed effects and $\log_{10}$-transformed concentration [$\log_{10}$(concentration + 1)] as a continuous predictor. Residual normality and homogeneity of variance were assessed using diagnostic plots, Shapiro–Wilk tests, and Levene's tests for homogeneity of variance. FI was analyzed on the original scale using Type III ANOVA, whereas HIX and E2/E3, which did not fully satisfy parametric assumptions, were further evaluated using aligned-rank transform (ART) ANOVA (Wobbrock, 2011). For ART analyses, concentration was treated as a categorical factor.

Significant ART results for HIX and E2/E3 were further assessed using Freedman–Lane permutation ANOVA with 5,000 permutations to confirm robustness of treatment effects without reliance on distributional assumptions (Frossard, 2021). ART was used for factorial rank-based inference, while permutation ANOVA was used to confirm the robustness of observed effects on raw responses.

PARAFAC fluorophores were analyzed separately using aligned-rank transform ANOVA because all components showed departures from parametric assumptions. Final component models included DOM source, PFAS species, pH, and their interactions. Concentration was excluded from the final component ART models because its inclusion generated aliased, non-estimable factorial designs. To confirm component-level treatment effects, raw PARAFAC component scores were additionally evaluated using Freedman–Lane permutation ANOVA with 5,000 permutations. Statistical significance was defined at $\alpha = 0.05$.

FTIR spectra were processed using the *prospectr* package to ensure consistent spectral treatment across samples (Stevens, 2025). Pre-processing steps were applied uniformly where appropriate to facilitate comparison of functional group regions among treatments. All figures were generated using *ggplot2* (Wickham, 2016).

3.4 Results and Discussion

3.4.1 DOM Composition and PARAFAC Characterization

PARAFAC modeling resolved four distinct fluorophores (Figure 5), including two humic-like (C1 and C2) and two protein-like (C3 and C4). These fluorophores represent chemically distinct DOM fractions with differing reactivity. The fluorophores were compared to the online database, Openfluor (Murphy, 2014), with high spectral similarity

(Tucker Congruency Coefficient, TCC = 0.95 for both excitation and emission) (Table 5). The identified fluorophores reflect the coexistence of both humified and microbially derived DOM fractions. Humic-like (C1 and C2) were associated with aromatic, terrestrially derived, and relatively recalcitrant organic matter, while the protein-like (C3) represents more labile, microbially derived material of tryptophan. C4 exhibited characteristics consistent with tyrosine-like fluorescence, indicative of autochthonous, protein-like DOM.

Relative contributions were assessed according to fluorophore classifications summarized in Table 5. This classification enabled the separation of humic-like and protein-like fluorophores, allowing for a more detailed evaluation of DOM composition across samples. Differences in the relative abundance of these components reflect shifts in DOM source characteristics and degree of humification. These compositional variations are particularly relevant for understanding fluorophore-specific responses to PFAS exposure.

The relative contributions of fluorophores varied across DOM sources (Figure 6 Figure 7). Humic-like fluorophores dominated all samples, particularly in Pahokee muck, which showed the highest contribution from the aromatic C2. In contrast, biosolids and cow manure exhibited greater relative contributions from protein-like (C3), indicating a higher proportion of labile, microbially derived organic matter. These differences demonstrate that the DOM source strongly controls compositional structure and fluorophore distribution.

3.4.2 Optical Indices

The fluorescence index (FI) is used to distinguish the dominant source of dissolved organic matter, with higher values indicating more microbially derived, protein-like DOM and lower values indicating more terrestrially derived, humic-rich DOM. FI values (Figure 8) were primarily controlled by DOM source, with biosolids highest (~2.10–2.30), followed by cow manure (~1.60–1.80) and Pahokee muck (~1.40–1.60).

Observed E2/E3 ratios varied primarily by DOM source, with Pahokee muck exhibiting the highest values (~5.5–7.5), followed by biosolids (~3.5–6.5) and cow manure (~3.5–4.1) (Figure 9). Across all DOM types, E2/E3 showed limited and inconsistent variation with increasing PFAS concentration, with no consistent trends observed. In biosolids, slight decreases in E2/E3 were observed at higher pH, whereas cow manure and Pahokee muck exhibited minor fluctuations across PFAS treatments and concentrations

The determined HIX values showed a slight attenuation with increasing PFAS concentration. This trend is attributed to changes in fluorophore behavior, such as alterations in aggregation or fluorescence intensity, rather than changes in DOM humification. Increased contributions from shorter-wavelength, protein-like emission can reduce the relative signal in the humic-like emission region used to calculate HIX, resulting in an apparent decrease in HIX without indicating a change in the underlying DOM composition.

Analysis of variance (Table 6) displays the statistical effects of DOM source, PFAS type, pH, and concentration on fluorescence responses. For FI, Type III ANOVA indicated significant effects of DOM, PFAS, and pH, as well as significant two-way interactions

among these factors. PFAS concentration was not a significant predictor of FI ($F = 0.06$, $p = 0.808$), indicating limited sensitivity of source-related fluorescence signatures to concentration across the tested range. Significant DOM × PFAS, DOM × pH, PFAS × pH, and DOM × PFAS × pH interactions further indicated that FI responses depended primarily on DOM composition and solution chemistry, with limited sensitivity to PFAS concentration across the tested range. FI remained highest in biosolids-derived DOM and lowest in Pahokee muck, consistent with greater microbial contributions in biosolids and more humified character in muck.

Because HIX and E2/E3 did not fully satisfy parametric assumptions, these responses were further evaluated using ART ANOVA (Table Appx. 7, Table Appx. 8). For HIX, significant main effects of DOM, PFAS, pH, and concentration were observed, along with significantly higher-order interactions, indicating that HIX responses depended strongly on the combined treatment conditions. Pairwise comparisons showed that HIX increased in the order PFBS < PFNA < PFOS, with PFOS producing the greatest red shift. Concentration also significantly influenced HIX, although its effect was smaller than that of DOM source and pH, suggesting that increasing PFAS levels produced modest but measurable red shift in the fluorescence spectra. These patterns are consistent with stronger interactions of longer-chain, more hydrophobic PFAS, particularly PFOS, with condensed aromatic and humified DOM domains through hydrophobic association, electrostatic bridging, and conformational changes within the DOM matrix. Similarly, E2/E3 exhibited significant main effects and interactions across all tested factors (all $p < 0.001$), confirming that DOM optical properties associated with apparent molecular size and aromaticity were sensitive to treatment combinations. Pairwise comparisons

indicated significant PFAS differences, with ranked responses ordered PFNA < PFOS < PFBS, demonstrating that PFAS headgroup chemistry and chain structure can differentially alter DOM optical properties. The limited sensitivity is consistent with the source-dependent nature of FI and E2/E3, which is primarily governed by DOM composition rather than short-term chemical interactions (McKnight, 2001).

Freedman–Lane permutation ANOVA (5,000 permutations, Table Appx. 5) confirmed that DOM source was the dominant factor influencing both HIX and E2/E3, yielding the largest F-statistics across all tested terms (HIX: F = 12,557.86; E2/E3: F = 12,762.96; p = 0.0002). PFAS identity and pH also significantly affected both indices, although their effects were smaller than those of DOM source. Concentration effects were significant but comparatively weak, particularly for E2/E3 (F = 4.32). Several interaction terms, including DOM × PFAS, DOM × pH, and PFAS × pH, were also highly significant for both indices, indicating that PFAS effects on DOM fluorescence responses depended strongly on DOM composition and solution chemistry.

Collectively, these findings indicate that DOM source and pH largely govern fluorescence behavior, whereas PFAS composition and concentration produce secondary but significant modifications to reactive fluorophore domains. Such shifts in DOM optical properties indicates PFAS complexation with DOM under variable conditions (pH and PFAS concentration) .

3.4.3 Fluorophore-Specific Responses

Normalized fluorescence (F/F_0) exhibited distinct patterns across fluorophores, DOM sources, and pH conditions (Figure 11). Humic-like fluorophores (C1 and C2) remained relatively stable across all treatments, indicating limited sensitivity to PFAS

exposure. In contrast, protein-like fluorophores (C3 and C4) showed greater variability, particularly in cow manure and Pahokee muck DOM, where PFOS and PFNA produced more pronounced increases in fluorescence at higher concentrations.

ART ANOVA demonstrated that PARAFAC component scores were significantly influenced by DOM source, PFAS species, and pH for all four components (Table 7; $p < 0.001$ for all main effects). Significant two-way interactions between DOM source and PFAS species, DOM source and pH, and PFAS species and pH were also observed across every component ($p < 0.001$), indicating that PFAS responses varied depending on DOM composition and solution chemistry. In addition, the three-way interaction among DOM source, PFAS species, and pH was significant for all components ($p < 0.001$), demonstrating that fluorophore-specific behavior was governed by the combined influence of DOM source, PFAS identity, and pH rather than by any single factor alone.

Among the components, Comp.3 exhibited the strongest factor responses, with particularly large effects for DOM source (F = 794.24), PFAS species (F = 324.83), and pH (F = 190.82), suggesting heightened sensitivity of this fluorophore region to environmental conditions. C1 and C2 also showed strong DOM and interaction effects, whereas Comp.4 displayed pronounced pH and PFAS × pH responses.

3.4.4 FTIR Evidence of PFOS–DOM Interactions

FTIR analysis provided complementary evidence of PFOS–DOM interactions. Increasing DOM concentration resulted in systematic spectral changes, particularly in the 1300–1000 cm^{-1} region corresponding to overlapping PFOS sulfonate (S=O) and C–F vibrations (Table 8). Increased peak intensities in this region indicate enhanced PFOS–DOM interactions with increasing DOM concentration (Figure 12).

Increasing DOM concentration resulted in systematic changes across all FTIR regions, with the most pronounced effects observed in the 1300–1000 cm^{-1} region corresponding to overlapping PFOS sulfonate (S=O) and C–F vibrations (Gao, 2012). Additional changes in the O–H (~3400 cm^{-1}) and aromatic/carbonyl (~1650 cm^{-1}) regions suggest that DOM functional groups participate in PFOS interactions through hydrogen bonding, electrostatic interactions, and hydrophobic associations (Wang, 2013). The emergence of features in the fingerprint region (~900 cm^{-1}) further supports changes in PFOS molecular environment in the presence of DOM.

3.5 Discussions

PARAFAC analysis revealed clear compositional differences among DOM sources, characterized by varying contributions of humic-like (C1, C2) and protein-like (C3, C4) fluorophores. Humic-like fluorophores dominated across all samples, particularly in Pahokee muck, indicating a greater contribution of aromatic, terrestrially derived organic matter. In contrast, biosolids and cow manure exhibited relatively higher contributions of protein-like fluorophores, reflecting a greater presence of labile, microbially derived DOM. These compositional differences establish the baseline chemical heterogeneity of the DOM and provide a framework for interpreting PFAS-induced fluorescence responses.

Despite clear compositional differences among DOM sources, fluorescence indices showed limited sensitivity to PFAS concentration. The E2/E3 ratio remained stable across PFAS concentration, pH, and DOM source (Figure 9), indicating no consistent changes in DOM molecular size or aromaticity proxies under the conditions studied. Similarly, HIX values exhibited minimal variation with increasing PFAS

concentration (Figure 10). At higher PFAS concentrations, modest attenuation in HIX was observed, consistent with trends reported by Olshansky (2025). The ANOVA results (Table 7) confirmed that DOM composition is the dominant control on optical properties, as evidenced by substantially larger F-values for DOM relative to PFAS concentration across all indices. While PFAS concentration significantly influenced E2/E3 and HIX statistically, these effects were comparatively small and not consistently observed across all indices, with no significant concentration effect detected for FI.

Fluorophore intensity analysis (F_0/F, *Figure 8*) showed humic-like fluorophores (C1 and C2) showed little change across PFAS concentration. Protein-like fluorophores (C3 and C4), however, displayed minor increases in fluorophore intensity positively correlated with PFAS intensity. This is especially true in Pahokee muck and cow manure, despite their humic-like dominance (Figure 6). PFBS showed more variability compared to PFOS and PFNA. PFOS showed high variability in Pahokee muck DOM with a trend towards quenching. Across PFAS species, PFOS generally exerted the strongest influence on fluorescence, followed by PFNA, while PFBS showed minimal impact. These trends suggest that PFAS interactions preferentially affect protein-like DOM fractions and are strongly influenced by both DOM composition and solution chemistry.

The inverse relationship between fluorophore intensity and HIX represents a redistribution of fluorescence emission rather than a change in DOM humification. As protein-like fluorescence increases, emission shifts toward shorter wavelengths, reducing the relative contribution of humic-like emission used to calculate HIX. This attenuation in HIX therefore reflects changes in fluorophore aggregation and intensity that effectively reveal proteinaceous fluorophores, rather than a loss of humified material. This behavior

could be potentially attributed to the liability of proteinaceous fluorophores through suppression of non-radiative relaxation pathways when weak associations are formed with PFAS. While hydrogen bonding interactions may contribute, the absence of substantial spectral shifts suggests that relaxation-based mechanisms likely dominate the fluorescence response.

In particular, weak non-covalent interactions may restrict molecular motion, reduce solvent-mediated quenching, and increase emission efficiency of protein-like fluorophores. This interpretation is supported by the FTIR results, which provide complementary evidence for subtle interactions between PFAS and DOM functional groups. Rather than indicating major structural transformation of the DOM matrix, the FTIR spectra suggest localized changes in bonding environments, consistent with hydrogen bonding, electrostatic association, and hydrophobic interactions that can alter fluorophore behavior without producing large shifts in bulk optical indices. This behavior suggests that DOM may enhance PFOS stabilization in solution, with important implications for PFAS mobility and transport in natural systems.

These interpretations were further supported by the nonparametric ART and Freedman–Lane permutation analyses, which confirmed that DOM source and pH were the dominant statistical controls on both bulk fluorescence indices and PARAFAC component intensities, while PFAS identity exerted smaller but significant secondary effects. For HIX and E2/E3, DOM source produced F-statistics several orders of magnitude greater than concentration effects, reinforcing that intrinsic DOM chemistry, rather than PFAS dose alone, governs most observed optical variability. At the component level, C3 exhibited the strongest response to PFAS species, pH, and

interaction terms, consistent with the pronounced sensitivity of protein-like fluorophores observed in the F_0/F analysis. This agreement between descriptive fluorescence trends and robust factorial statistics indicates that PFAS effects are not uniformly distributed across the DOM pool but are concentrated within specific reactive fluorophore domains. Environmentally, these selective interactions suggest that relatively minor DOM fractions may disproportionately influence PFAS complexation, stabilization, and transport, particularly under acidic conditions or in amendment-derived DOM enriched in labile proteinaceous material.

3.6 *Conclusions*

Modest decreases in HIX concurrent with increases in protein-like fluorophore intensity indicate that PFAS interactions shift the relative distribution of DOM fluorescence rather than altering bulk DOM composition. Reduced HIX suggests a diminished contribution of humified, aromatic DOM, while enhanced protein-like fluorescence reflects increased emission efficiency of labile fluorophores. These patterns are consistent with preferential PFAS interactions with protein-like DOM fractions.

Mechanistically, these responses support non-covalent PFAS–DOM complexation driven by hydrophobic interactions between the fluorinated PFAS tail and organic moieties, as well as electrostatic associations with functional groups such as amines. These interactions likely modify the local fluorophore environment by restricting molecular motion and reducing solvent-mediated quenching, enhancing fluorescence without substantially altering DOM structure. FTIR results further support this interpretation, indicating that PFAS associates with DOM rather than remaining freely dissolved.

The inverse relationship between HIX and fluorophore intensity underscores the importance of component-level analysis for resolving these interactions. These results provide a mechanistic framework for understanding PFAS–DOM binding behavior and highlight the need for future work to directly quantify PFAS–DOM associations and evaluate their role in controlling PFAS fate under dynamic environmental conditions.

References

Bolan NS, Adriano DC, Kunhikrishnan A, James T, McDowell R, Senesi N. 2011. Dissolved organic matter: biogeochemistry, dynamics, and environmental significance in soils. Advances in agronomy 110:1-75 https://doi.org/10.1016/B978-0-12-385531-2.00001-3.

Buck RC, Franklin J, Berger U, Conder JM, Cousins IT, De Voogt P, Jensen AA, Kannan K, Mabury SA, van Leeuwen SP. 2011. Perfluoroalkyl and polyfluoroalkyl substances in the environment: terminology, classification, and origins. Integrated Environmental Assessment and Management 7:513-541 https://doi.org/10.1002/ieam.258.

Carmosini N, Lee LS. 2008. Partitioning of fluorotelomer alcohols to octanol and different sources of dissolved organic carbon. Environmental science & technology 42:6559-6565 https://doi.org/10.1021/es800263t.

Evich MG, Davis MJB, McCord JP, Acrey B, Awkerman JA, Knappe DRU, Lindstrom AB, Speth TF, Tebes-Stevens C, Strynar MJ, Wang Z, Weber EJ, Henderson WM, Washington JW. 2022. Per- and polyfluoroalkyl substances in the environment. Science 375:eabg9065 https://doi.org/10.1126/science.abg9065.

Frossard J, Renaud O. 2021. Permutation tests for regression, ANOVA, and comparison of signals: the permuco package. Journal of Statistical Software 99:1-32 https://doi.org/https://doi.org/10.18637/jss.v099.i15.

Gao X, Chorover J. 2012. Adsorption of perfluorooctanoic acid and perfluorooctanesulfonic acid to iron oxide surfaces as studied by flow-through ATR-FTIR spectroscopy. Environmental Chemistry 9:148-157 https://doi.org/10.1071/EN11119.

Higgins CP, Luthy RG. 2006. Sorption of perfluorinated surfactants on sediments. Environmental Science & Technology 40:7251-7256 https://doi.org/10.1021/es061000n.

Johnson GR. 2022. PFAS in soil and groundwater following historical land application of biosolids. Water Research 211:118035 https://doi.org/10.1016/j.watres.2021.118035.

Lazcano K, Choi R, Jeong Y, Mashtare ML, Lee LS. 2020. Characterizing and comparing per-and polyfluoroalkyl substances in commercially available biosolid and organic non-biosolid-based products. Environmental science & technology 54:8640-8648 https://doi.org/10.1021/acs.est.9b07281.

Masoner JR, Kolpin DW, Cozzarelli IM, Akob DM, Conaway CH, Givens CE, Hladik ML, Hubbard LE, Lane RF, McCleskey RB. 2025. Land application of biosolid, livestock, and drilling wastes to US farmland: a potential pathway for the redistribution of contaminants in the environment. Environmental Science: Processes & Impacts 27:3372-3402 https://doi.org/10.1039/D5EM00312A.

McKnight DM, Boyer EW, Westerhoff PK, Doran PT, Kulbe T, Andersen DT. 2001. Spectrofluorometric characterization of dissolved organic matter for indication of precursor organic material and aromaticity. Limnology and Oceanography 46:38-48 https://doi.org/10.4319/lo.2001.46.1.0038.

Murphy KR, Stedmon CA, Wenig P, Bro R. 2014. OpenFluor–an online spectral library of auto-fluorescence by organic compounds in the environment. Analytical methods 6:658-661 https://doi.org/10.1039/C3AY41935E.

Olshansky Y, Lawhon J, Ojeda A, Melina N, Knappenberger T. 2025. Impact of dissolved organic matter chemical properties on perfluorooctane sulfonate solution binding affinities and adsorption on soils. 0047-2425. Wiley Online Library.

Panieri E, Baralic K, Djukic-Cosic D, Buha Djordjevic A, Saso L. 2022. PFAS molecules: a major concern for the human health and the environment. Toxics 10:44 https://doi.org/10.3390/toxics10020044.

Posit team. 2026. RStudio: integrated development environment for R. 2025.5.1.513 ed. Posit Software, PBC, Boston, MA.

Pucher M, Wünsch U, Weigelhofer G, Murphy K, Hein T, Graeber D. 2019. staRdom: versatile software for analyzing spectroscopic data of dissolved organic matter in R. Water 11:2366

Qi Y, Cao H, Pan W, Wang C, Liang Y. 2022. The role of dissolved organic matter during Per- and Polyfluorinated Substance (PFAS) adsorption, degradation, and plant uptake: A review. J Hazard Mater 436:129139 https://doi.org/10.1016/j.jhazmat.2022.129139.

R Core Team. 2026. R: a language and environment for statistical computing. R Foundation for Statistical Computing.

Stevens A, Ramirez-Lopez L. 2025. *An introduction to the prospectr package*. R package Vignette.

Sunderland EM, Hu XC, Dassuncao C, Tokranov AK, Wagner CC, Allen JG. 2019. A review of the pathways of human exposure to poly- and perfluoroalkyl substances (PFASs) and present understanding of health effects. Exposure Science & Environmental Epidemiology 29:131-147 https://doi.org/10.1038/s41370-018-0094-1.

Thompson JT, Robey NM, Tolaymat TM, Bowden JA, Solo-Gabriele HM, Townsend TG. 2023. Underestimation of Per- and Polyfluoroalkyl Substances in Biosolids: Precursor Transformation During Conventional Treatment. Environ Sci Technol 57:3825-3832 https://doi.org/10.1021/acs.est.2c06189.

Wang K, Li W, Gong X, Li Y, Wu C, Ren N. 2013. Spectral study of dissolved organic matter in biosolid during the composting process using inorganic bulking agent: UV–vis, GPC, FTIR and EEM. International Biodeterioration & Biodegradation 85:617-623 https://doi.org/10.1016/j.ibiod.2013.03.033.

Wickham H. 2016. *ggplot2: Elegant Graphics for Data Analysis*. Springer-Verlag New York.

Wickham H, Francois R, Henry L, Muller K, Vaughan D. 2026a. *dplyr: A Grammar of Data Manipulation*.

Wickham H, Vaughan D, Girlich M, Ushey K. 2026b. *tidyr: Tidy Messy Data.*

Wobbrock JO, Findlater L, Gergle D, Higgins JJ. 2011. The aligned rank transform for nonparametric factorial analyses using only anova procedures. Proceedings of the SIGCHI conference on human factors in computing systems, pp 143-146.

Xie Y, Jiang L, Mei W, Tang J, Li J, Luo C. 2025. The role of DOM on the allocation of PFASs between water and sediment within a river system. Environmental Pollution 127350 https://doi.org/10.1016/j.envpol.2025.127350.

Figures and Tables

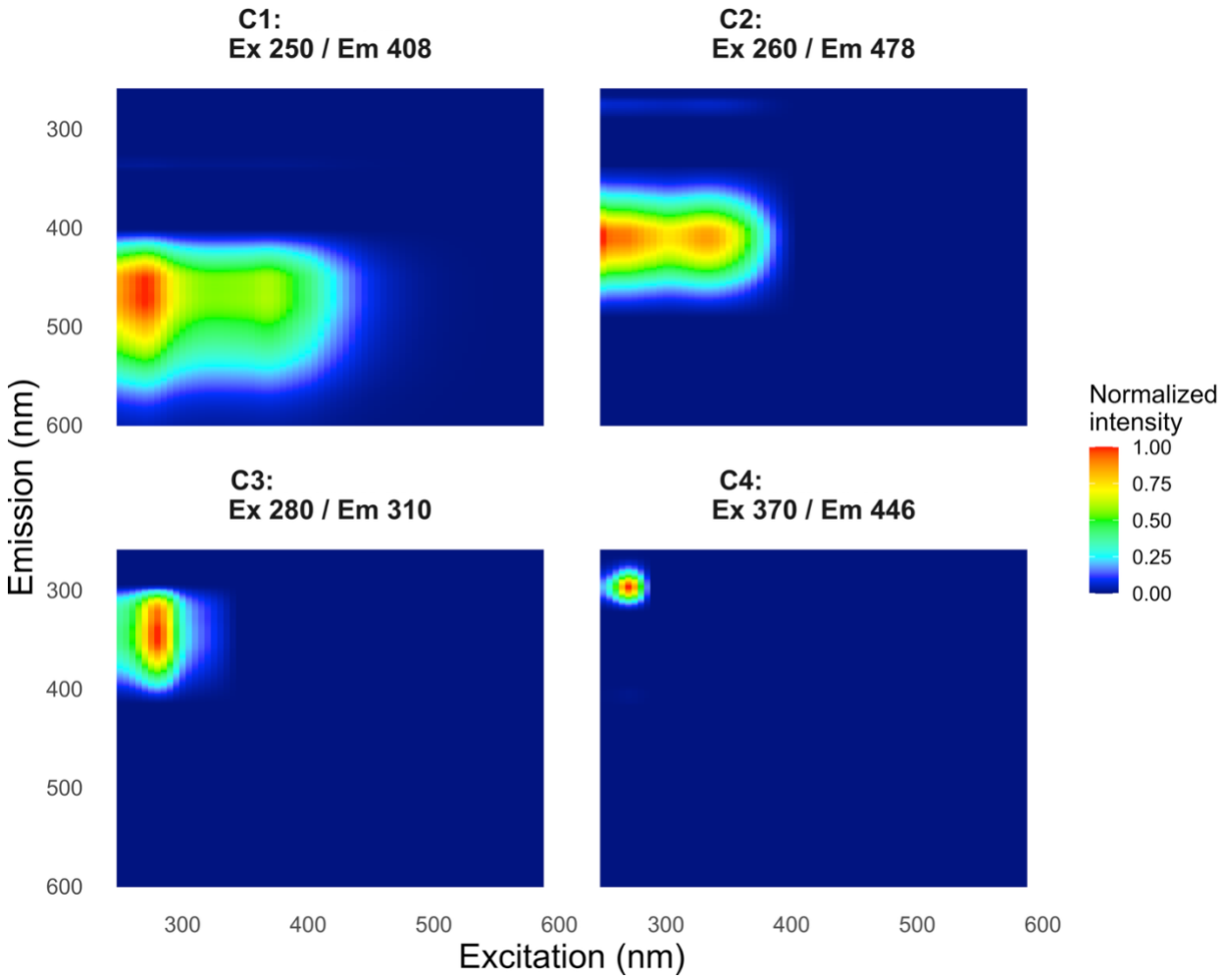

Figure 5 Excitation-emission matrices of the four principal fluorophores obtained from the PARAFAC model.

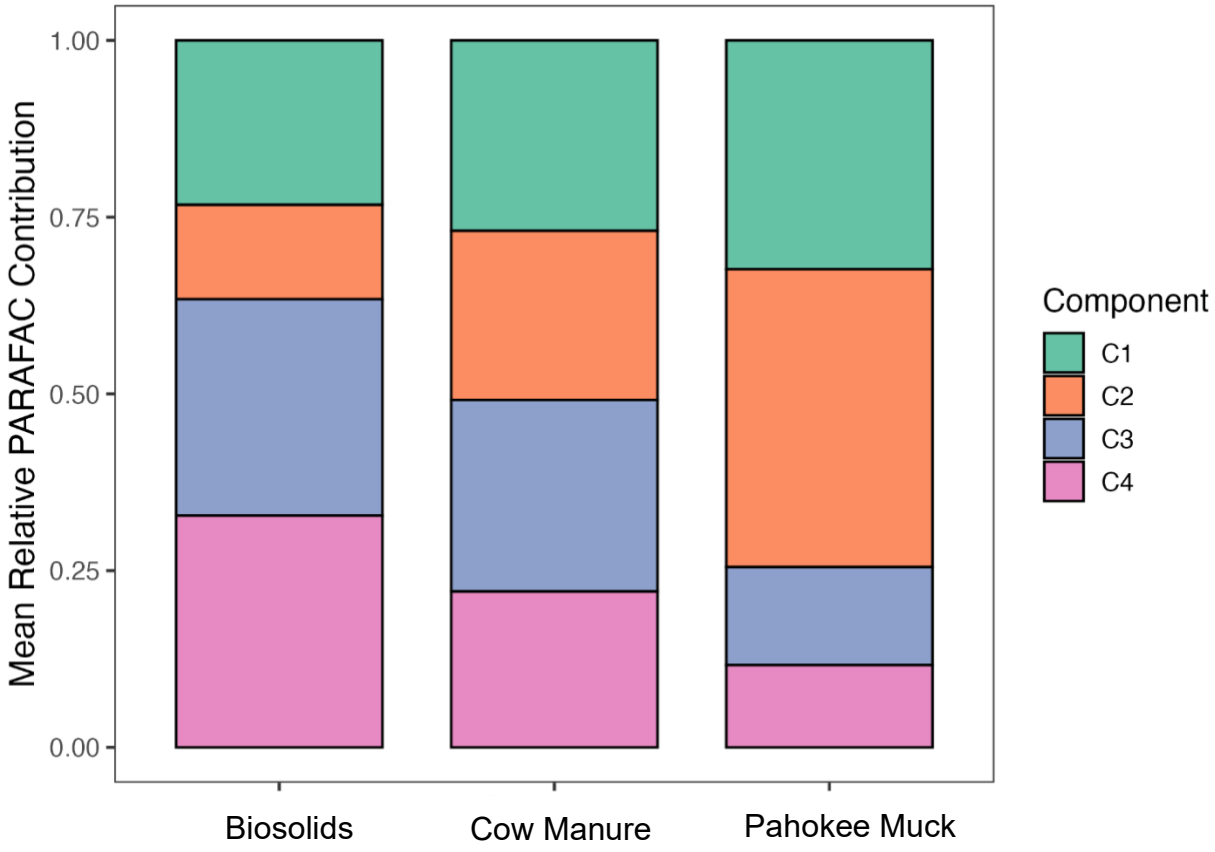

Figure 6 Mean relative contributions of fluorophores (C1–C4) in the studied DOM. Component contributions are normalized within each DOM source.

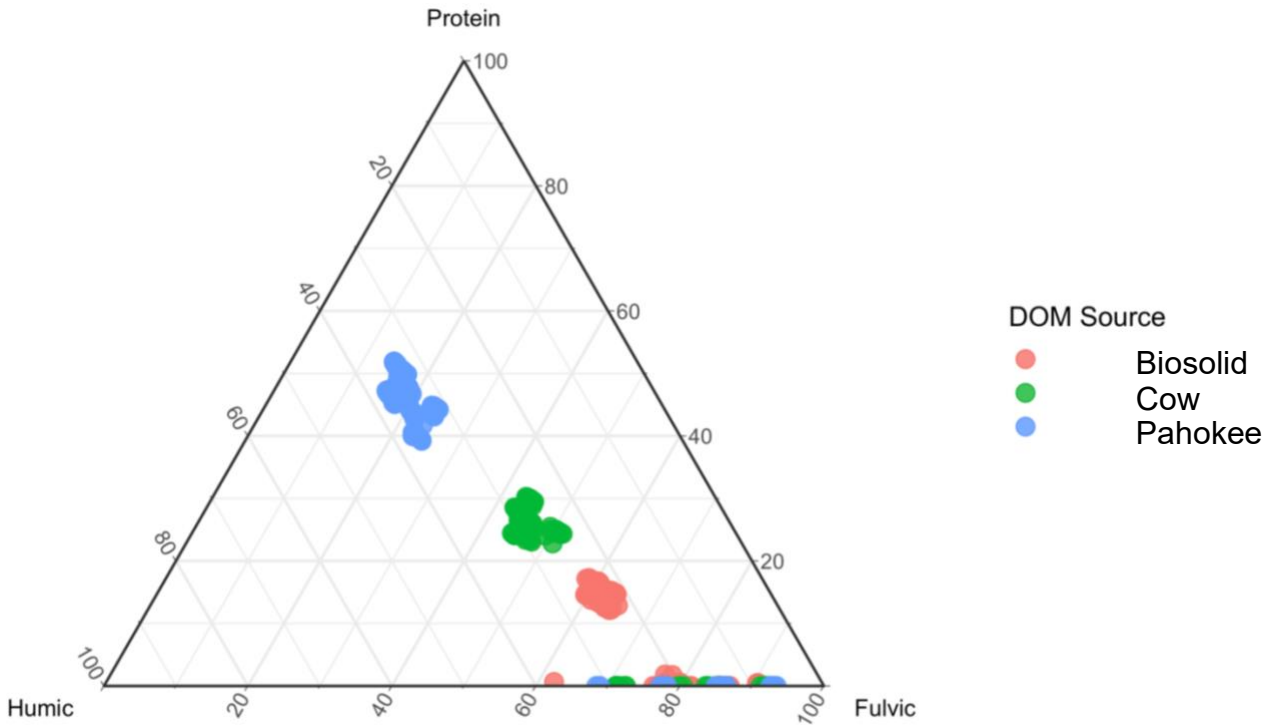

Figure 7 Ternary diagram showing the relative contributions of humic-like, fulvic-like, and protein-like fluorophores in the analysis of the studied DOM.

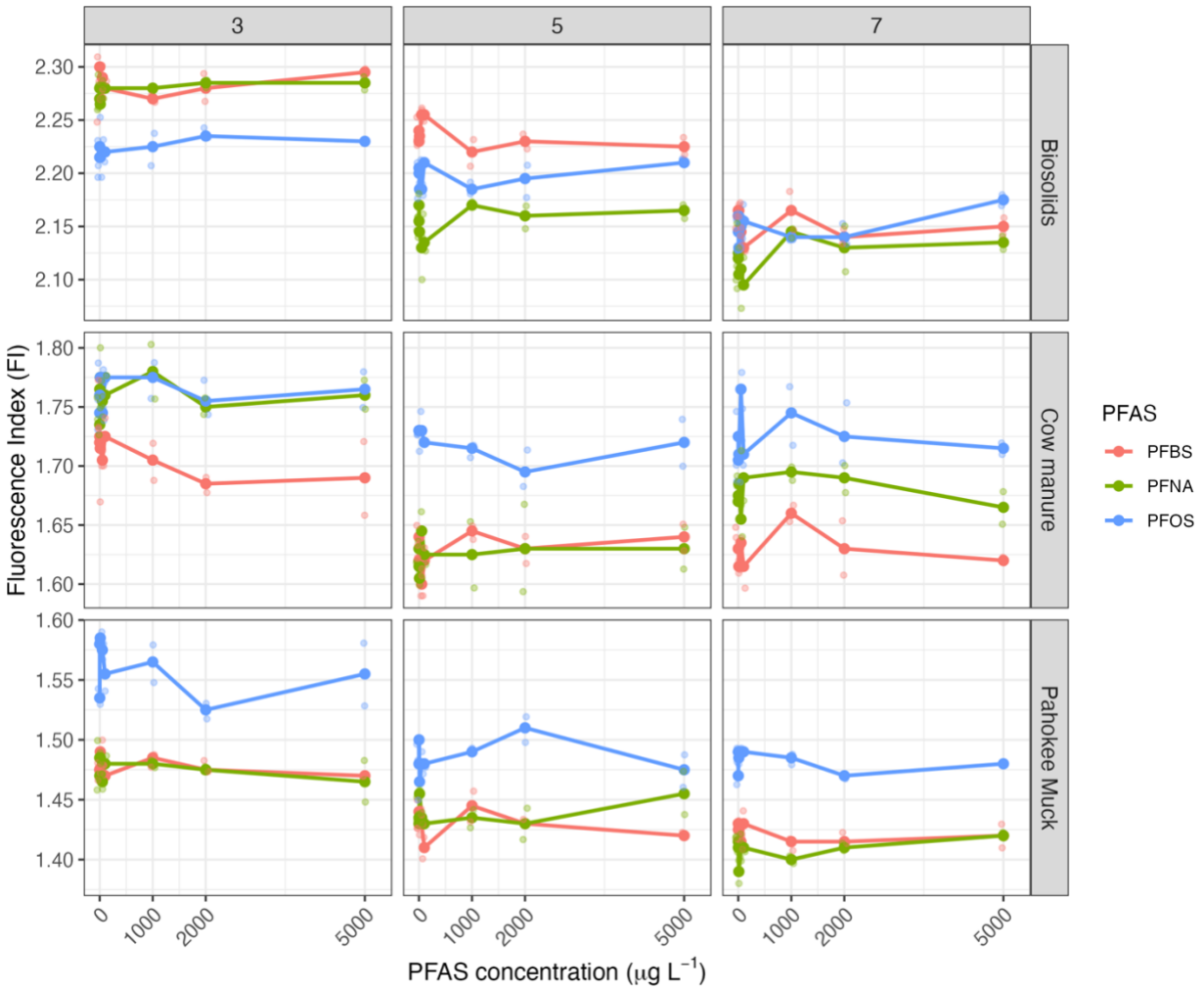

Figure 8 FI response as a function of PFAS concentration across DOM sources, PFAS species, and pH conditions. Panels show FI values measured over increasing PFAS concentrations (1–5000 μg L⁻¹). Points represent individual measurements and lines connect mean responses across concentration levels.

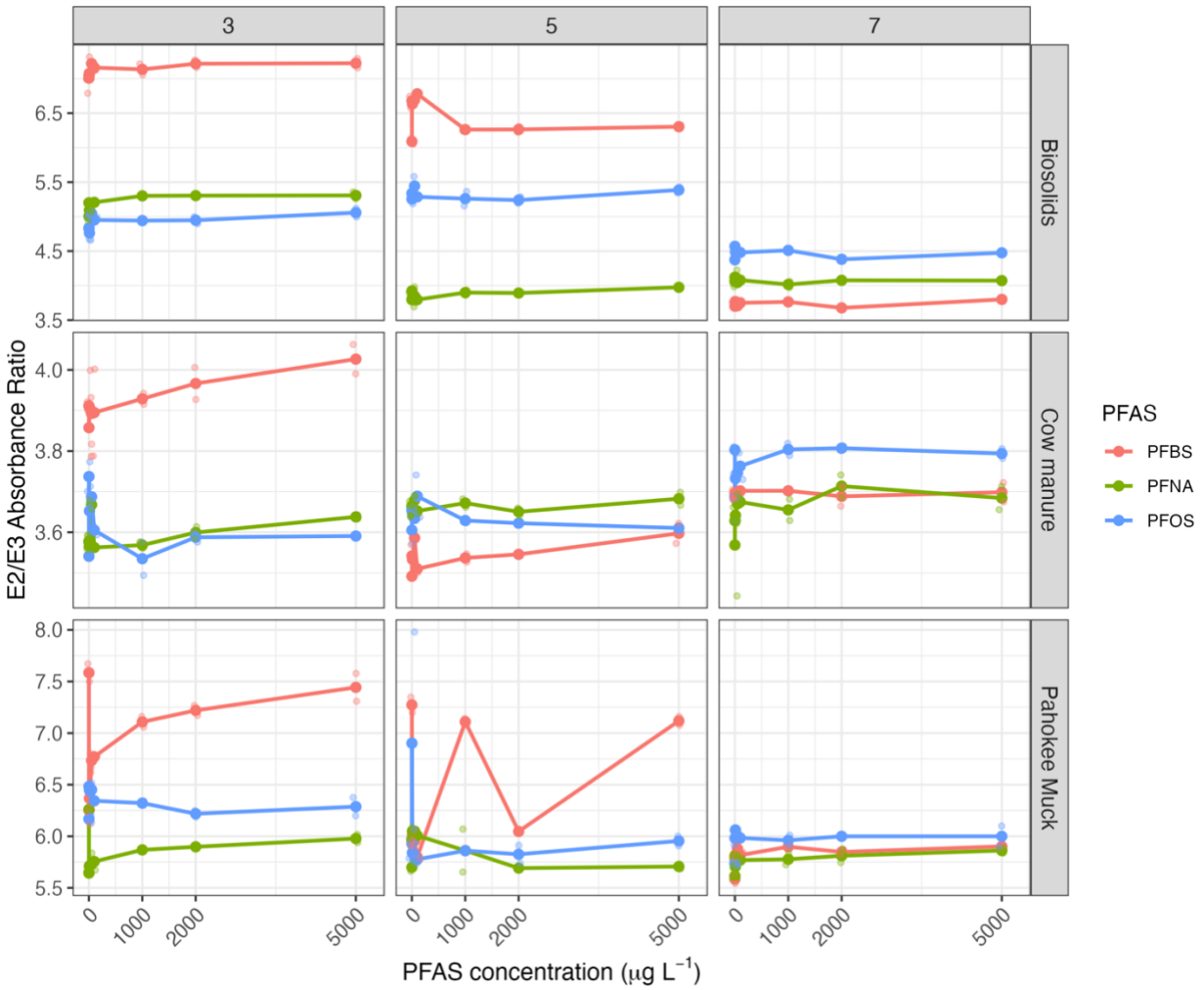

Figure 9 E2/E3 (250–365 nm) absorbance ratio as a function of PFAS concentration across DOM sources, PFAS species, and pH conditions. Panels show E2/E3 values measured over increasing PFAS concentrations (1–5000 μg L⁻¹). Points represent individual measurements

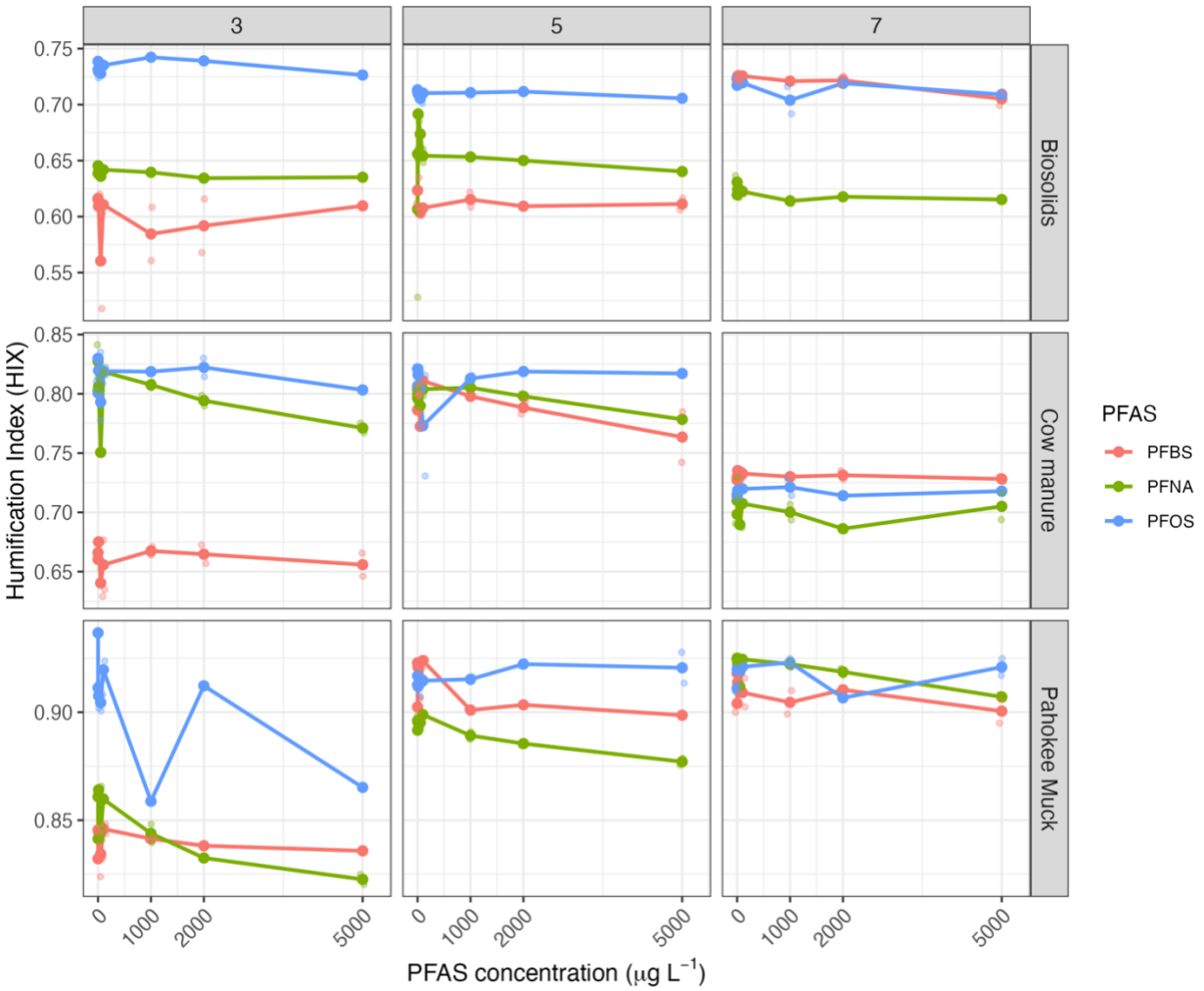

Figure 10 Humification index (HIX) responses across DOM sources, PFAS compounds, and pH conditions as a function of PFAS concentration. Panels show HIX values measured across increasing PFAS concentrations (1-5000 μg L⁻¹) Points represent individual measurements

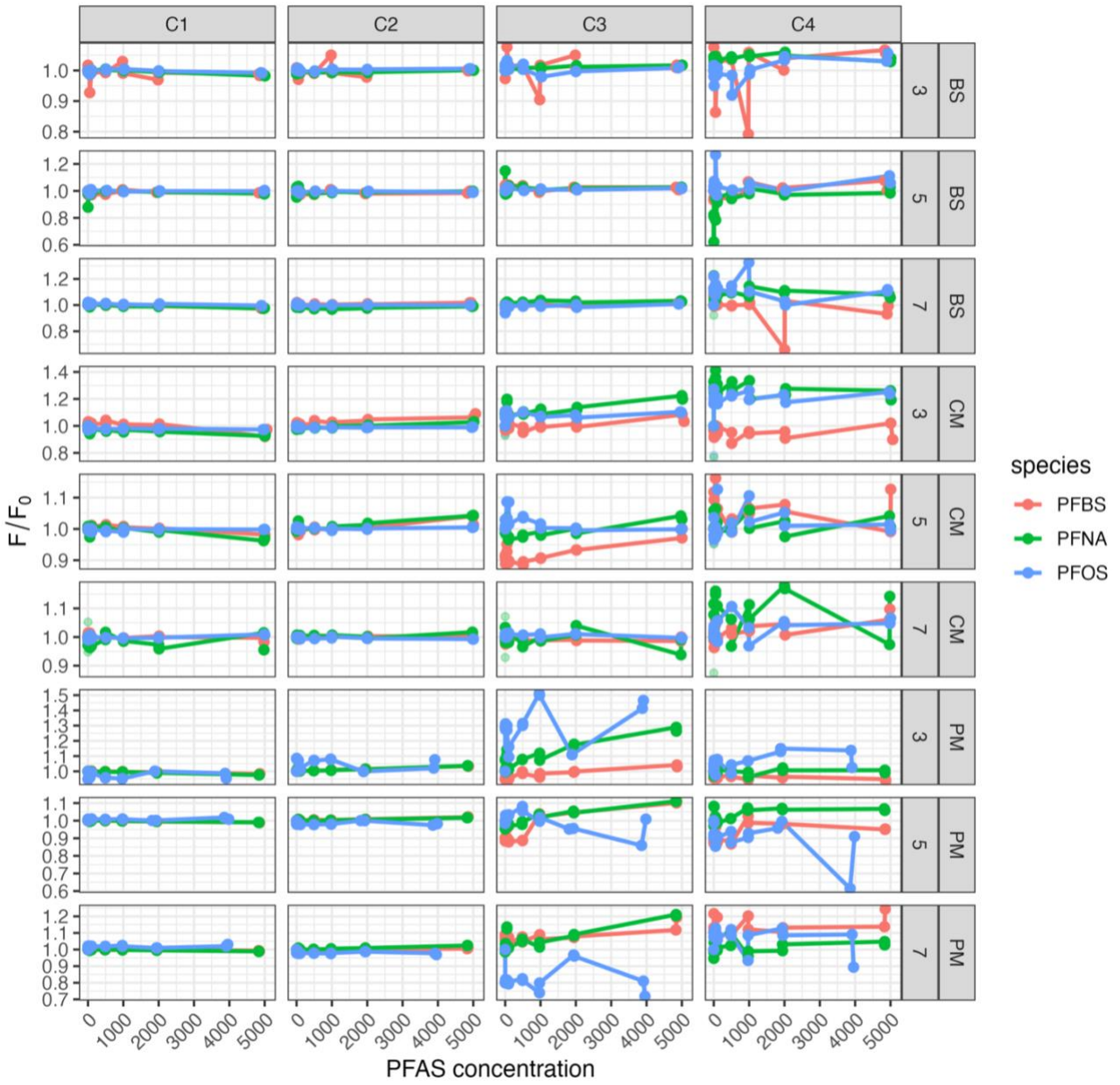

Figure 11 Fluorophore intensity plot of normalized fluorescence (F_0/F) as a function of PFAS concentration. Panels show PARAFAC components across DOM sources and pH and PFAS concentration (1-5000 µg L^{-1}). Humic-like fluorescence remains relatively stable, whereas

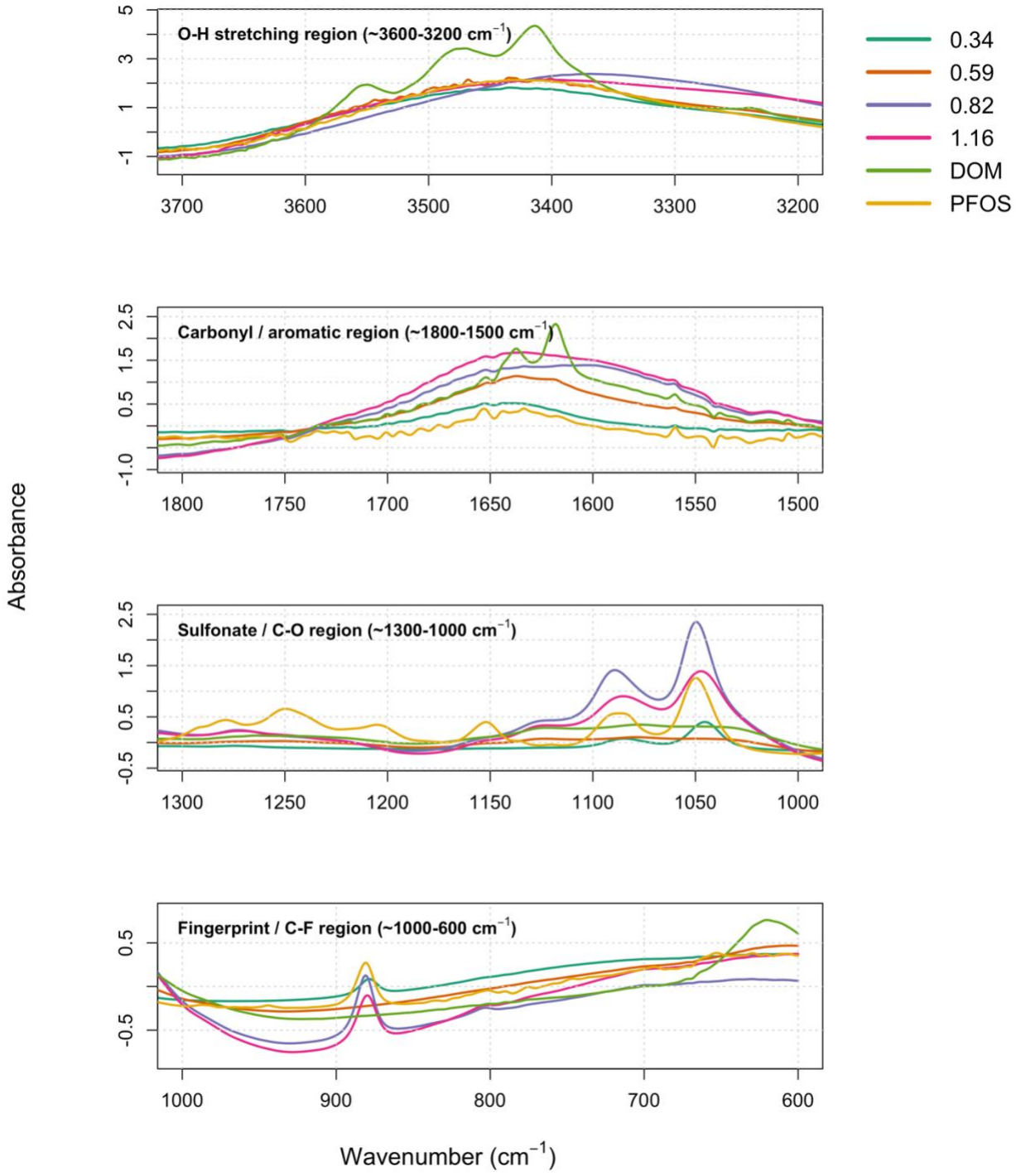

Figure 12 FTIR spectra of DOM, PFOS, and DOM–PFOS mixtures across selected wavenumber regions. Panels show the O–H stretching region (~3600–3200 cm⁻¹), carbonyl/aromatic region (~1800–1500 cm⁻¹), sulfonate/C–O region (~1300–1000 cm⁻¹), and fingerprint/C–F region (~1000–600 cm⁻¹). Lines represent DOM concentrations ranging from 0.3379 to 1.155 mg L⁻¹ with a constant PFOS-only

concentration of 5 mg L $^{-1}$ (± 0.007 mg L $^{-1}$) and a DOM-only concentration of 2.13 mg L $^{-1}$ (± 0.039 mg L $^{-1}$).

Table 3 List of organic amendment-derived DOMs used with their corresponding sources.

Name (Abbreviation)	Source
Type B Biosolids (BS)	Auburn Wastewater Facility, Auburn, AL
Pahokee Muck (PM)	International Humic Substance Society
Cow Manure (CM)	Cow feces collected fresh with no additives (Auburn, AL)

Table 4 List of PFAS compounds used in this study and their respective formula, molar mass, and structure.

PFAS Compound (CF chain length)	Formula	Molar Mass g mol^{-1}	Structure
PFNA(8)	C9F17O2	462.963	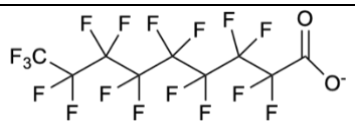
PFOS (8)	C8F17SO3	498.930	
PFBS (4)	C4F9SO3	298.943	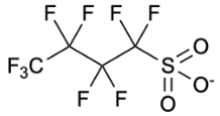

Table 5 PARAFAC component excitation–emission maxima and fluorophore assignments.

PARAFAC Component	Excitation/Emission Maxima (nm)	Characteristic	Source/Character	Reference
C1	275/456	Humic-like	Aromatic, humified, recalcitrant DOM	(Sharma, 2017)
C2	250/408	Humic-like	Terrestrially derived, aromatic DOM	(Olshansky, 2025)
C3	280/316	Protein-like (Tryptophan)	Microbial, labile, bioavailable DOM	(Bastidas Navarro, 2022)
C4	265/290	Protein-like (Tyrosine)	Autochthonous, labile DOM	(Coble, 2014)

Table 6 Summary of statistical analyses for bulk fluorescence indices (FI, HIX, and E2/E3). Includes analytical approach, significant treatment effects, pairwise PFAS differences, and environmental interpretation of PFAS–DOM responses.

Response Variable	Analysis Method	Significant Main Effects	Significant Interactions	Key PFAS Pairwise Differences	Interpretation
FI	Type III ANOVA	DOM, PFAS, pH	DOM × PFAS, DOM × pH, PFAS × pH	PFAS effects significant overall	FI was driven primarily by DOM source and pH, with PFAS contributing secondary but significant effects on fluorescence origin characteristics.
HIX	ART ANOVA	DOM, PFAS, pH, Concentration	Multiple two-way and higher-order interactions were significant	PFBS < PFNA < PFOS ($p < 0.001$)	Humification responses were strongly influenced by combined environmental conditions, with PFOS producing the greatest ranked HIX response.
E2/E3	ART ANOVA	DOM, PFAS, pH, Concentration	Multiple two-way and higher-order interactions were significant	PFNA < PFOS < PFBS ($p < 0.001$)	Apparent molecular size/aromaticity responses varied significantly across treatments.

Table 7 Aligned-rank transform ANOVA results for PARAFAC component scores.

Component	Term	Df	F value	p value
C1	DOM source	2	364.26	<0.001
	PFAS species	2	25.52	<0.001
	pH	2	58.82	<0.001
	DOM × PFAS	4	88.42	<0.001
	DOM × pH	4	131.88	<0.001
	PFAS × pH	4	33.17	<0.001
	DOM × PFAS × pH	8	35.00	<0.001
C2	DOM source	2	305.64	<0.001
	PFAS species	2	261.44	<0.001
	pH	2	83.42	<0.001
	DOM × PFAS	4	26.99	<0.001
	DOM × pH	4	120.96	<0.001
	PFAS × pH	4	36.55	<0.001
	DOM × PFAS × pH	8	29.38	<0.001
C3	DOM source	2	794.24	<0.001
	PFAS species	2	324.83	<0.001
	pH	2	190.82	<0.001
	DOM × PFAS	4	124.11	<0.001
	DOM × pH	4	184.79	<0.001
	PFAS × pH	4	63.27	<0.001
	DOM × PFAS × pH	8	49.89	<0.001
C4	DOM source	2	318.13	<0.001
	PFAS species	2	124.32	<0.001
	pH	2	172.33	<0.001
	DOM × PFAS	4	40.17	<0.001
	DOM × pH	4	68.00	<0.001
	PFAS × pH	4	82.25	<0.001
	DOM × PFAS × pH	8	30.46	<0.001

Table 8 Major FTIR bands observed in DOM, PFOS, and DOM–PFOS mixtures with corresponding functional group assignments. Wavenumber ranges are approximate, and assignments are tentative due to overlapping contributions between DOM and PFOS, particularly in the 1300–1000 cm^{-1} region. Peak assignments were based on Coates (2000).

Wavenumber (cm^{-1})	Tentative assignment	Interpretation
~3400	O–H stretching	DOM hydroxyl groups and hydrogen-bonded water
~1630–1650	Aromatic C=C and conjugated C=O vibrations	Aromatic/humic-like DOM structures
~1250	S=O asymmetric stretching with C–F overlap	PFOS sulfonate headgroup signature
~1150–1100	C–O stretching / oxygenated functional groups	DOM oxygenated functional groups
~1150–1090	S=O symmetric stretching with C–F overlap	PFOS-associated band, enhanced in mixed systems
~890	PFOS fingerprint band	Suggestive of PFOS molecular environment in DOM–PFOS mixtures
~625	Lower fingerprint / possible inorganic residue contribution	Likely secondary, not primary DOM assignment

Overall Conclusions and Environmental Implications

This research demonstrates that PFAS behavior in environmental systems is strongly governed by interactions with co-occurring materials, particularly microplastics (MPs) and dissolved organic matter (DOM). Across both studies, it is evident that PFAS cannot be considered in isolation, as their transport, retention, and bioavailability are controlled by complex, multiphase interactions.

The study revealed that environmental weathering fundamentally alters the role of MPs in PFAS sorption. Weathered PE MPs exhibited increased surface oxidation, heterogeneity, and mineral association, resulting in enhanced adsorption of long-chain PFAS relative to pristine MPs and MP-free sediments. In contrast, pristine MPs reduced PFAS adsorption or introduced sorption hysteresis, indicating kinetically constrained interactions. These findings suggest that weathering processes shift microplastics from relatively inert surfaces to active sorbents capable of modifying PFAS partitioning. Importantly, the more reversible sorption observed in weathered MPs indicates a greater potential for PFAS remobilization under dynamic environmental conditions, highlighting their role as vectors for contaminant transport rather than permanent sinks.

This work shows that thePFAS interactions are highly dependent on organic matter composition and solution chemistry. Although DOM is often assumed to enhance PFAS sorption, results indicate that its effects are variable and governed by competing mechanisms, including complexation, site competition, and bridging interactions with mineral surfaces. Fluorescence-based analyses showed that changes in DOM fluorophore intensity were sensitive to PFAS exposure; however, conventional bulk optical indices (e.g., FI, HIX, E2/E3) were often insufficient to capture these subtle

interactions. This suggests that PFAS–DOM associations may occur through weak, non-covalent interactions that are not readily detectable using traditional metrics. Additionally, environmental factors such as pH played a critical role in modulating these interactions, reinforcing the importance of solution chemistry.

Together, these findings highlight that PFAS fate is controlled by the combined influence of particle aging, organic matter composition, and environmental conditions. Rather than acting as passive co-contaminants, both weathered microplastics and DOM function as active regulators of PFAS partitioning and mobility. Notably, the results suggest that DOM composition and environmental chemistry may exert a stronger influence on PFAS behavior than concentration alone, challenging traditional assumptions used in predictive models.

From an environmental perspective, these results have important implications for PFAS transport in soils and sediments, particularly in systems impacted by plastic pollution and organic amendment applications. Weathered microplastics may enhance PFAS mobility, while heterogeneous DOM can either facilitate or inhibit PFAS retention depending on its composition. Therefore, accurate prediction of PFAS fate requires incorporation of these interacting factors into risk assessment frameworks.

Future research should focus on quantifying PFAS transport under dynamic flow conditions, evaluating long-term eco-corona development on microplastics, and further resolving DOM–PFAS interaction mechanisms using complementary spectroscopic and molecular-level techniques. Expanding studies to more environmentally relevant concentration ranges and complex matrices will be critical for improving our understanding of PFAS behavior in real-world systems.

Appendix

Appendix Text:

Appendix Tabes:

Appendix Figures:

Text Appx. 1 Specific surface area using Brunauer–Emmett–Teller (BET) method.

The specific surface area of sediment was determined by nitrogen (N_2) adsorption–desorption isotherms measured at 77 K using a Micromeritics 3Flex surface characterization analyzer (Micromeritics Instrument Corporation, Norcross, GA, USA). Prior to analysis, samples were degassed under vacuum at 80 °C for 72 hours to remove adsorbed gases and moisture. The Brunauer–Emmett–Teller (BET) method was applied over the relative pressure (P/P_0) to calculate the surface area (Brunauer, 1938). Additionally, the total organic carbon content of the sediment was determined using an Elementar Vario MICRO Cube, following the ASTM D5373 protocol, with four replicates. Sediment is put in an (12 M HCl) acid bath for 24 hours and in the oven (60°C TEMP) for 24 hours prior to analysis to remove inorganic carbon (Bisutti, 2004).

Text Appx. 2 XPS peak integration and relative atomic abundance calculations.

Peak area (P) can be determined using EQ 2 where I is the intensity at E, binding energy (mV). $E1$ is the E at the start of the peak and $E2$ is the end of the peak, also referred to as the peak window (mV). The relative abundance of specific atomic bonding environments, either within a single electron shell or as a combined summary from multiple shells within a sample was calculated by EQ 3 where SF is the sensitivity factor, $\boldsymbol{n}$ is the total number of elements, and the denominator is the sum of all corrected peaks.

$$P = \int_{E1}^{E2} I(E)d(E) \tag{2}$$

$$Atomic\ bonding\% = \frac{P/SF}{\sum_{i=1}^{n}(\frac{P_i}{SF_I})} \times 100 \tag{3}$$

Text Appx. 3 Liquid chromatography–high resolution mass spectrometry (LC-HRMS) conditions for PFAS quantification.

Analyses were performed using a Vanquish Flex Binary ultra-performance liquid chromatography (UPLC) system (Thermo Scientific) equipped with a PFAS-free kit (P/N 80100-62142), a delay column (Hypersil GOLD, 1.9 µm, 175 Å, 3 × 50 mm), and a separation column (Accucore RP-MS, 2.6 µm, 2.1 × 100 mm), coupled to a quadrupole Orbitrap mass spectrometer (Orbitrap Exploris 120, Thermo Scientific) operated with heated electrospray ionization (H-ESI) in negative mode using Xcalibur software (v. 4.4.16.14). The separation column was maintained at 40 °C. A 10 µL aliquot of standard or sample was injected onto the C18 separation column.

The mobile phase, delivered at 200 µL min^{-1}, consisted of (A) 2 mM ammonium acetate in water and (B) 100% acetonitrile. The gradient program was as follows: 0% B for 1.5 min, increased to 20% B at 1.8 min, ramped to 95% B at 13.4 min, held at 95% B for 1.6 min, returned to 20% B at 16 min, followed by 4 min re-equilibration.

The MS scan range was m/z 200–1000 with a resolution of 120,000. The automatic gain control (AGC) target was set to standard, RF lens to 70%, and maximum injection time to auto, with EASY-IC enabled at run start. The spray voltage was 2,500 V, the ion transfer tube temperature was 320 °C, and the vaporizer temperature was 275 °C. Sheath gas and auxiliary gas were set to 30 and 5 (arbitrary units), respectively. Mild trapping was disabled. Data were processed using Xcalibur 4.4 Quan Browser with a 5-ppm mass tolerance window.

Table Appx. 1 Relative Surface Functional Group Composition Derived From High-Resolution C1s and O1s XPS Spectra. High-resolution C1s spectra were deconvoluted into C–C/C–H (hydrocarbon), C–O (C–OH), and O–C=O (carboxyl) components. O1s spectra were deconvoluted into O–C and O–Si components. Binding energy windows (E_1–E_2), peak binding energies, sensitivity factors, raw peak areas, and sensitivity factor–corrected relative abundances (%) are reported for pristine and aged microplastics.

Element scan	E1	E2	Peak E	Sensitivity Factor	Pristine Peak Area	Aged Peak Area	Pristine Relative Abundance	Aged Relative Abundance
C1s C-C	298.08	279.08	284.5	1	13739	3734	100	77
C1s C-OH	298.08	279.08	285.9	1	NA	737	NA	15
C1s C-OOH	298.08	279.08	288.4	1	NA	374.3	NA	8
O1s O-C	545.08	525.08	531.3	2.881	1499	3552	100	77
O1s O-Si	545.08	525.08	532.72	2.881	NA	1080.8	NA	23

Table Appx. 2 surface elemental composition determined from xps survey spectra. Changes in surface atomic composition from XPS Survey Spectra. Survey spectra were used to quantify the relative atomic abundance (%) of major surface elements based on sensitivity factor–corrected peak areas of characteristic core-level signals (C1s, O1s, Si2p, and other detected elements).

Element scan	E1	E2	Peak E	Sensitivity Factor	Pristine Peak Area	Weathered Peak Area	Pristine Atomic (%)	Weathered Atomic (%)	Surface Element Enrichment (%)
C1s	291.58	277.08	285.13	1.0	813547	32947	98.1	67.3	-30.8
O1s	536.58	526.08	526.08	2.8	27868	31398.9	1.4	26.5	+25.1
Si2p	106.58	96.58	102.81	0.9	NA	3027.1	NA	6.2	+6.2

Table Appx. 3 surface elemental composition of unwashed weathered microplastics determined by XPS survey spectra. Binding energy ranges (E_1–E_2), peak binding energies (Peak E), relative sensitivity factors (SF), and calculated relative atomic abundances (%) for elements detected on unwashed weathered microplastics as determined from XPS survey spectra. Relative abundances were calculated using sensitivity factor–corrected peak areas.

Element Scan	E1	E2	Peak E	Sensitivity Factor	Relative Abundance (%)
O1s	541.0	532.1	522	2.9	34.2
F1s	694.0	687.1	677	4.1	13.2
C1s	295.5	285.3	278.5	1	24.9
Na1s	1078	1072.3	1063.5	10.6	4.2
Si2p	109.0	102.9	92	0.9	9.6
Fe2p	736.0	711.3	697.5	14.4	5
Al2p	83.50	74.4	71	0.6	5.8
Cl2p	209.0	200.0	187	2.7	3.0

Table Appx. 4 Compound-Specific LC–HRMS Parameters, Retention Times, and Limits of Quantification for Target PFAS. LC–HRMS acquisition parameters for individual PFAS, including exact mass (m) and charge (z), retention time (RT), and method limits of quantification (LOQ)

Acronym	Exact mass (m)	Charge (z)	RT (min)	Extraction Window (min)	Collision Energy (%)	LOQ (ng/L)
PFBS	298.943	-1	6.7	1.5	50	68.4
PFOA	412.9664	-1	9.04	2	14	2.70
PFHxS	398.9366	-1	9.2	2	40	140
PFOS	498.9302	-1	10.3	2	50	1.80
PFNA	462.9632	-1	9.85	2	12	560
PFHpA	362.9696	-1	8.3	1	14	50

Table Appx. 5 Freedman–Lane Permutation ANOVA Results (5,000 permutations) for the Effects of DOM Source, PFAS Type, pH, and Concentration Group on HIX and E2/E3. Reported values are numerator degrees of freedom (df), F-statistics, and permutation-based p-values.

Response	Term	df	F	Permutation p-value	Significance
HIX	DOM	2	12557.86	0.0002	***
HIX	PFAS	2	712.14	0.0002	***
HIX	pH	2	194.28	0.0002	***
HIX	Concentration	7	10.77	0.0002	***
HIX	DOM × PFAS	4	135.42	0.0002	***
HIX	DOM × pH	4	352.16	0.0002	***
HIX	PFAS × pH	4	343.65	0.0002	***
HIX	DOM × Concentration	14	1.99	0.0244	*
HIX	PFAS × Concentration	14	1.96	0.0252	*
HIX	pH × Concentration	14	2.55	0.0064	**
HIX	DOM × PFAS × pH	8	97.79	0.0002	***
HIX	DOM × PFAS × Concentration	28	1.38	0.0992	ns
HIX	DOM × pH × Concentration	28	1.53	0.0574	ns
HIX	PFAS × pH × Concentration	28	1.73	0.0234	*
HIX	DOM × PFAS × pH × Concentration	56	1.45	0.0434	*
E2/E3	DOM	2	12762.96	0.0002	***
E2/E3	PFAS	2	1006.65	0.0002	***
E2/E3	pH	2	1182.23	0.0002	***
E2/E3	Concentration	7	4.32	0.0020	**
E2/E3	DOM × PFAS	4	335.96	0.0002	***
E2/E3	DOM × pH	4	565.43	0.0002	***
E2/E3	PFAS × pH	4	454.75	0.0002	***
E2/E3	DOM × Conc	14	5.00	0.0004	***
E2/E3	PFAS × Conc	14	5.37	0.0004	***
E2/E3	pH × Conc	14	4.04	0.0012	**
E2/E3	DOM × PFAS × pH	8	244.30	0.0002	***
E2/E3	DOM × PFAS × Conc	28	8.19	0.0002	***
E2/E3	DOM × pH × Conc	28	3.30	0.0016	**

Response	Term	df	F	Permutation p-value	Significance
E2/E3	PFAS × pH × Conc	28	2.26	0.0166	*
E2/E3	DOM × PFAS × pH × Conc	56	3.89	0.0002	***

Significance codes: *** p ≤ 0.001; ** p ≤ 0.01; * p ≤ 0.05; ns = not significant.

Table Appx. 6 Type III ANOVA Results for FI with DOM source, PFAS Species, pH, and log_{10}-transformed concentration as predictors.

Term	df	F	p-value	Significance
DOM source	2	20381.00	<0.001	***
PFAS species	2	77.99	<0.001	***
pH	2	311.56	<0.001	***
Conc	1	0.06	0.808	ns
DOM × PFAS	4	57.05	<0.001	***
DOM × pH	4	19.77	<0.001	***
PFAS × pH	4	11.10	<0.001	***
DOM × Conc	2	0.90	0.409	ns
PFAS × Conc	2	2.68	0.070	ns
pH × Conc	2	0.35	0.706	ns
DOM × PFAS × pH	8	10.69	<0.001	***
DOM × PFAS × Conc	4	0.41	0.802	ns
DOM × pH × Conc	4	0.76	0.550	ns
PFAS × pH × Concentration	4	0.52	0.720	ns
DOM × PFAS × pH × Conc	8	1.61	0.120	ns

Significance codes: *** p ≤ 0.001; ** p ≤ 0.01; * p ≤ 0.05; ns = not significant.

Table Appx. 7 Aligned-rank transform (ART) ANOVA results for HIX. Reported values include numerator degrees of freedom (Df), residual degrees of freedom (Df.res), F-statistics, and p-values.

Term	Df	Df.res	F value	p-value	Significance
DOM	2	209	817.37	<0.001	***
PFAS	2	209	501.41	<0.001	***
pH	2	209	384.07	<0.001	***
Conc_group	7	209	45.23	<0.001	***
DOM × PFAS	4	209	276.56	<0.001	***
DOM × pH	4	209	457.44	<0.001	***
PFAS × pH	4	209	608.50	<0.001	***
DOM × Conc	14	209	11.37	<0.001	***
PFAS × Conc	14	209	19.98	<0.001	***
pH × Conc	14	209	17.15	<0.001	***
DOM × PFAS × pH	8	209	193.81	<0.001	***
DOM × PFAS × Conc	28	209	6.69	<0.001	***
DOM × pH × Conc	28	209	8.25	<0.001	***
PFAS × pH × Conc	28	209	12.39	<0.001	***
DOM × PFAS × pH × Conc	56	209	5.16	<0.001	***

Significance codes: *** p ≤ 0.001; ** p ≤ 0.01; * p ≤ 0.05; ns = not significant.

Table Appx. 8 Aligned-rank transform (ART) ANOVA results for HIX. Reported values include numerator degrees of freedom (Df), residual degrees of freedom (Df.res), F-statistics, and p-values.

Term	Df	Df.res	F value	p-value	Significance
DOM	2	209	805.76	<0.001	***
PFAS	2	209	727.99	<0.001	***
pH	2	209	731.28	<0.001	***
Conc_group	7	209	23.70	<0.001	***
DOM × PFAS	4	209	462.40	<0.001	***
DOM × pH	4	209	691.88	<0.001	***
PFAS × pH	4	209	810.94	<0.001	***
DOM × Conc	14	209	20.76	<0.001	***
PFAS × Conc	14	209	28.31	<0.001	***
pH × Conc	14	209	19.69	<0.001	***
DOM × PFAS × pH	8	209	382.91	<0.001	***
DOM × PFAS × Conc	28	209	30.78	<0.001	***
DOM × pH × Conc	28	209	13.12	<0.001	***
PFAS × pH × Conc	28	209	14.95	<0.001	***
DOM × PFAS × pH × Conc	56	209	10.58	<0.001	***

Table Appx. 9 Freedman–Lane permutation ANOVA Results (5,000 permutations) for the Effects of DOM Source, PFAS Species, and pH on PARAFAC Component Intensities. Reported values are numerator degrees of freedom (df), F-statistics, and permutation-based p-values.

Component	Term	df	F	p-value	Significance
	DOM source	2	54.92	0.0002	***
	PFAS species	2	0.34	0.7144	ns
	pH	2	0.45	0.6482	ns
C1	DOM × PFAS	4	1.78	0.1292	ns
	DOM × pH	4	2.95	0.0174	*
	PFAS × pH	4	0.29	0.8892	ns
	DOM × PFAS × pH	8	0.31	0.9646	ns
	DOM source	2	21.00	0.0002	***
	PFAS species	2	10.35	0.0002	***
	pH	2	3.24	0.0338	*
C2	DOM × PFAS	4	0.88	0.4754	ns
	DOM × pH	4	4.32	0.0018	**
	PFAS × pH	4	1.29	0.2792	ns
	DOM × PFAS × pH	8	0.90	0.5014	ns
	DOM source	2	1149.51	0.0002	***
	PFAS species	2	28.30	0.0002	***
	pH	2	21.59	0.0002	***
C3	DOM × PFAS	4	12.13	0.0002	***
	DOM × pH	4	26.33	0.0002	***
	PFAS × pH	4	6.93	0.0002	***
	DOM × PFAS × pH	8	4.14	0.0004	***
	DOM source	2	39.86	0.0002	***
	PFAS species	2	5.26	0.0050	**
	pH	2	5.14	0.0060	**
C4	DOM × PFAS	4	0.61	0.6568	ns
	DOM × pH	4	0.60	0.6648	ns
	PFAS × pH	4	1.32	0.2522	ns
	DOM × PFAS × pH	8	0.60	0.7782	ns

Significance codes: *** $p \leq 0.001$; ** $p \leq 0.01$; * $p \leq 0.05$; ns = not significant.

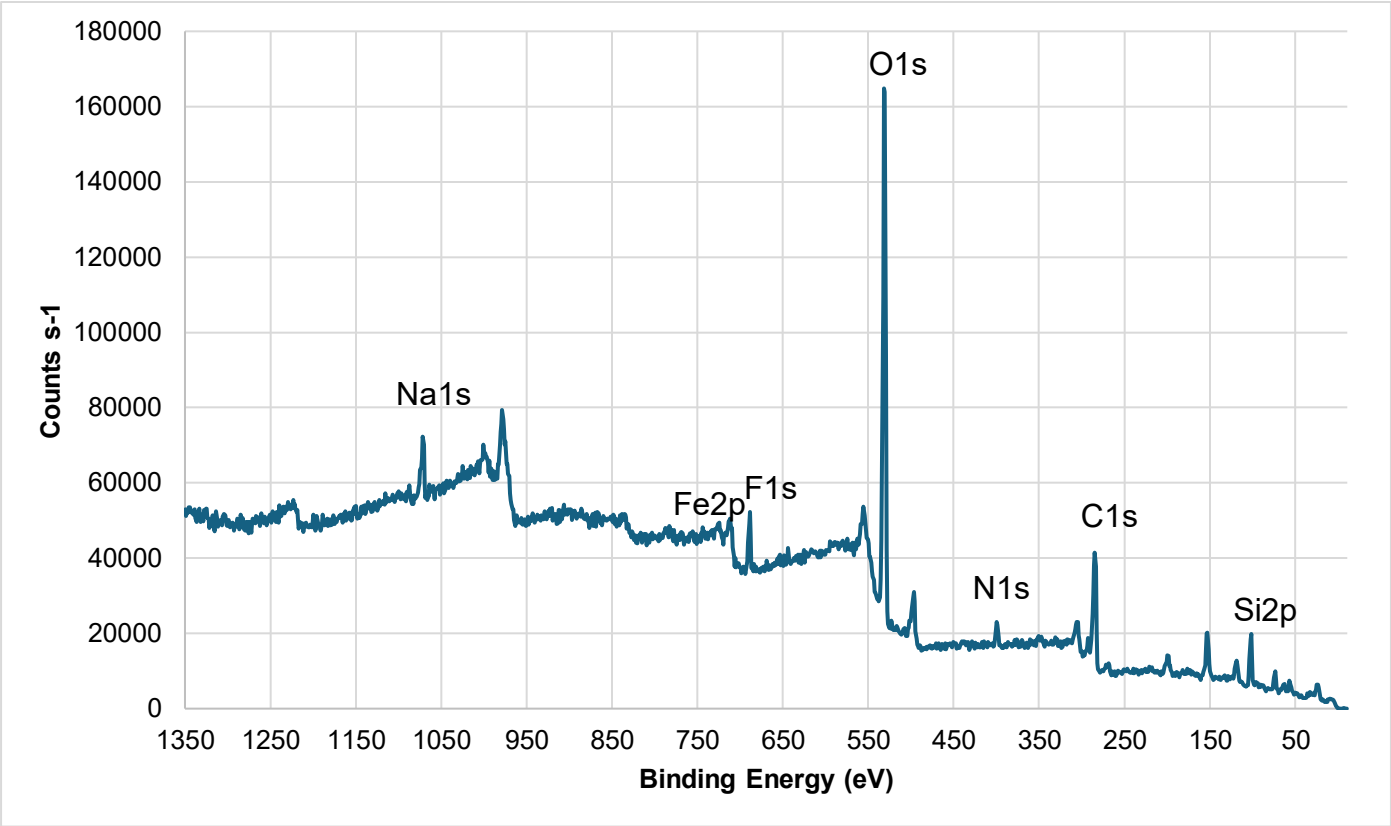

Figure Appx. 1 XPS Survey and High-Resolution Spectra of Unwashed Weathered Microplastics. XPS spectra of weathered microplastics prior to solvent washing, showing the presence of sediment-associated elements and surface-bound species. Peak assignments were performed using Advantage software (v. 5.99, Thermo Scientific). The detected Na, Fe, Al, Cl, F, and Si signals indicate weakly associated mineral and ionic surface constituents consistent with environmentally derived surface coatings

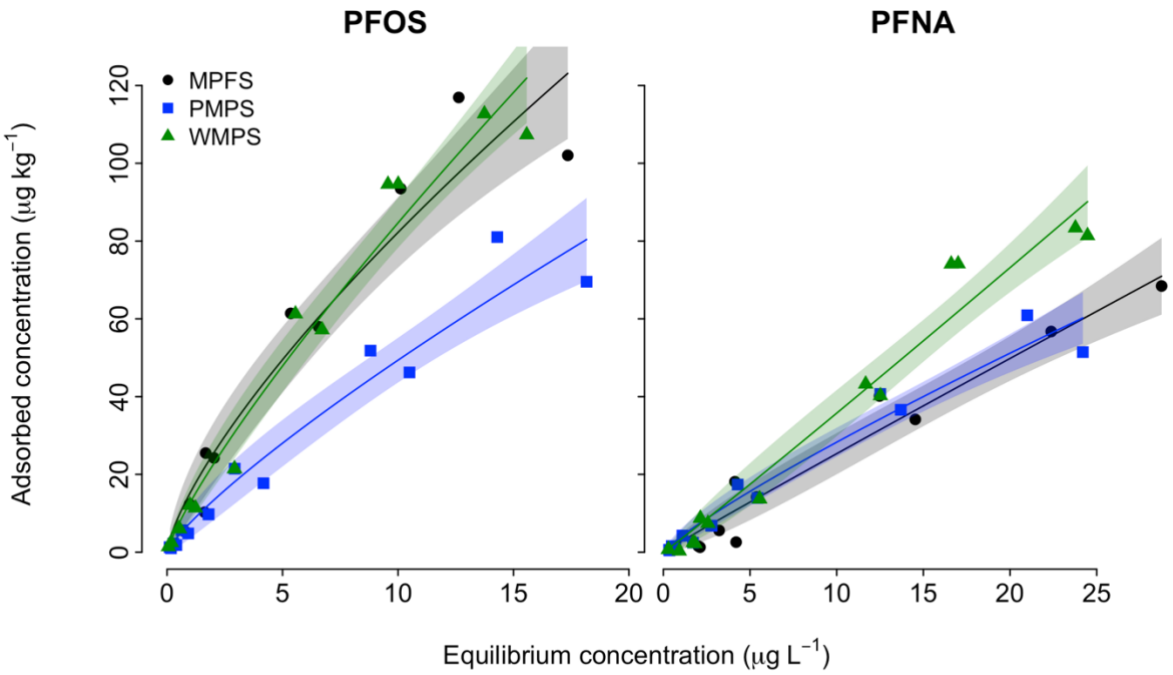

Figure Appx. 2 Comparison of PFOS and PFNA Adsorption Across Sediment Treatments. Adsorption isotherms of PFOS and PFNA on microplastic-free sediments (MPFS), sediments containing pristine microplastics (PMPS), and sediments containing weathered microplastics (WMPS). Data points represent measured values, and fitted lines correspond to the Freundlich model. Shaded regions indicate 95% confidence intervals for model predictions.

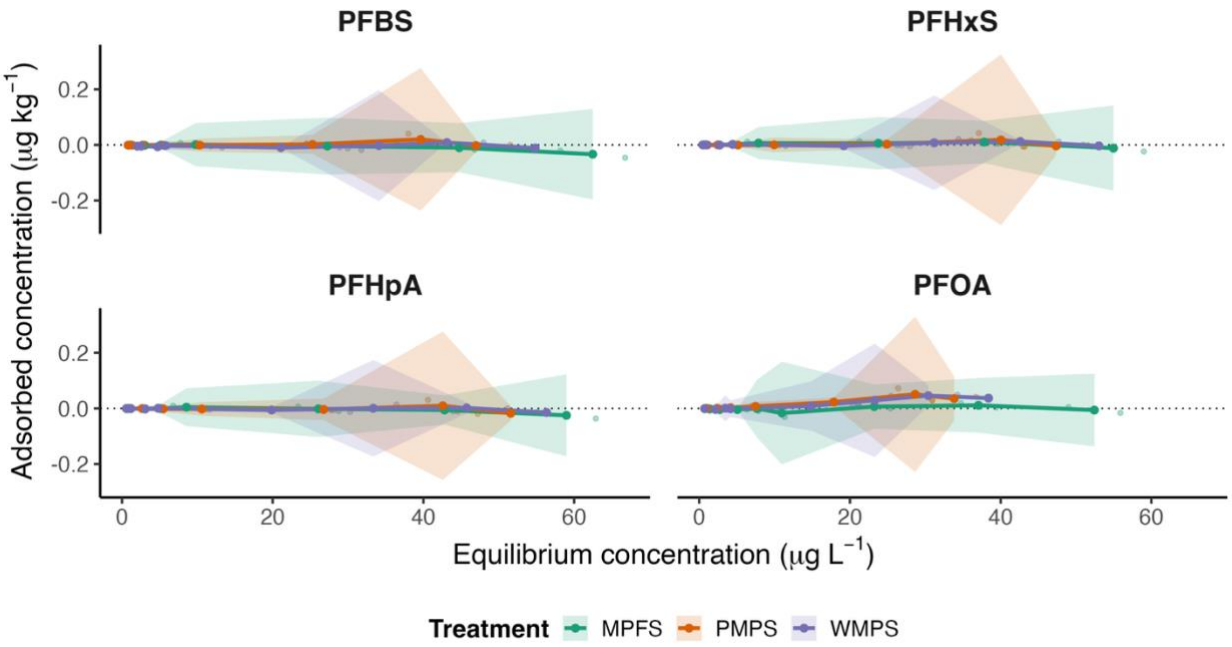

Figure Appx. 3 Adsorption of Short-Chain PFAS Under Microplastic Treatments with 95% Confidence Intervals. Adsorption isotherms for PFBS, PFHxS, PFHpA, and PFOA comparing microplastic-free sediment (MPFS), weathered microplastic sediment (WMPS), and pristine microplastic sediment (PMPS). Points represent measured replicate data, solid lines represent treatment means, and shaded ribbons indicate the 95% confidence interval calculated from replicate measurements. Panels are faceted by PFAS compound.

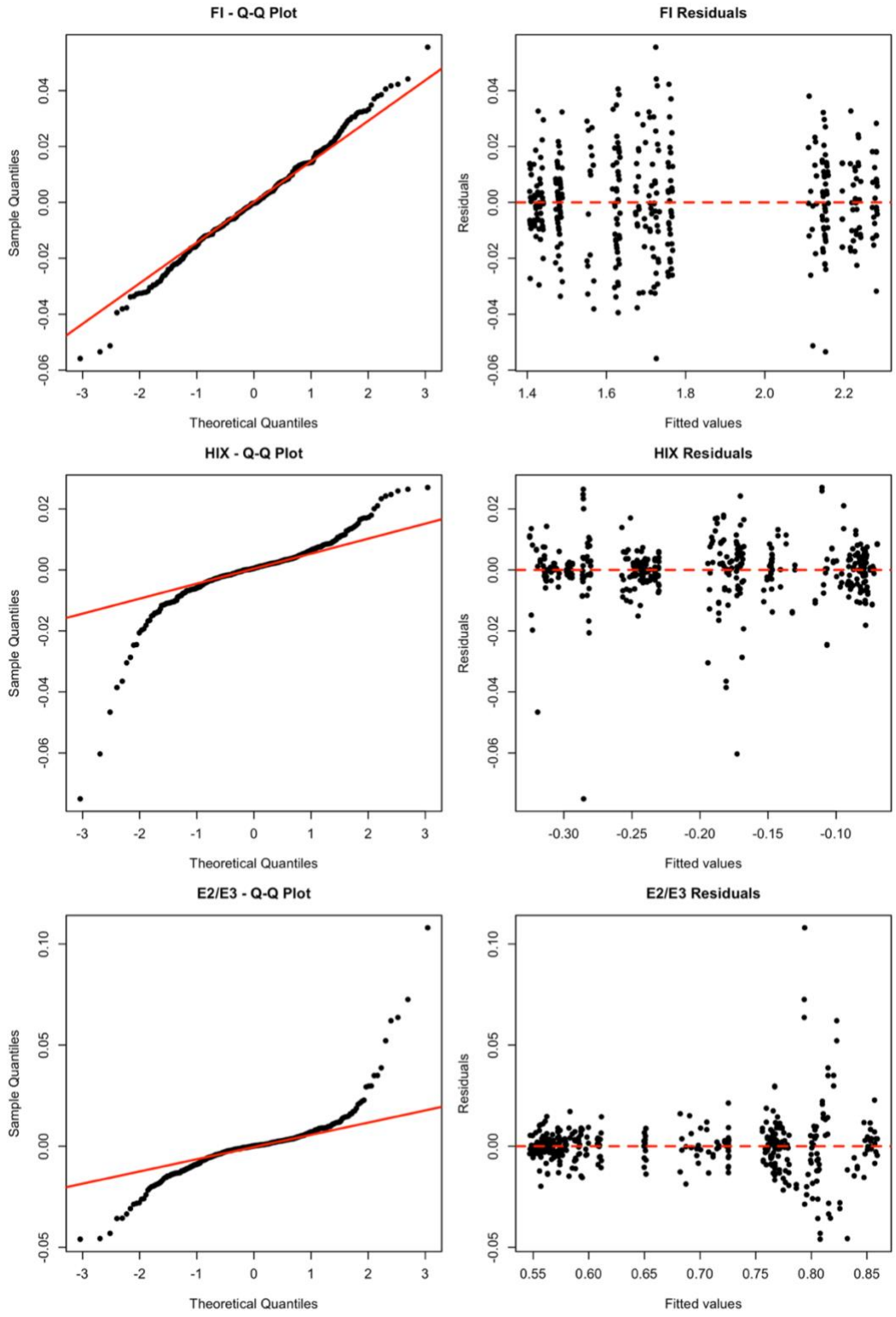

Figure Appx. 4 Residual diagnostic plots for fluorescence index (FI), humification index (HIX), and E2/E3 models.

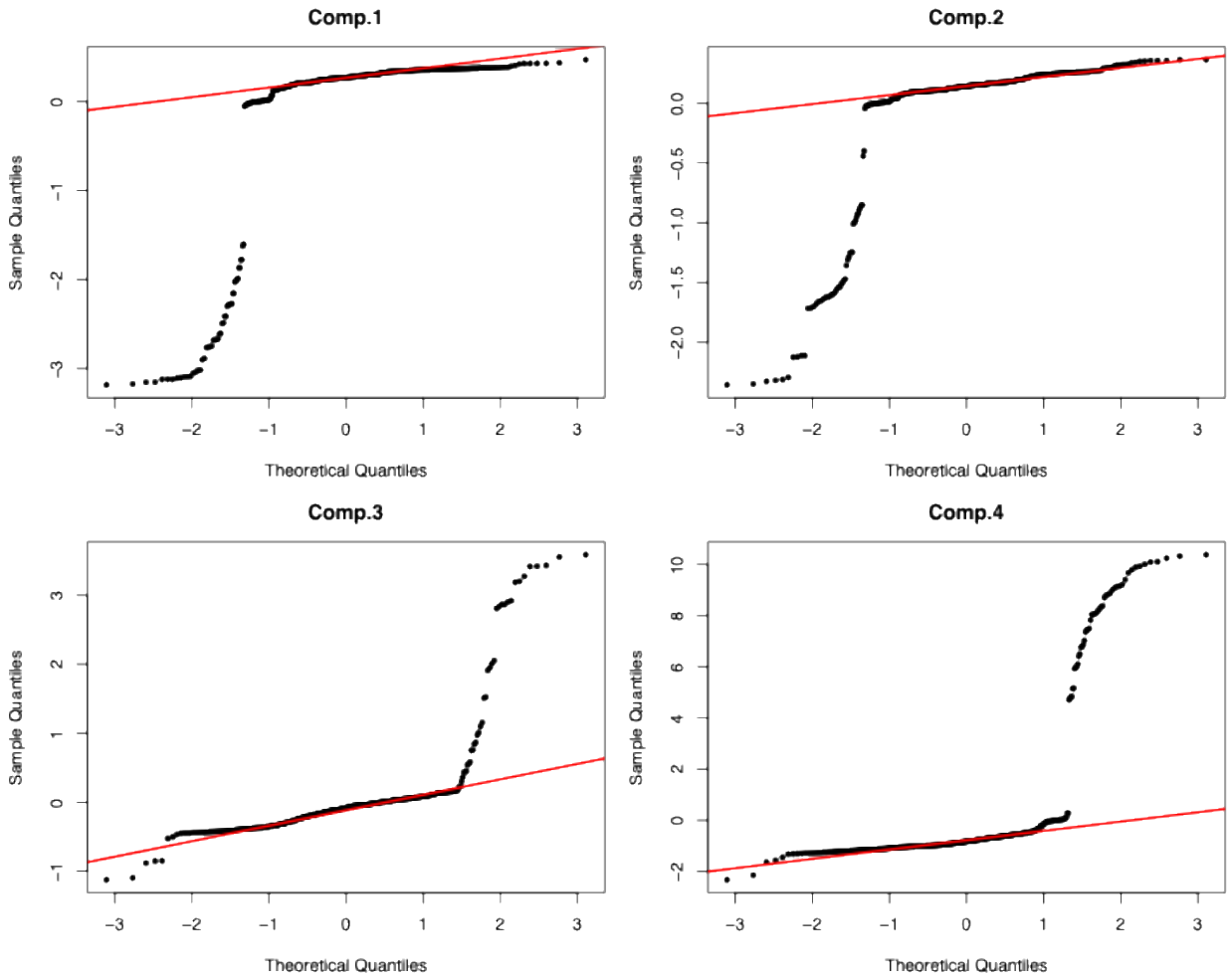

Figure Appx. 5 Quantile–quantile (Q–Q) plots of residuals for PARAFAC component score models (C1–C4) used to assess normality assumptions prior to aligned-rank transform ANOVA.

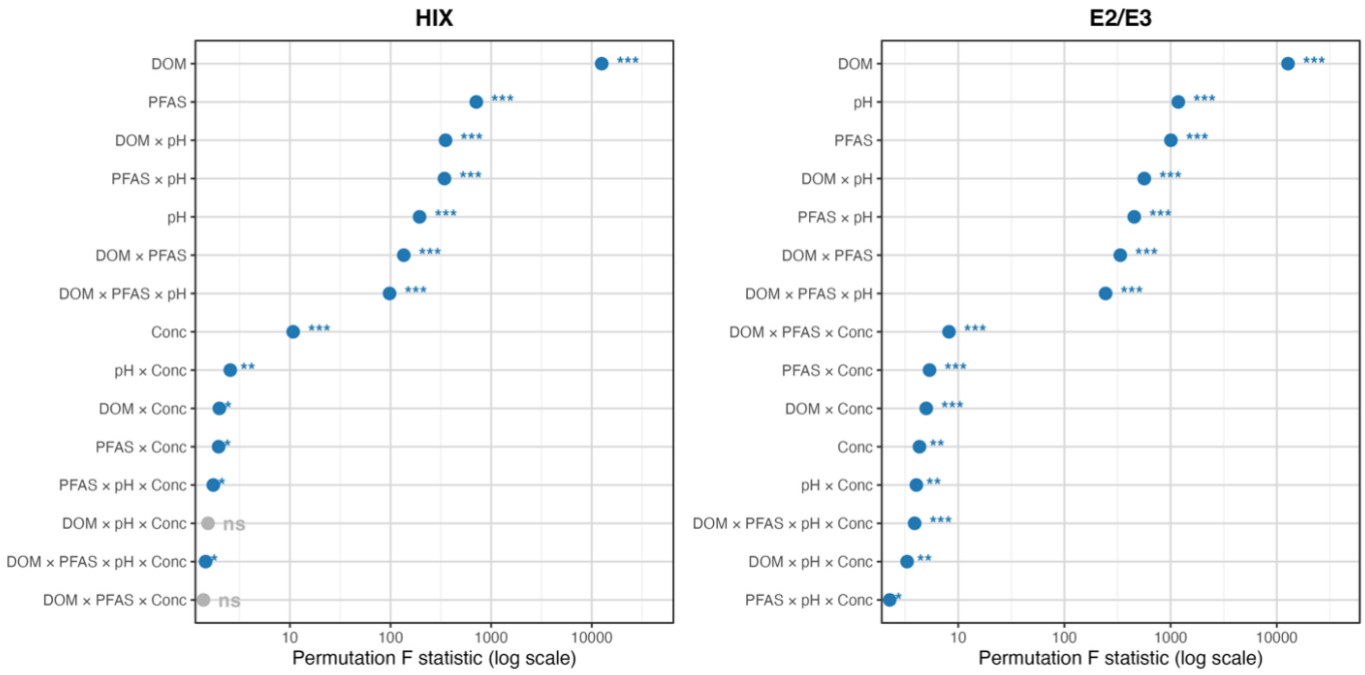

*Figure Appx. 6 Relative Importance of Experimental Factors Controlling HIX and E2/E3 Based on Permutation ANOVA. Points represent Freedman–Lane permutation ANOVA F-statistics (log scale) for factors influencing HIX and E2/E3, with significance indicated by asterisks. Significance codes: *** p ≤ 0.001; ** p ≤ 0.01; * p ≤ 0.05; ns = not significant*

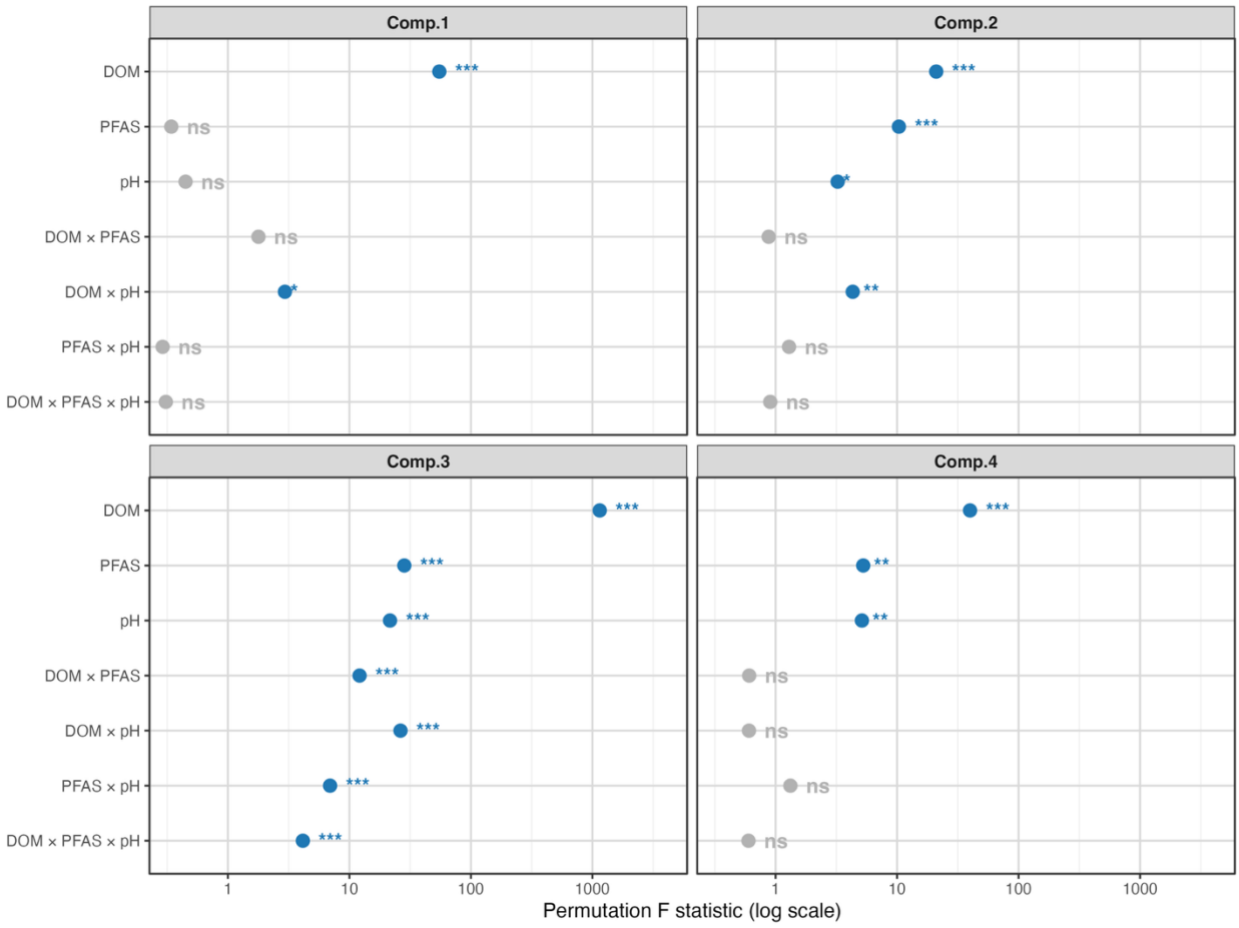

*Figure Appx. 7 Relative Importance of DOM Source, PFAS Species, and pH on PARAFAC Component Intensities Based on Permutation ANOVA. Points represent Freedman–Lane permutation ANOVA F-statistics (log scale) for factors affecting PARAFAC component intensities, with significance indicated by asterisks. Significance codes: *** p ≤ 0.001; ** p ≤ 0.01; * p ≤ 0.05; ns = not significant.*

Appendix References:

Bisutti I, Hilke I, Raessler M. 2004. Determination of total organic carbon–an overview of current methods. TrAC Trends in Analytical Chemistry 23:716-726

Brunauer S, Emmett PH, Teller E. 1938. Adsorption of gases in multimolecular layers. Journal of the American chemical society 60:309-319